Interphase Transfer of Low-Molecular-Weight Compound between Immiscible Polymer Pairs

NAWAPHORN KUHAKONGKIAT

Japan Advanced Institute of Science and Technology

Interphase Transfer of Low-Molecular-Weight Compound between Immiscible Polymer Pairs

by

NAWAPHORN KUHAKONGKIAT

Submitted to
Japan Advanced Institute of Science and Technology
in partial fulfillment of the requirements for the degree of
Doctor of Philosophy

Supervisor: **Professor Dr. Masayuki Yamaguchi**

School of Materials Science
Japan Advanced Institute of Science and Technology

September 2016

Referee-in-chief : **Professor Dr. Masayuki Yamaguchi**
Japan Advanced Institute of Science and Technology

Referees : **Associate Professor Ken-ichi Shinohara**
Japan Advanced Institute of Science and Technology

Associate Professor Kazuaki Matsumura
Japan Advanced Institute of Science and Technology

Associate Professor Tsutomu Hamada
Japan Advanced Institute of Science and Technology

Professor Dr. Shuichi Maeda
Yamaguchi University

Preface

In multi-component system, the addition of a low-molecular-weight compound as a third component is frequently carried out to provide desirable properties of a material. Understanding and controlling the distribution state of a third component have to be seriously considered because it decides the quality of a product. Generally, the distribution state of a third component is determined by the difference in the miscibility with each polymer, which is dependent upon the temperature. Furthermore, the distribution state may change by the interphase transfer when it is different from that in the equilibrium state.

In this thesis, the interphase transfer behavior of a low-molecular-weight compound as a third component between immiscible polymers is studied considering the effect of the ambient temperature. I hope this thesis will help to establish a new concept of the material design for multi-component polymer systems, which will lead to a novel smart material.

Nawaphorn Kuhakongkiat

Contents

Chapter 1

General Introduction

1.1 Introduction

The science and technology of polymeric materials have been significantly developed due to their unique properties and light weight, and further development is expected to meet a demand of various applications [1-4]. Research activities in the past have been concentrated mainly on the chemical approach such as catalyst and polymerization techniques. Since these routes have become increasingly complex and lead to poor cost performance, blending, as an alternative technique, has been focused these days.

Some of polymer blends have been successfully commercialized with the combination of excellent properties, which cannot be attained from one polymer species. This strategy is known as one of the powerful approaches with the advantages of good cost performance and easy processing. Additionally, polymer blends can cover a wide range of material properties by changing the blend composition.

Polymer blends are of great importance also in the rubber industry, especially for automotive and transportation applications [5-8]. It is an effective and economic approach to satisfy the divergent requirements of properties compared to synthesizing new elastomers. Prospestive commitments of rubber blends are (1) product uniformity, (2) good processability, (3) efficient productivity, and (4) rapid formulation changes and manufacture flexibility. Moreover, the addition of a low-molecular-weight additive has been often carried

out to satisfy properties for a final product. For example, the addition of curatives such as sulfur to create a three-dimensional network vulcanization [9] and a processing oil to provide flexibility and processability [10].

Because commercial rubbers have generally high molecular weight, their blends are typically not miscible due to the lack of the contribution of mixing entropy as explained later. In the case of an immiscible polymer blend containing a low-molecular-weight compound as a third component, the overall phase-separated morphology is governed by not only the properties of individual components, but also the interaction among them. In particular, the distribution state of a low-molecular-weight compound is determined by the difference in the miscibility with each rubber component, which is expressed by the Flory-Huggins interaction parameter [11, 12]. In general, a third component prefers to reside in a polymer component with the low interaction parameter. In addition, the interaction parameter is dependent upon the ambient temperature, pressure and flow field. In other words, the distribution state of a low-molecular-weight additive in a blend changes with these conditions.

Moreover, the distribution state may change during storage. In fact, some researchers have reported that the distribution state of a compound in an immiscible rubber blend changes by the interphase transfer phenomenon. Since the factors controlling the distribution, e.g., the interaction parameter, is a function of the temperature, the preferable distribution state of a third component can be controlled by the ambient temperature when the diffusion is allowed for a third component. In this case, the amount of a third component in each phase changes with the ambient temperature. This will lead to a novel material

design. In this thesis, the effect of the temperature on the distribution will be focused, which has not been carried out before to the best of my knowledge.

This chapter covers the background information prior to the discussion on the transfer phenomenon. The fundamental of miscibility of a polymer blend, the rubber technology, and the distribution of a low-molecular-weight compound in a rubber blend are explained in the combination with literature reviews. Finally, the objective of the thesis is mentioned.

1.2 Polymer-Polymer Miscibility

1.2.1 Polymer blend and morphology

Processability and mechanical properties of a polymer blend are strongly dependent on morphology [3, 13]. Therefore, the control of morphology is the key factor in the field of polymer blends. Most polymer blend systems are immiscible and exhibit phase-separated morphology. Two notable morphologies for immiscible blends are co-continuous morphology and sea-island morphology, which can be characterized by various methods [14-17]. The morphology of an immiscible polymer blend depends on (1) mixing procedure, (2) rheological properties of the components, and (3) interfacial tension.

The mixing process is the first step to control the morphology. The model mechanism was initially proposed by Scott and Macosko [18, 19], in which the shape of the dispersed amorphous polyamide is deformed from spheres to platelets under the shear field in the polystyrene matrix as shown in Figure 1.1. Their experimental results demonstrated the morphology development at the processing. Jordhamo *et al.* [20] noted the essential condition to create co-continuous morphology as follows;

$$\frac{\eta_1\theta_2}{\eta_2\theta_1} = 1 \qquad (1.1)$$

where η_1, η_2 and θ_1, θ_2 are the viscosity and weight fraction of each component in the blend.

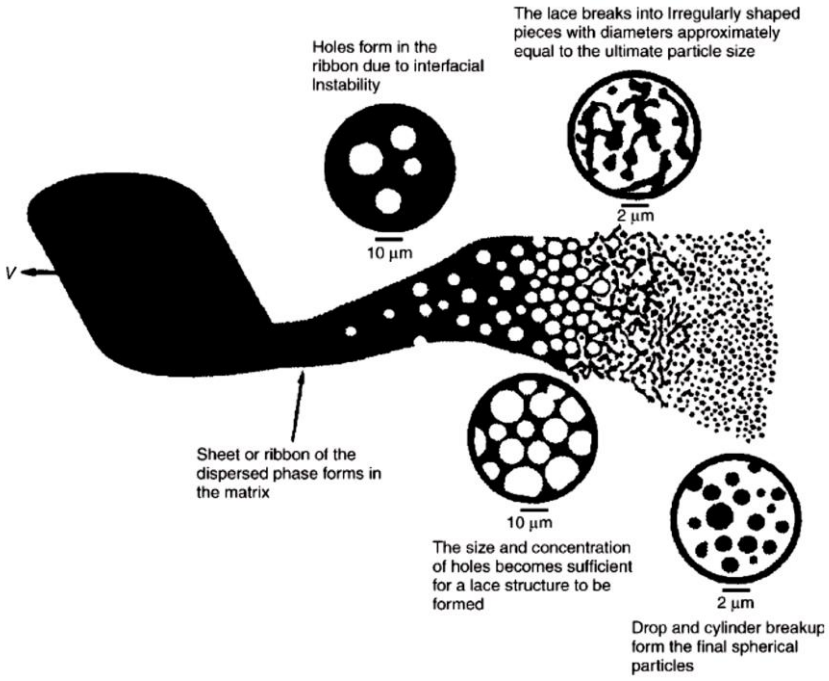

Figure 1.1 Morphology development of a polymer blend at mixing process. [18]

1.2.2 Thermodynamics of miscibility

The structure of a polymer blend is primarily determined by the miscibility of the components. In the equilibrium state, the miscibility is governed by the Gibbs free energy of mixing ΔG_m [21];

$$\Delta G_m = \Delta H_m - T\Delta S_m \tag{1.2}$$

where ΔH_m is the enthalpy of mixing (heat of mixing), and ΔS_m is the entropy of mixing determined by the Boltzmann relationship. Since the entropy term is negligible for polymer blends, ΔH_m is the key factor to decide the miscibility.

Assuming that ΔS_m is zero, the miscibility is determined by ΔH_m, as follows.

1. Miscible blend: ΔH_m is negative due to the specific interaction between components, e.g., ion-dipole interaction, hydrogen bond, etc. Both components are dissolved together in a molecular scale.

2. Immiscible blend: ΔH_m is positive. The phase separated morphology is observed.

The miscibility is, of course, affected by the mixing entropy. This becomes very important when components have low molecular weight. For a polymer-polymer blend, ΔS_m is small because of the high molecular weights. The assumption in the Flory-Huggins theory based on the lattice model [11, 12, 22, 23] is applied to determine the entropy of mixing for the mixture as illustrated in Figure 1.2.

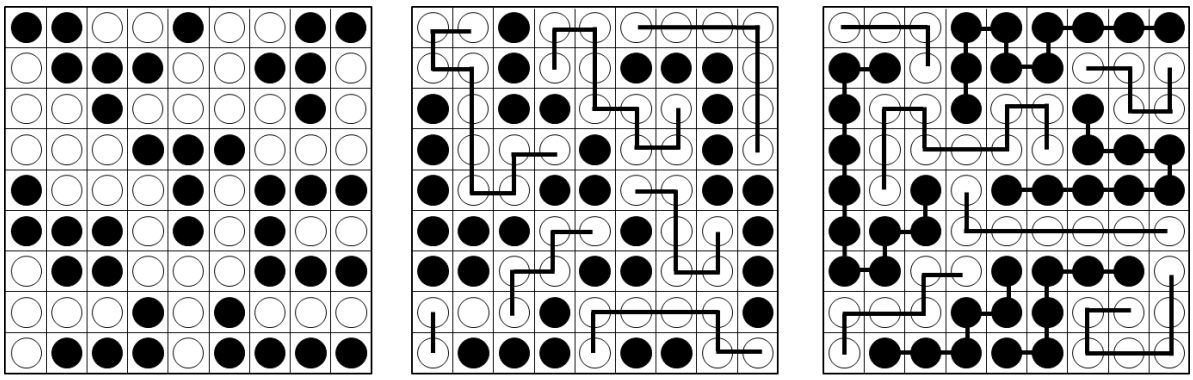

Figure 1.2 Lattice model for (a) solvent-solvent blend, (b) solvent-polymer blend, and (c) polymer-polymer blend.

From the figure, the lattice is comprised of *N* cells with a volume of *v*. Each cell is occupied by one segment of any molecule. The entropy change of mixing can be derived through the number of cites of a lattice as follows;

$$\Delta S_m = -k_B(N_1 \ln \phi_1 + N_2 \ln \phi_2) \tag{1.3}$$

$$\Delta S_m = -k_B V(\frac{\phi_1}{r_1} \ln \phi_1 + \frac{\phi_2}{r_2} \ln \phi_2) \quad \text{(molecular basis)} \tag{1.4}$$

$$\Delta S_m = -RV(\frac{\phi_1}{r_1} \ln \phi_1 + \frac{\phi_2}{r_2} \ln \phi_2) \quad \text{(molar basis)} \tag{1.5}$$

where k_B is the Boltzmann constant, V is the total volume, R is the gas constant, and ϕ_i and r_i are the volume fraction and the number of polymer segment i.

As mentioned that most polymer pairs have a small value of ΔS_m. Therefore, the miscibility is usually determined by the contribution of ΔH_m. The term of enthalpy change has relation with the Flory-Huggins interaction parameter χ_{12} by the following equation.

$$\Delta H_m = \phi_1 \phi_2 RTV \frac{\chi_{12}}{v_r} \tag{1.6}$$

where v_r is the reference volume.

Consequently, the following two expressions are obtained to express the Gibbs free energy of mixing.

$$\Delta G_m = k_B TV\left[\frac{\phi_1}{r_1} \ln \phi_1 + \frac{\phi_2}{r_2} \ln \phi_2\right] + \phi_1 \phi_2 \chi_{12} k_B TV / v_r \quad \text{(molecular basis)} \tag{1.7}$$

$$\Delta G_m = RTV\left[\frac{\phi_1}{r_1} \ln \phi_1 + \frac{\phi_2}{r_2} \ln \phi_2\right] + \phi_1 \phi_2 \chi_{12} RTV / v_r \quad \text{(molar basis)} \tag{1.8}$$

The general style of the Flory-Huggins equation is given;

$$\Delta G_m = RTV\left[\frac{\rho_1\phi_1}{r_1}\ln\phi_1 + \frac{\rho_2\phi_2}{r_2}\ln\phi_2\right] + \chi_{12}\phi_1\phi_2 V \tag{1.9}$$

where ρ_i is the density of the component *i*.

Finally, the following equation is obtained, assuming $\rho_1 = \rho_2 = 1$.

$$\frac{\Delta G_m}{V} = RT\left[\frac{\phi_1}{r_1}\ln\phi_1 + \frac{\phi_2}{r_2}\ln\phi_2\right] + \chi_{12}\phi_1\phi_2 \tag{1.10}$$

It has been reported that most polymer pairs have positive ΔH_m. Consequently, there are a lot of immiscible systems. In other words, two polymers can be miscible only when they have specific interactions between the components ($\Delta H_m < 0$), e.g., hydrogen bonding and ion-dipole interaction.

There are two famous critical temperatures to illustrate a phase diagram of a polymer blend, i.e., upper critical solution temperature (UCST) and lower critical solution temperature (LCST). The phase diagram including the critical temperature is illustrated in Figure 1.3, in which the blend ratio and the temperature are the variables.

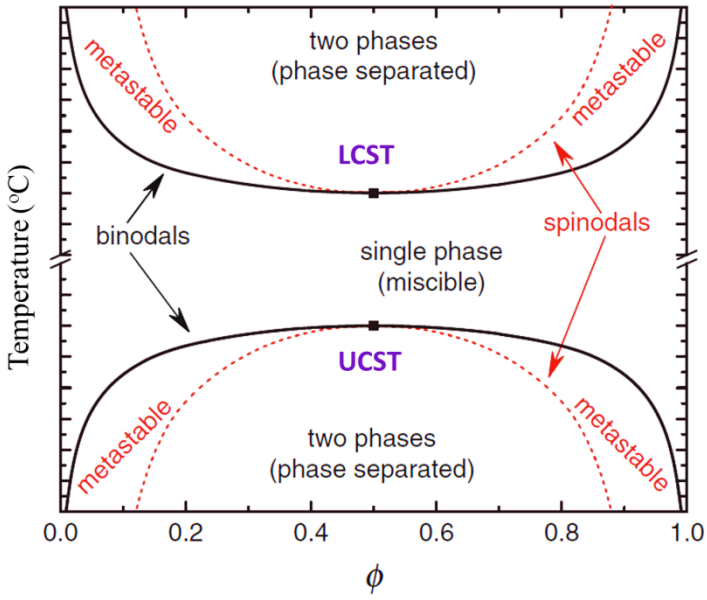

Figure 1.3 Phase diagram showing LCST and UCST behavior for blend systems.

In the classical lattice theory, polymer blends can show only UCST but not LCST, because χ_{12} is given as follows;

$$\chi_{12} = \frac{z\Delta\varepsilon}{k_B T} \quad \text{(molecular basis)} \quad \text{or} \tag{1.11}$$

$$\chi_{12} = \frac{z\Delta\varepsilon}{RT} \quad \text{(molar basis)} \tag{1.12}$$

where z is the coordinate number of the lattice model.

The term of $\Delta\varepsilon$ is the difference in the interaction energies between chain segments of components, which is derived from the relationship;

$$\Delta\varepsilon = \frac{1}{2}\left(\varepsilon_{11} + \varepsilon_{22}\right) - \varepsilon_{12} \tag{1.13}$$

where ε_{ij} is the constant energy of contacts between components i and j.

Then, the Flory-Huggins interaction parameter can be written as follows;

$$\chi_{12} = \frac{z}{k_B T}\left(\frac{\varepsilon_{11} + \varepsilon_{12}}{2} - \varepsilon_{12}\right) \quad \text{(molecular basis)} \quad \text{or} \tag{1.14}$$

$$\chi_{12} = \frac{z}{RT}\left(\frac{\varepsilon_{11} + \varepsilon_{12}}{2} - \varepsilon_{12}\right) \quad \text{(molar basis)} \tag{1.15}$$

In 1960, Freeman and Rowlinson found that several hydrocarbon polymers can be dissolved in hydrocarbon solvents [24]. These nonpolar polymer solutions exhibited the phase separation at high temperature, known as LCST behavior. This seldom happens in a mixture of low-molecular-weight compounds. Of course, the original Flory-Huggins theory assuming eq. (1.11) and (1.12) cannot describe the phenomenon. Flory and co-workers [25-31] then developed the new theory for the solutions, which can predict the LCST behavior. Furthermore, various models have been proposed such as the Prigogine-Flory-Patterson theory [27, 32-34], the lattice-with-holes theory [35, 36], and Sanchez-Lacombe lattice fluid model [37, 38]. They are called “equations of state theories”.

The equation of state is basically a mathematical relationship between volume, temperature, and pressure, which can be written by three parameters: v^* (characteristic reduced volume), T^* (characteristic reduced temperature), and P^* (characteristic reduced pressure). The reduced variables are defined as

$$\tilde{T} = T / T^* \tag{1.16}$$

$$\tilde{P} = P / P^* \tag{1.17}$$

$$\tilde{v} = v / v^* \tag{1.18}$$

The volume v^* is that of a polymer segment and v is the actual volume of a segment. Thus $\tilde{v}$ is the reduced value per segment. The values of $\tilde{v}$ and $\tilde{P}$ were estimated by thermal expansion coefficient. The Flory-Huggins interaction parameter χ_{12} can be expressed using the reduced variables as follows;

$$\frac{\chi_{12}}{M_1\tilde{v}_{1,sp}} = \frac{P_1^*}{RT_1^*}\left[\frac{\tilde{v}_1^{1/3}X_{12}}{\left(\tilde{v}_1^{1/3}-1\right)P_1^*}\right] + \left[\frac{\tilde{v}_1^{1/3}}{2\left(\frac{4}{3}-\tilde{v}_1^{1/3}\right)}\right] + \left[\left(1-\frac{T_1^*}{T_2^*}\right)^2\right] \tag{1.19}$$

where M_1 is the molecular weight of a polymer and X_{12} is an exchange interaction parameter between polymer and solvent.

The interaction term X_{12} is similar to χ_{12} in the Flory lattice theory, but has the dimensions of energy density as given by;

$$P^* = \phi_1 P_1^* + \phi_2 P_2^* - \phi_1\theta_2 X_{12} \tag{1.20}$$

where ϕ_i is the volume fraction of component i and θ_2 is the segment surface fraction.

In the modified theory, the following three principle contributions are important for the interaction parameter, i.e, dispersion force contribution, free volume contribution, and the contribution of specific interaction. In general, the dispersive force and specific interaction are inversely proportional to temperature as shown in eqs. (1.14) and (1.15), whereas the contribution of free volume is always increasing with temperature as a positive value. These two opposite contributions are responsible for the LCST behavior as shown in Figure 1.4.

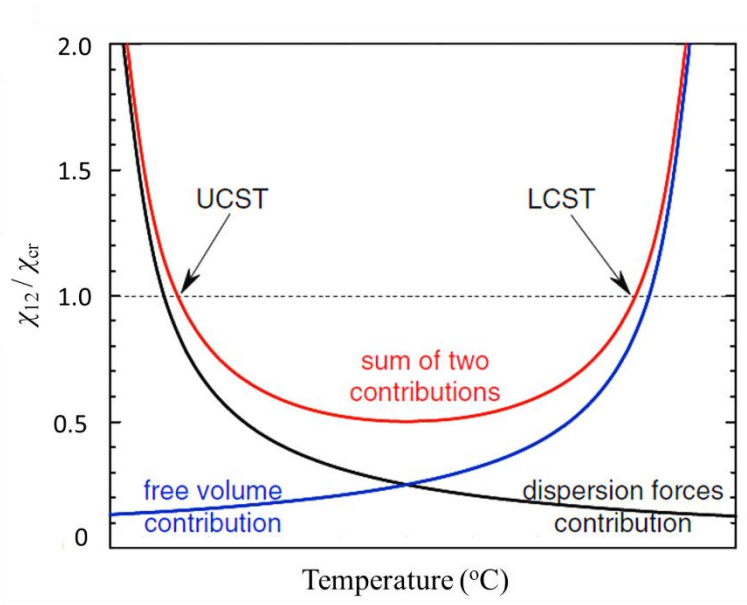

Figure 1.4 Schematic diagram of the UCST and LCST phase diagrams for liquid mixtures relating to the free energy of mixing contributions

The miscibility can only be achieved when χ_{12} is lower than χ_{cr}, where χ_{cr} is the maximum value (> 0) to show the miscibility. The dotted line ($\chi_{12}/\chi_{cr} = 1$) is the temperature at which the miscibility changes. Furthermore, χ_{cr} can be obtained as follows;

$$\chi_{cr} = \frac{1}{2}\rho\left[\frac{1}{r_1^{1/2}} + \frac{1}{r_2^{1/2}}\right]^2 \tag{1.21}$$

where ρ is the average density.

When the specific interactions such as hydrogen bonding and electrostatic interactions governs the miscibility, the phase diagram is written in Figure 1.5.

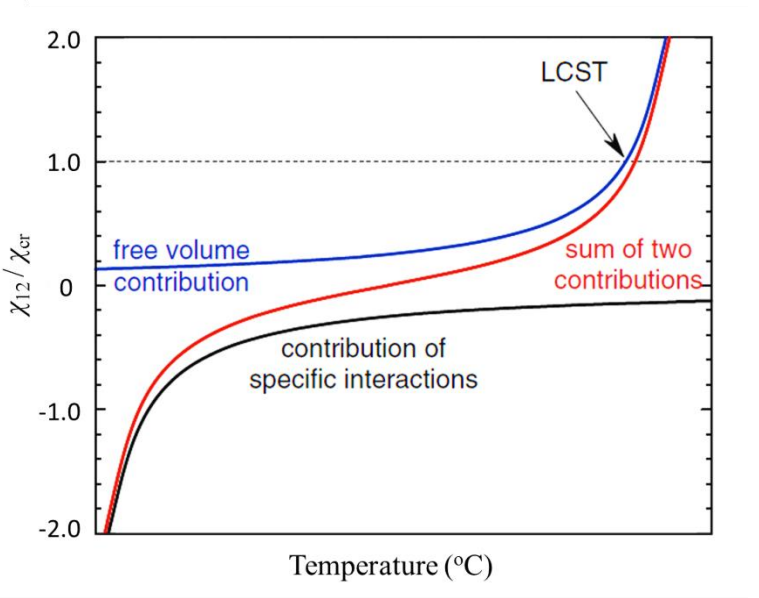

Figure 1.5 LCST phase behavior of polymer blend controlling the interaction parameter by the contribution of the specific interactions

The free volume contribution was explained by using other characteristics of polymer chains. Lohse et al. studied the miscibility of saturated hydrocarbon elastomer blends using small-angle neutron scattering and *PVT* measurements [39, 40]. The *PVT* data provide the cohesive energy density $CED = U/V$, which has a close relation with the internal pressure $\Pi_{IP} = \partial U/\partial V$. This parameter depends on not only the chemical composition, but also their chain packing density.

The packing length is defined as the ratio of the occupied volume V_{occ} of the chain, defined by eq. (1.22), to the radius of gyration r_g. V_{occ} is the occupied volume of a unit polymer, which is directly defined by the polymer density.

$$V_{OCC} = \frac{M}{\rho N_A} \tag{1.22}$$

where N_A and M are the Avogadro's number and molecular weight of a component, respectively.

Since the average of r_g^2 in the melt is proportional to M, V_{occ}/r_g^2 is independent of the molecular weight, the packing length l_p is defined as follows;

$$l_p = \frac{V_{OCC}}{r_g^2} = \frac{M}{r_g^2 \rho N_A} \tag{1.23}$$

It has been reported that the packing length is correlated with the solubility parameter by the following expression;

$$\delta = \frac{\rho N_A}{m_0}\left[\frac{2\pi\varepsilon a^3}{\left(1+\left(\frac{l_p}{2\pi a}\right)\right)}\right]^{1/2} \tag{1.24}$$

where m_0 is the molecular weight of a repeating unit. The parameters a and ε represent the length and energy scales of the component associated with the entanglement spacing.

The solubility parameter is inversely proportional to the packing length as long as both a and ε are constant. In other words, a smaller packing length provides a large solubility parameter. This is reasonable because small packing length leads to large radius of gyration, which can overlap the neighboring polymer chains with a strong interaction. The difference in the packing length is, therefore, used to predict the miscibility of non-polar systems [41-44].

1.2.3 Solubility parameter concept

The solubility parameter is known as a conventional parameter to predict the miscibility. When two materials have similar solubility parameters, then they may be miscible. This concept was firstly introduced by Scatchard [45], who defined the cohesive energy density as the energy of evaporation ΔE_v per unit volume. Then Hildebrand and Scott [46] further developed to obtain the following equation;

$$\delta = (CED)^{1/2} = \left(\frac{\Delta E_v}{V} \right)^{1/2} \tag{1.25}$$

The value is noted to be influenced by the specific solvent internal pressure [47]. For most of low-molecular-weight materials, e.g., organic liquids, the value can be estimated by several sources such as the heat of evaporization. In the case of high-molecular-weight polymers, the heat of evaporation cannot be measured directly. Therefore, the solubility parameter is typically estimated by viscosity or swelling of a crosslinked sample in a series of solvents.

Hansen [48] further considered the solubility parameter using three components, i.e., dispersion interaction δ_d, polarity δ_p, and hydrogen bonding δ_h. The total solubility parameter δ_t is given by the root mean square of these components.

$$\delta_t^2 = \delta_d^2 + \delta_p^2 + \delta_h^2 \tag{1.26}$$

Another approach has been used to predict the solubility parameter without physical experiments, which is known as the group contribution method, firstly developed by Small [49]. This method was further developed by van Krevelan [50], Hoy [51], and Coleman [52].

For this method, values of molar attraction constants are required as illustrated in Figure 1.6. The Small's formula is given by;

$$\delta_t = \frac{\rho \sum G_{Mi}}{M} \tag{1.27}$$

where ρ is the density, ΣG_{Mi} is the summation of the molar attraction constants of *i*-group, and M is the molar mass of a repeating unit.

Group	Molar attractive $[(MPa)^{1/2}/mole]$	Group	Molar attractive $[(MPa)^{1/2}/mole]$
Single bonded		H(variable)	164-205
$-CH_3$	439	O, ethers	144
$-CH_2-$	273	CO, Ketones	564
$-CH<$	57	COO, esters	636
$>C<$	-191	CN	841
Double bonded		Cl(mean)	533
$CH_2=$	390	Cl, single	554
$-CH=$	228	Cl,twinned as in $>CCl_2$	533
$>C=$	39	Cl, triple as in $-CCl_3$	513
Triple bonded		Br,single	697
$CH \equiv C-$	584	I,single	871
$-C \equiv C-$	455	CF_2, CF_3 n-fluorocarbons only	308, 562
Aromatic		S,sulfides	461
Phenyl	1507	SH, thiols	646
Phenylene (*o,m,p*)	1404	ONO_2-nitrates	~902
Naphthyl	2349	NO_2-,(aliphatic nitrocompounds)	~902
Others		PO_4 (organic phosphates)	1025
Ring, 5-membered	215-236	Si (in silicones)	78
Ring, 6-membered	195-215		
Conjugations	41-62		

Figure 1.6 Group molar attraction constants [49]

The Flory-Huggins interaction parameter χ_{12} is an important tool for quantifying the degree of miscibility for polymers. It can be presented with the correlation with the solubility parameters by combining Hidebrand-Scatchard solution theory as follows;

$$\chi_{12} = \frac{V}{RT}(\delta_1 - \delta_2)^2 \tag{1.28}$$

Based on this equation, however, the interaction parameter never become a negative value. Although this situation is not correct, the calculated value can be used to predict the miscibility roughly.

As seen in eq. (1.25), the solubility parameter is the square root of the cohesive energy density of the pure liquid. In the case of nonpolar liquid, i.e., saturated hydrocarbon, the cohesive energy is related approximately to its internal pressure. It can be determined by *PVT* measurements, which leads to;

$$\delta_{PVT} = \left(T \frac{\alpha(T)}{\beta(T)} \right)^{1/2} \tag{1.29}$$

where α is the thermal expansion coefficient of a liquid and β is the isothermal compressability.

As mentioned, a solubility parameter is dependent upon the temperature. Table 1.1 shows the *PVT* results of several polyolefin materials at various temperatures.

Table 1.1 Characteristic components on *PVT* data for several polyolefin materials [53]

Species	T (^oC)	$\alpha\,(T)$ x 10^4 (K^{-1})	$\beta\,(T)$ x 10^4 (MPa^{-1})	$\delta_{PVT}\,(T)$ ($MPa^{1/2}$)
PP atactic polypropylene	27	7.28	6.47	18.37
	51	7.55	7.54	18.02
	83	7.31	8.73	17.25
	121	7.30	10.44	16.60
	167	7.52	13.14	15.87
EP57 copolymer of ethylene and propylene (23 wt.% propylene)	27	6.77	5.89	18.57
	51	7.06	6.88	18.24
	83	7.12	7.87	17.94
	121	7.41	9.28	17.73
	167	8.10	11.49	17.61
PEP alternating copolymer of ethylene ad propylene	27	6.60	5.82	18.45
	51	6.78	6.74	18.06
	83	6.69	7.87	17.39
	121	6.88	9.30	17.07
	167	7.33	11.50	16.74
PIB polyisobutylene	27	5.52	4.80	18.58
	51	5.72	5.52	18.33
	83	5.53	6.29	17.68
	121	5.68	7.41	17.38
	167	6.08	8.85	17.38

1.3 Basics of Rheology

Rheology is a science of the deformation and flow. Therefore, elastic and viscous properties are frequently dealt in this field. In general, most polymer melts exhibit both elastic and viscous responses, i.e., viscoelasticity. The elastic response of a polymer liquid is attributed to the entanglement couplings of long molecules.

Hooke's law is applicable to a perfect elastic body by the following equation.

$$\sigma = E\varepsilon \tag{1.30}$$

where σ and ε are the stress and strain, respectively and E is the modulus.

Viscosity expresses the resistance to flow. Following the Newton's law, viscosity η is defined as the ratio of the stress ($\sigma = F/A$) and strain rate $\dot{\varepsilon}$ as follows;

$$\sigma = \eta\dot{\varepsilon} \tag{1.31}$$

1.3.1 Oscillatory modulus

The response of dynamic oscillatory stress and strain is expressed in Figure 1.7.

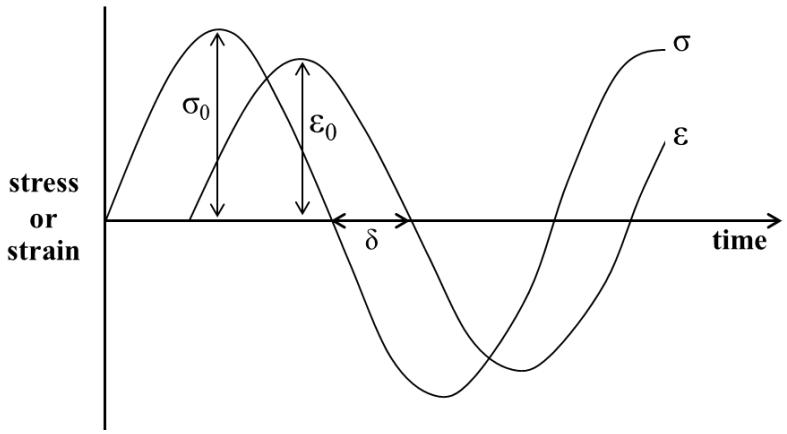

Figure 1.7 Sinusoidal oscillating stress and strain with a phase angle δ

The sinusoidal response with strain as a function of angular frequency ω, given by the following expressions;

$$\sigma(t) = \sigma_0 \sin(\omega t + \delta) \tag{1.32}$$

$$\varepsilon(t) = \varepsilon_0 \sin(\omega t) \tag{1.33}$$

where δ ($0 \leq \delta \leq \pi/2$) is a phase lag of the response.

When an oscillatory deformation ($\varepsilon = \varepsilon_0 e^{i\omega t}$) is applied to a viscoelastic body, the stress is generated as follows;

$$\sigma = E^*(\omega)\varepsilon \tag{1.34}$$

$$\sigma = \left[E'(\omega) + iE''(\omega)\right]\varepsilon \tag{1.35}$$

where $E^*(\omega)$ is complex modulus, E' is elastic storage modulus, and E'' is viscous loss modulus.

The complex modulus is given by;

$$E^* = \frac{\omega^2 z^2}{1+\omega^2 z^2} E + i \frac{\omega z}{1+\omega^2 z^2} E \tag{1.36}$$

where z is the relaxation time.

$$E^* = E' + iE'' \tag{1.37}$$

$$\tan\delta = \frac{E''}{E'} \tag{1.38}$$

1.3.2 Rheological four regions

Temperature dependence of viscoelastic behaviors is shown in Figure 1.8. In general, a polymer has four regions such as glassy region, transition region, rubbery region, and flow region from the low temperature.

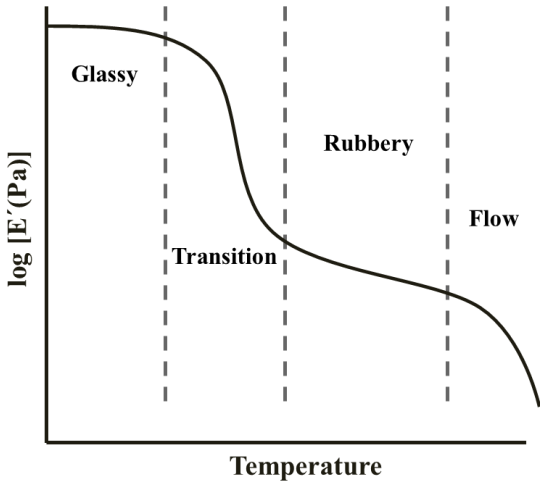

Figure 1.8 Four regions of an amorphous polymer

In the glassy region, Brownian motion is prohibited and only vibrations and short-range rotational motions are allowed. This region is observed in the low temperature range or high frequencies. Young's modulus is around 10^9-10^{10} Pa.

In the glass-to-rubber transition region, the Brownian motion starts to occur. The modulus is 10^6-10^{10} Pa and drops off greatly in a narrow temperature range. In this region, the glass transition temperature T_g is the important physical property, which can be defined as the peak temperature of loss modulus E''.

Beyond T_g, the modulus becomes almost a constant (10^5-10^6 Pa as a tensile modulus), known as the rubbery plateau modulus. In this region, Brownian motion is allowed between entanglement couplings. In other words, entanglement couplings act as crosslink points. The length of the plateau is dependent on the molecular weight. The molecular weight between entanglements M_e can be evaluated from the modulus at the rubbery plateau G_N^0 by the following equation using the classical rubber theory.

$$M_e = \frac{\rho RT}{G_N^0} \tag{1.39}$$

In the flow region, the relaxation time associated with entanglement couplings is shorter than the observation time. Consequently, a material shows viscous flow. Although elastic properties are still detected, viscosity is a dominant characteristic for mechanical behaviors of a polymer.

1.4 Elastomer Blend

Conventional unsaturated elastomers, e.g., natural rubber (NR), synthetic polybutadiene (BR), and poly(styrene-*co*-butadiene) rubber (SBR), are commercially important in the automotive tire manufactures. However, they are usually used in blends to satisfy the properties, e.g., chemical, physical, and processing benefits for each application [54-57].

Table 1.2 lists the important components of tire and the typical blends used for them. It is known that most rubber blends show phase-separated morphology because of their high molecular weight.

Table 1.2 Elastomer blends for automotive tires [58, 59]

	Passenger tires	**Truck tires**
Tread	SBR-BR	NR-BR or SBR-BR
Belt	NR	NR
Carcass	NR-SBR-BR	NR-BR
Sidewall	NR-BR or NR-SBR	NR-BR
Liner	NR-SBR-IIR	NR-IIR

IIR = isobutylene-isoprene rubber or butyl rubber

1.4.1 Distribution of third component in immiscible elastomer blend

Various compounds are added in rubber blends as a third component, including plasticizers, processing oil, antioxidants, and vulcanizing agents. Their distribution state dramatically influences properties of a final product as well as the processability.

Rubber compounds are mixed in the highly viscous state above their glass transition temperatures, in which additives may be distributed in one component or at the interface. Besides, the transfer phenomenon from one phase to another may occur during mixing and/or post-processing annealing. Therefore, it is significantly important for the material design to select an appropriate third component in each rubber blend.

1.4.2 Transfer of curatives

Sulfur is often used as a crosskinking agent especially for unsaturated rubbers, while peroxide system is used for saturated rubbers. Activators and accelerators are other kinds of ingredients to promote crosslinking without side reactions. The distribution of these

curatives is significantly important for rubber blends to control the mechanical properties. Curatives are initially located within a continuous phase at mixing. However, the difference in the miscility leads to the uneven distribution. Because most curatives are composed of polar molecules, they preferably reside in a polar rubber. When the distribution state after mixing is far from that in the equilibrium, the transfer through the interface may take place as demonstrated by a number of researchers [60-63].

1.4.2.1 Blooming

This is not a transfer from one rubber to another, but the diffusion from a rubber to outside. It occurs when the amount is beyond the critical volume at a given temperature. One example is the migration of sulfur to the surface, which is eventually crystallized [64]. Therefore, a patent to use specific sulfur in a particular compound was filed to eliminate blooming [65]. Mastromatteo et al. [66] reported that the use of accelerators with longer alkyl chains can provide non-blooming cure system for ethylene-propylene diene momomer (EPDM) and results in good physical properties of acrylonitrile-butadiene rubber (NBR) blend with EPDM.

1.4.2.2 Diffusion

When the solubility of curatives is limited, the diffusion occurs to be in the equilibrium condition. Gardiner [61, 62] showed that conventional curatives usually diffuse from less polar rubber to more polar one across the boundary of phases, which occurs very

quickly during both mixing and vulcanization procedures. He estimated the diffusion coefficient from the concentration changes as a function of distance and time. The diffusion coefficients of sulfur and accelerators from isobutylene-isoprene rubber or butyl rubber (IIR) to other rubbers are listed in Table 1.3.

Table 1.3 Interphase transfer of curatives in elastomer blends

Curatives	**From**	**To**	**Diffusion coefficient, D x 10^7 (cm^2/s)**
Accelerator (TDDC)	IIR	BR	12.66
		EPDM	1.09
		CR	1.08
		SBR	0.58
		NR	0.70
Sulfur	IIR	SBR	4.73
		SBR & 50PHR N700 CB	17.2
		NR	2.82

TDDC = Tellurium diehyldithiocarbamate
CR = Polychloroprene or chloroprene rubber
N700 CB = reinforcing type carbon black

In many cases in industry, co-vulcanization is required, e.g., a blend of EPDM and unsaturated rubbers, at which the curative distribution is a key technology to provide more uniform crosslinking. Grafting of accelerators onto EPDM prior to blending or addition of a long-chain dithiocarbamate are alternative ways to improve both co-crosslinking and compatibility [67].

The large difference in the solubility parameter leads to the rapid transfer of curatives at the vulcanization temperature. In order to prevent the lack of co-vulcanization in the

blends, the accelerators with the same difference in the solubility parameter with each rubber component should be added [68]. Attempts to determine the solubility parameters of sulfur and accelerators have been carried out for a long time [64, 68-71]. The solubilities of several curatives and rubbers are given in Figure 1.9.

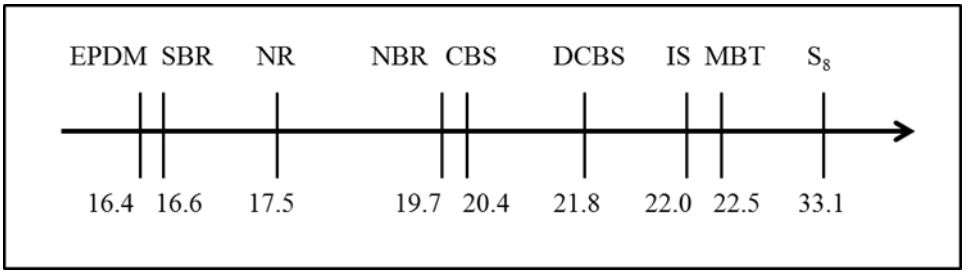

CBS = *N*-cyclohexylbenzothiazole-2-sulphenamide
DCBS = *N*-dicyclohexylbenzothiazole-2-sulphenamide
IS = insoluble sulfur
MBT = 2-mercaptobenzothiazole
S_8 = eight-membered ring sulfur or octasulfur

Figure 1.9 Solubility parameter $[(MPa)^{1/2}]$ of various rubbers and some curatives. [71]

Besides fillers and curatives, the transfer of other additives such as wax, antioxidant, antiozonant, processing oil, and plasticizer, also play an important role in the properties of a blend [10, 72-75]. In the rubber formulation, petroleum wax can cause the transfer and/or blooming, as similar to sulfur. The wax blooming is, however, used to protect a vulcanized rubber surface against ozone attack due to the carbon-carbon double bond (C=C) of elastomer chains. Lewis et al. [63] showed that antiozonants prefers to migrate from EPDM to SBR during curing. It has been reported that the extent of migration depends on not only solubility, but also mobility of wax. The latter is affected by rubber composition and the ozone exposure conditions, such as time and temperature [76, 77].

The primary role of oil and plasticizer is to increase flexibility of polymeric chains and to improve the rheological properties suitable for processing operations by lowering the glass transition temperature T_g and viscosity. Oil and plasticizer are dissolved into rubber with no chemically bonding and act as an internal lubricant. However, bleeding out may occur for these additives with poor miscibility.

In addition, the tackifier is another type of low-molecular-weight compounds with high softening point, which commonly enhances the adhesion of vulcanized rubbers. According to Basak et al. [78], good adhesion between the vulcanized and unvulcanized EPDM is improved by the addition of a tackifier, which can be explained by the "single side interdiffuion" concept. Doan *et al.* [79] found that the tackifier transfer occurs from BR to SBR due to the miscibility difference.

1.5 Characterization of Transfer Process

1.5.1 Diffusion theory

As well known, Einstein developed and established the theory of Brownian motion in 1905 [80, 81]. Diffusion of spherical particles is expressed by the following relation;

$$\left\langle \left|\Delta r(t)\right|^2 \right\rangle = 6D \tag{1.40}$$

$$D = k_B T b \tag{1.41}$$

where $\left\langle |\Delta r(t)|^2 \right\rangle$ is the mean-square displacement, D is the diffusion coefficient, k_B is the Boltzmann constant, b is the mobility constant of a particle or segment, and T is the absolute temperature.

Einstein also showed that the diffusion coefficient is inversely proportional to the friction coefficient ξ, known as the Nernst-Einstein relation.

$$D_r = \frac{k_B T}{\xi} \tag{1.42}$$

In the case of large particles, there is no tendency for the solution to slip at the surface of the spherical particle. The value of ξ can be obtained by the Stokes law as follows;

$$\xi = 6\pi\eta R \tag{1.43}$$

where R is the radius of particles and η is the viscosity of a medium.

By combining the Nernst-Einstein relation and the Stokes law, the following equation is given [82];

$$D_r = \frac{k_B T}{6\pi\eta R} \tag{1.44}$$

This equation is widely used to explain the diffusion of a spherical nanoparticles, whose radius is larger than the radius of gyration of a polymer chains [83-85].

The presence of a liquid fraction is significant importance for rheological and physical properties. During compounding, liquids may penetrate from one rubber to another acrossing the boundary of interphase, which is described by the Fick's law of diffusion. The diffusion process is characterized by a dimensionless parameter called the Deborah number

for diffusion D_b. This number is defined as a ratio of the characteristic time of a fluid λ_f to the characteristic time for the diffusion process θ_D [86].

$$D_b = \frac{\lambda_f}{\theta_D} \tag{1.45}$$

The diffusion of small molecules in a polymer or in a network of highly entangled chains is often observed at a temperature well above T_g, leading to the small value of Deborah number of diffusion. At this state, the diffusion process is classified into Fickian type based on the rate of diffusion. The Fick's first law says that the flow of molecules or mass flux J is proportional to the concentration gradient [87];

$$J = -D\frac{\partial c}{\partial x} \tag{1.46}$$

where D is the mass diffusion coefficient [$m^2\ s^{-1}$] and $\frac{\partial c}{\partial x}$ is the concentration gradient.

The Fick's second law expresses the time evolution of the concentration profile, which is obtained from the mass balance of a diffusing molecule in a unit volume [88];

$$\frac{\partial c}{\partial t} = D\frac{\partial^2 c}{\partial x^2} \tag{1.47}$$

$$\frac{\partial c}{\partial t} = \frac{\partial}{\partial c}\left(D\frac{\partial c}{\partial x}\right) \tag{1.48}$$

When the diffusion process occurs through a flat sheet of thickness l, whose surfaces are maintained at constant concentrations c_1 and c_2, the steady state is reached when the concentration in the sheet is constant;

$$\frac{\partial^2 c}{\partial x^2} = 0 \tag{1.49}$$

$$\frac{\partial c}{\partial x} = \text{constant} \tag{1.50}$$

By further integration at the conditions of x=0 and x=l, it can be written by;

$$c = \frac{c_2 - c_1}{l} x + c_1 \tag{1.51}$$

leading to

$$J = -D\frac{\partial c}{\partial x} = D\frac{c_1 - c_2}{l} \tag{1.52}$$

The diffusion coefficient in a polymer matrix with molecular weight of M is described by a power law [89].

$$D = KM^{-\alpha} \tag{1.53}$$

where K and α are constants.

The value of the exponent α was reported to be 2 [90, 91]. Moreover, the diffusion coefficient is a function of temperature, which is expressed by the Arrhenius equation.

$$D = D_0 \exp\left[-\frac{E_D}{RT}\right] \tag{1.54}$$

where D_0 is the pre-exponential factor and E_D is the activation energy of the diffusion. The experimental results revealed that E_D is given by the following equation;

$$E_D \approx d^2 \Delta E_v \tag{1.55}$$

where d is the diameter of a molecule and ΔE_v is the cohesive energy [92, 93];

The diffusion in a polymer is accelerated by sufficient free volume in the molten state [94, 95], because penetrant molecules can migrate only in a free space. Therefore, the diffusion is accelerated in a polymer with a number of chain ends, i.e., low molecular

weight. Moreover, the crystallinity and temperature are the factors influencing the diffusivity.

The diffusion occurs significantly slow below the glass transition temperature T_g [96, 97]. At this temperature, the free volume fraction, i.e., $V_f /(V_f + V_o)$, is believed to be 2.5%. Beyond T_g, the free volume fraction increases rapidly with temperature as illustrated in Figure 1.10.

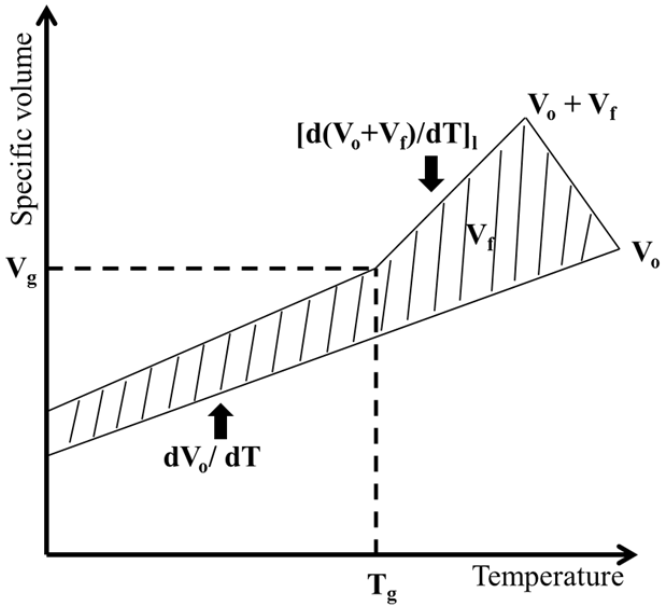

Figure 1.10 Temperature dependence of occupied volume (V_o) and free volume (V_f)

1.6 Objective of This Research

For a multi-component system, especially for an immiscible polymer blend, the addition of a low-molecular-weight compound as a third component is a significant importance to provide required properties of a final product. The distribution state of a third

component is generally determined by the miscibility between a third component and each polymer, which can be changed by ambient temperature.

The transfer phenomenon of a third component between dissimilar polymers can occur from one phase to another through the boundary of the phases. This will lead to the uneven distribution of this component in the blend, which depends upon the temperature. Previous researches on the transfer phenomenon were carried out at a fixed temperature, which is significantly different from my research.

The main objective of this research is to study "the temperature dependence of the distribution state of various types of liquid compounds in an immiscible polymer blend", as well as the interphase transfer phenomenon between immiscible polymers. The difference in the miscibility as a function of temperature will be discussed using solubility parameter and Flory-Huggins interaction parameter. It should be underlined that T_g is determined by a liquid concentration. Therefore, it is expected to control T_g of each phase when the amount of a liquid can change with ambient temperature.

At first, in the following Chapter 2, a plasticizer was introduced in a binary polyolefin elastomer blend, which is composed of ethylene-propylene copolymer and poly(isobutylene). The interphase transfer due to the difference in the temperature dependence of the Flory-Huggins interaction parameter is discussed. Then the transfer of a coumarone-indene tackifier between immiscible conventional rubbers, such as natural rubber and poly(isobutylene), was investigated in Chapter 3. In this chapter, the crystallization of NR is found to accelerate the tackifier transfer at low temperature. Furthermore, controlling transparency driven by the interphase transfer of a low-molecular-weight compound with

low refractive index between ethylene-vinyl acetate copolymer and poly(vinyl butyral) is discussed in Chapter 4. Finally, the details of this research are summarized in Chapter 5.

Through this research, a better understanding of the interphase transfer of a third component is expected. Furthermore, the uneven distribution of a third component in an immiscible blend can be precisely controlled by the ambient temperature. This would be applicable to the development of a high-performance immiscible polymeric materials.

References

1. Paul, D. R.; Newman, S., *Polymer Blends*. Academic Press: New York, 1978.
2. Robeson, L. M., *Polymer Engineering & Science* **1984,** *24* (8), 587-597.
3. Utracki, L. A., *Polymer Blends Handbook*. Springer Netherlands: Dordrecht, 2003.
4. Vaia, R. A.; Giannelis, E. P., *MRS Bulletin* **2001,** *26* (05), 394-401.
5. Cheremisinoff, N. P.; Cheremisinoff, P. N., *Elastomer Technology Handbook*. CRC Press: Florida, 1993.
6. De, S. K.; White, J. R., *Rubber Technologist's Handbook*. Rapra Technology Limited: 2001.
7. Findik, F.; Yilmaz, R.; Köksal, T., *Materials & Design* **2004,** *25* (4), 269-276.
8. Feng, W. I., A. I., *Journal of Materials Science* **2005,** *40* (11), 2883-2889.
9. Noriman, N. Z.; Ismail, H.; Rashid, A., *Polymer-Plastics Technology and Engineering* **2008,** *47* (10), 1016-1023.
10. Nakason, C.; Kaewsakul, W., *Journal of Applied Polymer Science* **2010,** *115* (1), 540-548.
11. Flory, P. J., *The Journal of Chemical Physics* **1942,** *10* (1), 51-61.
12. Huggins, M. L., *The Journal of Physical Chemistry* **1942,** *46* (1), 151-158.
13. Alfrey, T. S., W. J., *Science* **1980,** *208* (23), 813-818.
14. Kumar, C. R.; George, K. E.; Thomas, S., *Journal of Applied Polymer Science* **1996,** *61* (13), 2383-2396.
15. Schuster, R. H., *Macromolecular Symposia* **2002,** *189* (1), 59-81.
16. Tsou, A.; Waddell, W., *Kautschuk und Gummi Kunstoffe* **2002,** *55* (7/8), 382-387.

17. Rocha, T.; Rosca, C.; Ziegler, J.; Schuster, R., *Kautschuk Gummi Kunststoffe* **2005,** *58* (1-2), 22-22.

18. Scott, C. E.; Macosko, C. W., *Polymer* **1994,** *35* (25), 5422-5433.

19. Scott, C. E.; Macosko, C. W., *Polymer* **1995,** *36* (3), 461-470.

20. Jordhamo, G. M.; Manson, J. A.; Sperling, L. H., *Polymer Engineering & Science* **1986,** *26* (8), 517-524.

21. Gibbs, J. W., *Transactions of the Connecticut Academy of Arts and Sciences* **1873,** *2*, 382-404.

22. Flory, P. J., *The Journal of Chemical Physics* **1941,** *9* (8), 660-660.

23. Huggins, M. L., *Journal of the American Chemical Society* **1942,** *64* (7), 1712-1719.

24. Freeman, P. I.; Rowlinson, J. S., *Polymer* **1960,** *1*, 20-26.

25. Flory, P. J.; Orwoll, R. A.; Vrij, A., *Journal of the American Chemical Society* **1964,** *86* (17), 3507-3514.

26. Flory, P. J.; Orwoll, R. A.; Vrij, A., *Journal of the American Chemical Society* **1964,** *86* (17), 3515-3520.

27. Flory, P. J., *Journal of the American Chemical Society* **1965,** *87* (9), 1833-1838.

28. Eichinger, B. E.; Flory, P. J., *Transactions of the Faraday Society* **1968,** *64* (0), 2035-2052.

29. Eichinger, B. E.; Flory, P. J., *Transactions of the Faraday Society* **1968,** *64* (0), 2053-2060.

30. Eichinger, B. E.; Flory, P. J., *Transactions of the Faraday Society* **1968,** *64* (0), 2061-2065.

31. Eichinger, B. E.; Flory, P. J., *Transactions of the Faraday Society* **1968,** *64* (0), 2066-2072.

32. Prigogine, I.; Trappeniers, N.; Mathot, V., *Discussions of the Faraday Society* **1953,** *15* (0), 93-107.

33. Prigogine, I., *The Molecular Theory of Solutions*. North-Holland Publishing Company: New York, 1957.

34. Patterson, D., *Macromolecules* **1969,** *2* (6), 672-677.

35. Simha, R.; Havlik, A. J., *Journal of the American Chemical Society* **1964,** *86* (2), 197-204.

36. Bonner, D. C.; Bellemans, A.; Prausnitz, J. M., *Journal of Polymer Science Part C: Polymer Symposia* **1972,** *39* (1), 1-9.

37. Sanchez, I. C.; Lacombe, R. H., *The Journal of Physical Chemistry* **1976,** *80* (21), 2352-2362.

38. Panayiotou, C.; Sanchez, I. C., *Macromolecules* **1991,** *24* (23), 6231-6237.

39. L. J. Fetters; D . J. Lohse; D. Richter; T . A. Witten; Zirkelt, A., *Macromolecules* **1994,** *27* (17), 4639-3647.

40. Lohse, D. J.; Garner, R. T.; Graessley, W. W.; Krishnamoorti, R., *Rubber Chemistry and Technology* **1999,** *72* (4), 569-579.

41. Lewis J. Fetters; David J. Lohse; Scott T. Milner; Graessley, W. W., *Macromolecules* **1999,** *32* (20), 6847-6851.

42. Lohse, D. J., *Journal of Macromolecular Science, Part C: Polymer Reviews* **2005,** *45* (4), 289-308.

43. White, R. P.; Lipson, J. E. G.; Higgins, J. S., *Macromolecules* **2012,** *45* (2), 1076-1084.

44. White, R. P.; Lipson, J. E. G., *Macromolecules* **2014,** *47* (12), 3959-3968.

45. Scatchard, G., *Chemical Reviews* **1931,** *8* (2), 321-333.

46. Hildebrand, J. H.; Scott, R. L., *The Solubility of Nonelectrolytes*. Reinhold: New York, 1950.

47. Hildebrand, J. H., *Journal of the American Chemical Society* **1916,** *38* (8), 1452-1473.

48. Hansen, C. M., *Journal Paint Technology* **1967,** *39* (505), 104-117.

49. Small, P. A., *Journal of Applied Chemistry* **1953,** *3* (2), 71-80.

50. Van Krevelen, D. W., *Properties of Polymers: Their Correlation with Chemical Structure; their Numerical Estimation and Prediction from Additive Group Contributions*. Elsevier Science: Oxford, 2009.

51. Hoy, K. L., *Journal of Paint Technology* **1970,** *42* (541), 76-118.

52. Coleman, M. M.; Painter, P. C.; Graf, J. F., *Specific Interactions and the Miscibility of Polymer Blends*. CRC Press: Pensylvania, 1995.

53. Krishnamoorti, R.; Graessley, W. W.; Dee, G. T.; Walsh, D. J.; Fetters, L. J.; Lohse, D. J., *Macromolecules* **1996,** *29* (1), 367-376.

54. Coran, A. Y., *Rubber Chemistry and Technology* **1995,** *68* (3), 351-375.

55. Coran, A. Y., *Journal of Applied Polymer Science* **2003,** *87* (1), 24-30.

56. Ibrahim, A.; Dahlan, M., *Progress in Polymer Science* **1998,** *23* (4), 665-706.

57. Jones, A. J. T. K. P., *Blends of Natural Rubber: Novel Technique for Blending with Speciality Polymers*. Chapman & Hall: London, 1998.

58. Hess, W. M.; Herd, C. R.; Vegvari, P. C., *Rubber Chemistry and Technology* **1993,** *66* (3), 329-375.

59. Coran, A. Y.; Patel, R., *Rubber Chemistry and Technology* **1980,** *53* (1), 141-150.

60. Amerongen, G. J. v., *Rubber Chemistry and Technology* **1964,** *37* (5), 1065-1152.

61. Gardiner, J. B., *Rubber Chemistry and Technology* **1968,** *41* (5), 1312-1328.

62. Gardiner, J. B., *Rubber Chemistry and Technology* **1969,** *42* (4), 1058-1078.

63. Lewis, J. E.; Jr., M. L. D.; Whittington, L. E., *Rubber Chemistry and Technology* **1969,** *42* (3), 892-902.

64. Guo, R.; Talma, A. G.; Datta, R. N.; Dierkes, W. K.; Noordermeer, J. W. M., *European Polymer Journal* **2008,** *44* (11), 3890-3893.

65. Guillaumond, F.-X., *Rubber Chemistry and Technology* **1976,** *49* (1), 105-111.

66. Mastromatteo, R. P.; Mitchell, J. M.; Jr., T. J. B., *Rubber Chemistry and Technology* **1971,** *44* (4), 1065-1079.

67. Amidon, R. W.; Gencarelli, R. A. Long Chain Hydrocarbon Dithiocarbamate Accelerators and Method of Making Same. US3674824 A, 1972.

68. Brimblecombe, A.; Hendra, P.; Wallen, P.; Chapman, A.; Jackson, K.; Loadman, J.; Kip, B.; Hofstraat, J.; Schreurs, H., *Kautschuk Gummi Kunststoffe* **1996,** *49* (5), 354-356.

69. Morris, M.; Thomas, A., *Rubber Chemistry and Technology* **1995,** *68* (5), 794-803.

70. Guillaumond, F., *Rubber Chemistry and Technology* **1976,** *49* (1), 105-111.

71. Guo, R. Improved Properties of Dissimilar Rubber-Rubber Blends Using Plasma Polymer Encapsulated Curatives: A Novel Ssurface Modification Method to Improve Co-Vulcanization. University of Twente, 2009.

72. Lloyd, D. G., *Materials & Design* **1991,** *12* (3), 139-146.

73. Im, S.-H.; Choi, S.-S., *Elastomers and Composites* **2009,** *44* (4), 397-400.

74. Choi, S. S., *Journal of Applied Polymer Science* **1999,** *74* (13), 3130-3136.

75. Audic, J. L.; Reyx, D.; Brosse, J. C., *Journal of Applied Polymer Science* **2003,** *89* (5), 1291-1299.

76. Torregrosa-Coque, R.; Álvarez-García, S.; Martín-Martinez, J. M., *Journal of Adhesion Science and Technology* **2012,** *26* (6), 813-826.

77. Torregrosa-Coque, R.; Álvarez-García, S.; Martín-Martínez, J. M., *International Journal of Adhesion and Adhesives* **2011,** *31* (1), 20-28.

78. Basak, G. C.; Bandyopadhyay, A.; Bhowmick, A. K., *Journal of Materials Science* **2011,** *47* (7), 3166-3176.

79. Doan, V. A.; Nobukawa, S.; Ohtsubo, S.; Tada, T.; Yamaguchi, M., *Journal of Materials Science* **2012,** *48* (5), 2046-2052.

80. Einstein, A., *Annalen der Physik* **1905,** *322* (8), 549-560.

81. Einstein, A., *Investigations on the Theory of the Brownian Movement*. Dover Publications: New York, 1956.

82. Edward, J. T., *Journal of Chemical Education* **1970,** *47* (4), 261.

83. Mason, T. G.; Weitz, D. A., *Physical Review Letters* **1995,** *74* (7), 1250-1253.

84. Liu, J.; Cao, D.; Zhang, L., *The Journal of Physical Chemistry C* **2008,** *112* (17), 6653-6661.

85. Cai, L.-H.; Panyukov, S.; Rubinstein, M., *Macromolecules* **2011,** *44* (19), 7853-7863.

86. Vrentas, J. S.; Duda, J. L., *Journal of Polymer Science: Polymer Physics Edition* **1977,** *15* (3), 441-453.

87. Fick, A., *Annalen der Physik* **1855,** *170* (1), 59-86.

88. Fick, A., *Philosophical Magazine Series 4* **1855,** *10* (63), 30-39.

89. Van Amerongen, G. J., *Journal of Applied Physics* **1946,** *17* (11), 972-985.

90. Gent, A. N.; Liu, G. L., *Journal of Polymer Science Part B: Polymer Physics* **1991,** *29* (11), 1313-1319.

91. Ito, T.; Aizawa, K.; Seta, J., *Colloid and Polymer Science* **1991,** *269* (12), 1224-1240.

92. Meares, P., *Journal of Polymer Science* **1958,** *27* (115), 391-404.

93. Meares, P., *Journal of Polymer Science* **1958,** *27* (115), 405-418.

94. Lipatov, Y. S., *Physical Chemistry: Relaxation and Viscoelastic Properties of Heterogeneous Polymeric Compositions*. Springer Berlin Heidelberg: Berlin, 1977.

95. Nechitailo, V. S., *International Journal of Polymeric Materials and Polymeric Biomaterials* **1992,** *16* (1-4), 171-177.

96. Turnbull, D.; Cohen, M. H., *The Journal of Chemical Physics* **1961,** *34* (1), 120-125.

97. Lipatov, Y. U. S.; Privalko, V. P., *Journal of Macromolecular Science, Part B* **1973,** *7* (3), 431-444.

Chapter 2

Interphase Transfer of Plasticizer between Immiscible Rubbers

2.1 Introduction

For a polymer blend, a third component is often added to satisfy the properties required for commercial applications. In particular, a low-molecular-weight compound is usually employed as a third component, because it is dissolved into polymers due to the contribution of mixing entropy. In many cases, however, the amount of a third component in each phase is not equivalent, i.e., the uneven distribution, because the the miscibility of a third component with each polymer is different [1-5].

The Flory-Huggins interaction parameter decides the miscibility of blends. This parameter includes the contribution of the mixing enthalpy and the other factors except for the combinatorial entropy [6, 7]. In addition, it has been reported that the interaction parameter is dependent upon the temperature, which affects the phase diagram [8-10]. With respect to a blend, the interaction parameter between a low-molecular-weight compound and a polymer also depends on the ambient temperature.

This situation leads to the transfer of a third component from one phase to another favorable phase through the boundary of the phases. Several researchers reported the transfer

phenomenon of a third component, e.g., tackifier and curative for rubbers, using laminate sheets and/or blends of the immiscible polymer pairs [11-16]. In this chapter, the plasticizer transfer in an immiscible rubber blend is discussed. Amorphous polyolefins of ethylene-propylene copolymer (EPR) and polyisobutylene (PIB) were selected as an immiscible pair. Di-2-ethylhexyl adipate (DOA), known as a plasticizer, was employed as a third component because it can decrease T_g greatly. Since the interaction parameter between EPR and PIB has been studied and found to decrease with temperature [17, 18], the difference in the interaction parameter between DOA and each rubber could also change with the ambient temperature. This will lead to the T_g control of each rubber phase in the blend by the interphase transfer of DOA. This can be a novel material design of all-season tire. The matrix is expected to show low glass transition temperature T_g in winter and high T_g in summer season due to the change in the amount of the plasticizer content.

2.2 Experimental

2.2.1 Materials

Amorphous polyolefins such as ethylene-propylene rubber (EPR) with ethylene content 52 wt.% (JSR EP11, JSR, Japan) and polyisobutylene (PIB) (Sigma-Aldrich, USA) were used as an immiscible pair. As a third component, di-2-ethylhexyl adipate (DOA) (New Japan Chemical, Japan) was employed in this study. The average molecular weights of the rubbers were evaluated using a gel permeation chromatography (HLC 8020, Tosoh, Japan) with polystyrene standard as follows; M_n = 3.4 x 10^6 and M_w = 4.7 x 10^6 for EPR and M_n = 5.6 x 10^6 and M_w = 7.5 x 10^6 for PIB, respectively.

2.2.2 Sample preparation

A rubber and 10 phr of DOA were blended in a mixed solvent of dichloromethane and toluene in 8 to 2 weight ratio. After slowly evaporating the solvent at room temperature, the obtained mixture, i.e., rubbers with DOA, were compressed into flat sheets with 1 mm thickness using a compression-molding machine at 100 ^{o}C under 20 MPa. The EPR and PIB sheets, each containing 10 phr of DOA, were laminated together under an applied slight pressure by manual operation. Then annealing was carried out without pressure at -20 and 40 ^{o}C for 5 days. The experimental procedure for the interphase transfer experiment is illustrated in Figure 2.1. Furthermore, one set of the laminated samples annealed at 40 ^{o}C (or -20 ^{o}C) was further annealed at -20 ^{o}C (or 40 ^{o}C) to confirm the reversibility of the DOA transfer phenomenon. The separated sheets were kept at room temperature for 3 days to homogenize the DOA distribution in a sheet prior to the characterization.

Moreover, the rubber samples were crosslinked to predict the difference in the interaction parameter between EPR-DOA and PIB-DOA. In this case, the vulcanization was performed using 2 phr of *N-tert*-butyl-2-benzothiazole sulfonamide (Alfa Aesar, UK) and 2 phr of sulfur (Kanto Chemical, Japan) as an accelerator and curing agent for each rubber, respectively. Furthermore, 3 phr of zinc oxide (Kanto Chemical, Japan) was used together with 1.5 phr of stearic acid (Sigma Aldrich, USA) as an activator. They were mixed at 60 ^{o}C in an internal batch mixer (Labo-Plastomill, Toyoseiki, Japan) with a blade rotation speed of 40 rpm. The sample was cured at 170 ^{o}C using a laboratory hydraulic compression-molding machine under 20 MPa for 15 min and subsequently cooled at 15 ^{o}C for 10 min. The thickness of the film was 1 mm.

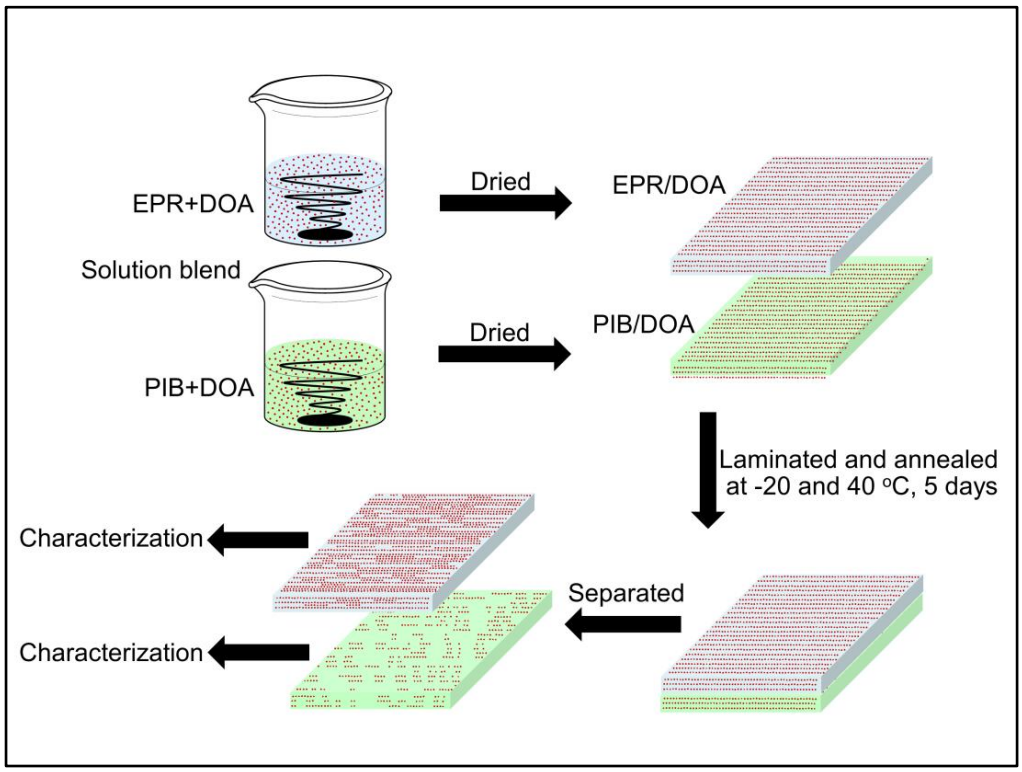

Figure 2.1 Schematic illustration of experimental procedure.

2.2.3 Measurements

The rectangular specimens with 5 mm in width and 20 mm in length were used. Start the temperature dependence of the dynamic tensile moduli was measured using a dynamic mechanical analyzer (DVE3, UBM, Japan). The sample was hated from -100 to 100 ^{o}C at a heating rate of 2 ^{o}C/min. The frequency was 10 Hz. In this research, the peak temperature in the tensile loss modulus E'' was defined as T_g.

Thermal properties were evaluated by a differential scanning calorimeter (DSC) (DSC 8500, Perkin Elmer, USA). Measurements were peformed from -100 to 25 ^{o}C at a heating rate of 10 ^{o}C/min.

Fourier–transform infrared spectroscopy (FT-IR) analyzer (Spectrum 100, Perkin Elmer, USA) was applied to determine the DOA content in each sheet using diamond as an ATR plate. The characteristic absorption peak at 1740 cm^{-1}, ascribed to the C=O=C stretching vibration mode, was utilized for the quantitative calculation of the DOA amount.

2.3 Results and Discussion

2.3.1 Role of plasticizer on the rubbers

The effect of the DOA addition on the dynamic tensile modulus is examined prior to the evaluation of the transfer phenomenon. The temperature dependence of tensile storage modulus E' and loss modulus E'' for pure rubbers and the rubbers with 10 phr of DOA were depicted in Figures 2.2 and 2.3. From the figures, the peak temperatures of E'', i.e., T_g, is found to shift to lower temperature by the addition of DOA for both EPR and PIB. The T_g shift for EPR is more pronounced than that for PIB, presumably due to higher T_g for EPR. The peak width is not much affected by the DOA addition, suggesting the narrow distribution of relaxation time, i.e., good miscibility. The rubbery plateau modulus slightly decreases by the DOA addition. This is reasonable because the entanglement density decreases.

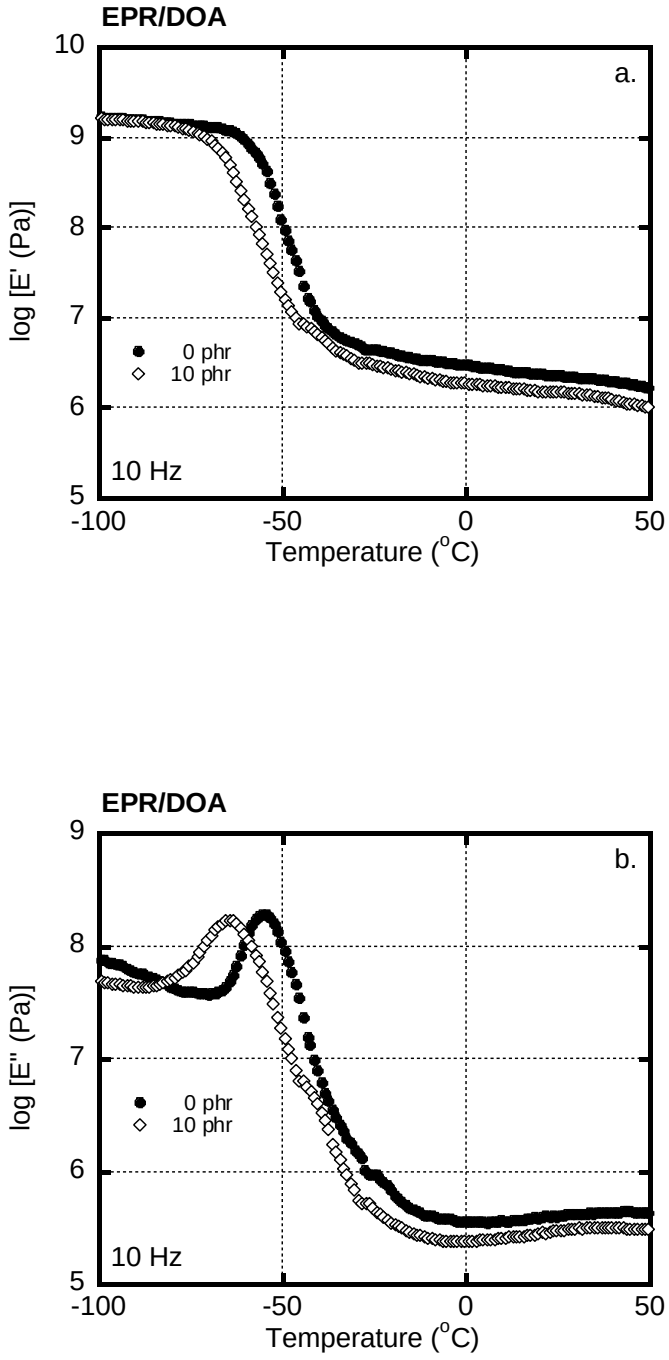

Figure 2.2 Temperature dependence of (a) storage modulus *E′* and (b) loss modulus *E″* for (closed circles) pure EPR and (open diamonds) EPR containing 10 phr of DOA.

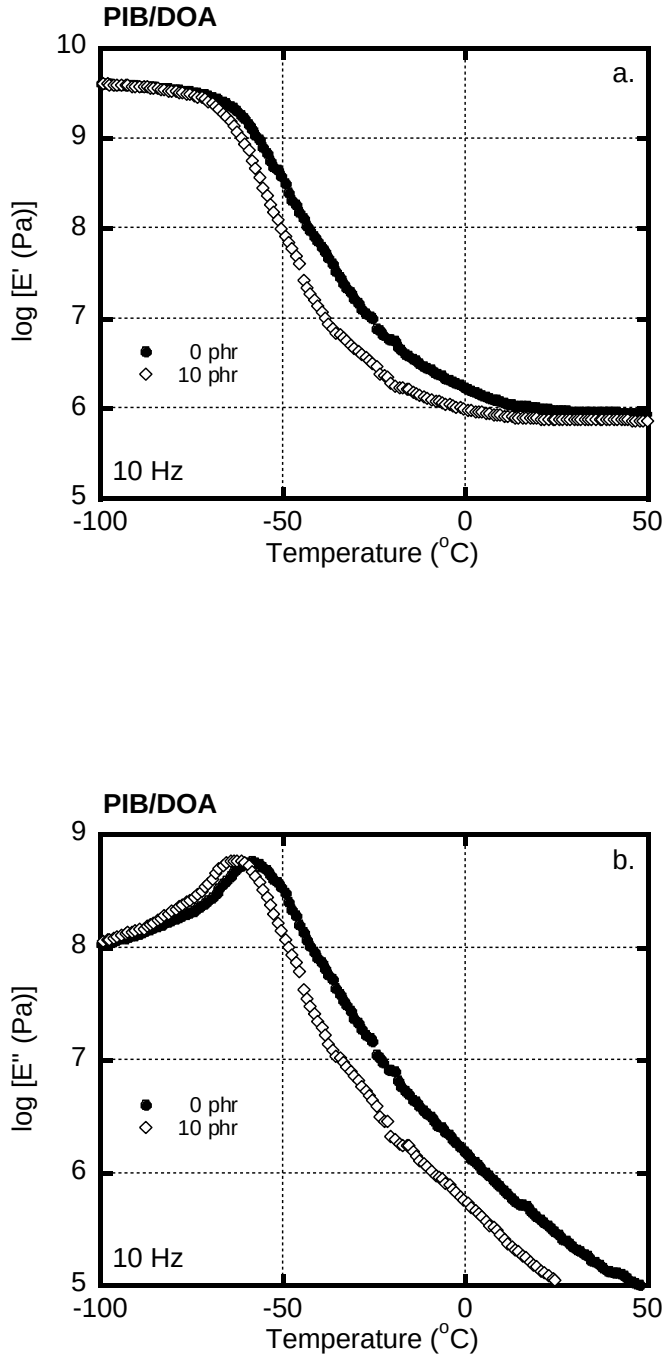

Figure 2.3 Temperature dependence of (a) storage modulus *E′* and (b) loss modulus *E″* for (closed circles) pure PIB and (open diamonds) PIB containing 10 phr of the DOA.

As mentioned, the peak intensity at 1740 cm^{-1} in the FT-IR spectra is employed to estimate the amount of DOA. This peak is ascribed to the carbonyl stretching vibration mode of DOA. The peak intensities of the EPR sheets containing various amounts of DOA were previously evaluated as shown in Figure 2.4. This peak is found to be a good candidate to estimate the DOA content, because (1) pure EPR does not show any absorbance and (2) good reproducibility with almost no experimental error. We did not normalize the absorbance peak. However, in this experiment, we can get a good calibration curve with almost no experimental error. The perfect contact with the ATR plate will be responsible for the reproducable measurements, as similar to the absorbance of a liquid compound. Regarding the concentration gradient, it can be ignored because the samples were kept for 3 days prior to the measurements to homogenize the DOA distribution in the sheet. Even if there could be the concentration gradient, the situation is the same with the measurements carried out to make a calibration curve.

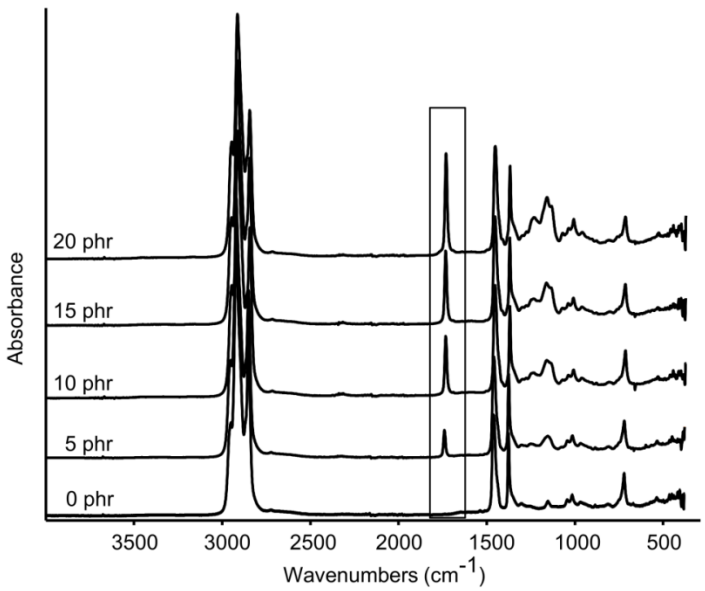

Figure 2.4 ATR-FT-IR spectra of EPR with various amounts of DOA.

2.3.2 Interphase transfer of the plasticizer

The annealing at the specific temperature, i.e., -20 and 40 °C for 5 days, was carried out using the laminate samples composed of EPR and PIB, in which each sheet contains 10 phr of DOA. A low-molecular-weight compound can diffuse in a rubber with 1 mm, i.e., the sheet thickness in 1 days, assuming that the diffusion constant is 10^{-11} m^2/s [19]. Hence, the distribution state of DOA is considered to be in the equilibrium owing to the long annealing period, i.e., 5 days. Furthermore, the laminate sheets can be easily separated each other after annealing, suggesting that the interfacial thickness λ is too thin to show a strong adhesion. This is because of a small number of the entanglement couplings at boundary of the rubbers, which is estimated from the following equation [20, 21].

$$\lambda = \frac{2b}{(6\chi)^{1/2}} \tag{2.1}$$

where λ is the interfacial thickness, χ is the polymer-polymer interaction parameter, and b is the statistical segment step length.

From the equation, the weak interfacial adhesion between EPR and PIB is also attributed to the immiscible nature among them. Although Krishnamoorti and Graessley reported that EPR and PIB exhibit the lower critical solution temperature (LCST) at approximately 25 ^oC [22], the high-molecular-weight of the rubbers used in this study provide the immiscibility. The interphase transfer of DOA between rubbers in the laminated sheets is evaluated by the characterization of the separated sheets after exposure to the annealing operation.

As mentioned, both rubber sheets contain 10 phr of DOA prior to the lamination at the specific temperature. The ATR spectra for the separated EPR/DOA sheets after annealing at different temperatures are expressed in Figure 2.5. Since the separated sheets were kept at room temperature for 3 days as similar to the sample sheets prepared for a calibration curve, the DOA distribution in the sheet must be homogeneous. From the figure, the annealing temperature greatly affects the peak intensity at 1740 cm^{-1}; a strong peak after annealing at -20 ^{o}C and a weak one at 40 ^{o}C.

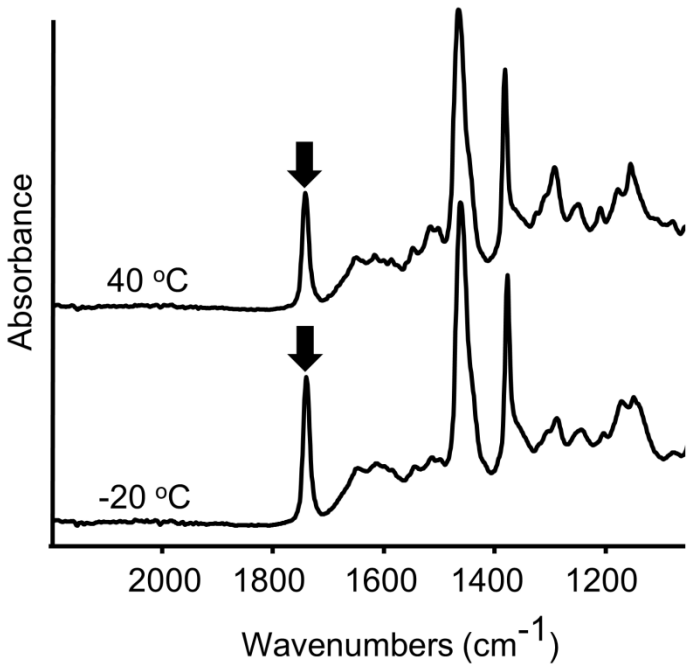

Figure 2.5 ATR-FT-IR spectra of the EPR sheets after annealing for 5 days at (bottom) -20 ^{o}C and (top) 40 ^{o}C

By the calibration curve of the EPR with DOA, the amount of DOA transfer during annealing was quantitatively estimated. Figure 2.6 shows that the absorbance is proportional to the weight percentage of DOA, in which the additional two dotted lines represent the absorbances of the EPR sheets after separation. From the results, 5.4 phr (5.2 wt.%) of DOA is calculated to transfer from PIB to EPR by the annealing procedure at -20 ^{o}C. The opposite direction is detected when the annealing was performed at 40 ^{o}C. It is found that 3.6 phr (3.5 wt.%) of DOA migrates from EPR to PIB. Moreover, the laminated samples were annealed again to observe the reversibility, e.g., -20 ^{o}C annealing after 40 ^{o}C annealing. It is found that the DOA amount is determined by the temperature at the final annealing procedure.

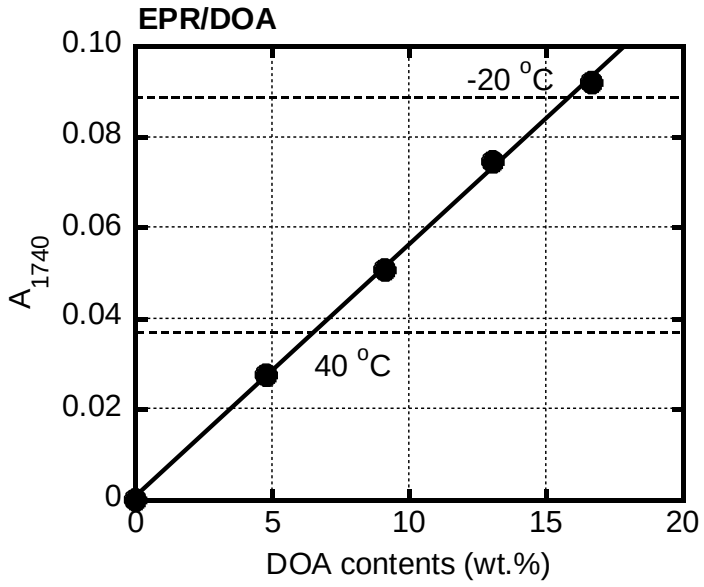

Figure 2.6 Absorbances at 1740 cm^{-1} for the EPR/DOA sheets containing various amounts of DOA. The absorbances after annealing are also indicated by the dotted lines.

As discussed above, the extent of DOA in each sheet is decided by the ambient temperature, i.e., annealing temperature. Therefore, T_g of each sheet after separation is affected by the annealing temperature. Figure 2.7 shows the temperature dependence of tensile loss modulus E'' of the separated sheets after annealing at -20 and 40 ^{o}C. At -20 ^{o}C annealing, T_g's of EPR and PIB shift to low and high temperatures, respectively, as compared with those of the original samples, i.e., the rubber containing 10 phr of DOA. It is reasonable because the DOA transfer occurs from PIB to EPR. In contrast, at 40 ^{o}C annealing temperature, the opposite transfer direction is detected, in which T_g of EPR shifts to higher temperature and vice versa. The results correspond with the FT-IR spectra.

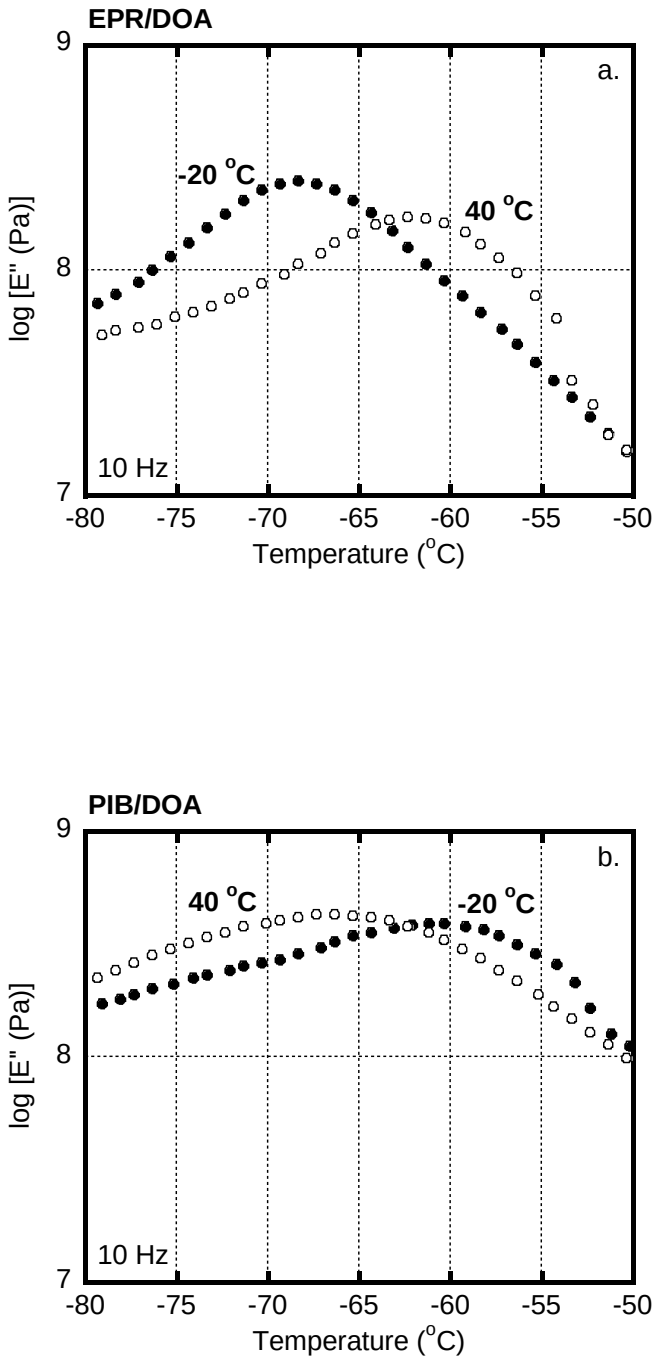

Figure 2.7 Temperature dependence of tensile loss modulus *E''* for the samples after annealing at (closed symbols) -20 °C and (open symbols) 40 °C; (a) EPR and (b) PIB.

2.3.3 The determination of the Flory-Huggins interaction parameter

The DOA transfer occurs by the difference in the Flory-Huggins interaction parameter, in which the initial concentration of DOA is 10 phr for both rubbers. Furthermore, the experimental results show that the interaction parameter must depend on the ambient temperature. The difference in the temperature dependence of the interaction parameter was estimated by the immersion experiments using crosslinked rubbers.

Prior to the swollen experiment, dynamic mechanical spectra were measured to confirm the vulcanization. It is found that T_g, i.e., the peak temperature of *E''*, is enhanced when the network structure is formed as shown in Figure 2.8. The tensile storage modulus *E'* for both crosslinked rubbers is slightly increased at high temperature due to the higher energy stored, as compared with those of the original samples without vulcanization as shown in Figure 2.9. Moreover, the peak absorption at 1520-1540 cm^{-1} in the FT-IR spectra is detected for both crosslinked EPR and PIB, which is ascribed to the bond formation of carbon-sulfur on the chain as shown in Figure 2.10.

At first, the crosslinked rubber films were immersed in toluene at 25 ^{o}C to evaluate the crosslink density. It is well known that the swell ratio is determined by the crosslink density together with the interaction parameter. According to the theory proposed by Flory and Rehner [23], it can be described as follows;

$$v^* = -\frac{\ln\left(1-q^{-1}\right)+q^{-1}+\chi q^{-2}}{V\left(q^{-1/3}-0.5q^{-1}\right)} \qquad (2.2)$$

where q is the swell ratio, v^* is the network chain density, and V is the partial molar volume of the solvent.

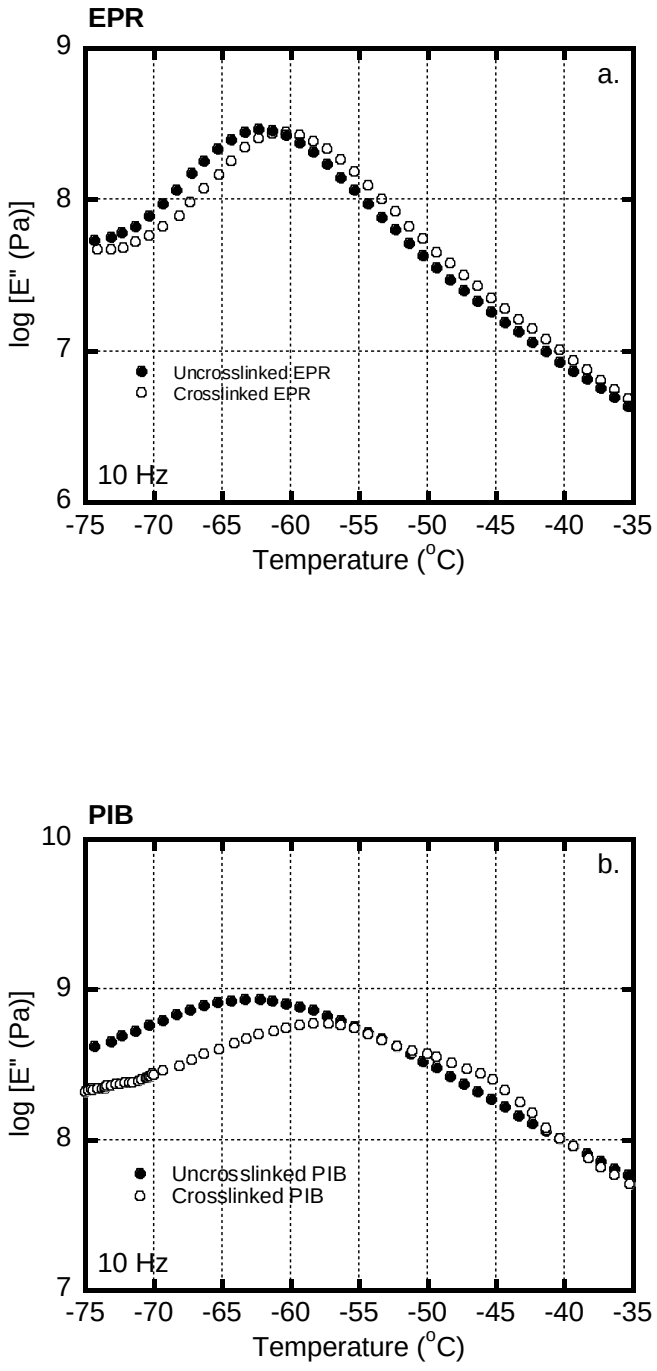

Figure 2.8 Temperature dependence of tensile loss modulus *E''* for the (closed symbols) uncrosslinked samples and (open symbols) crosslinked samples; (a) EPR and (b) PIB.

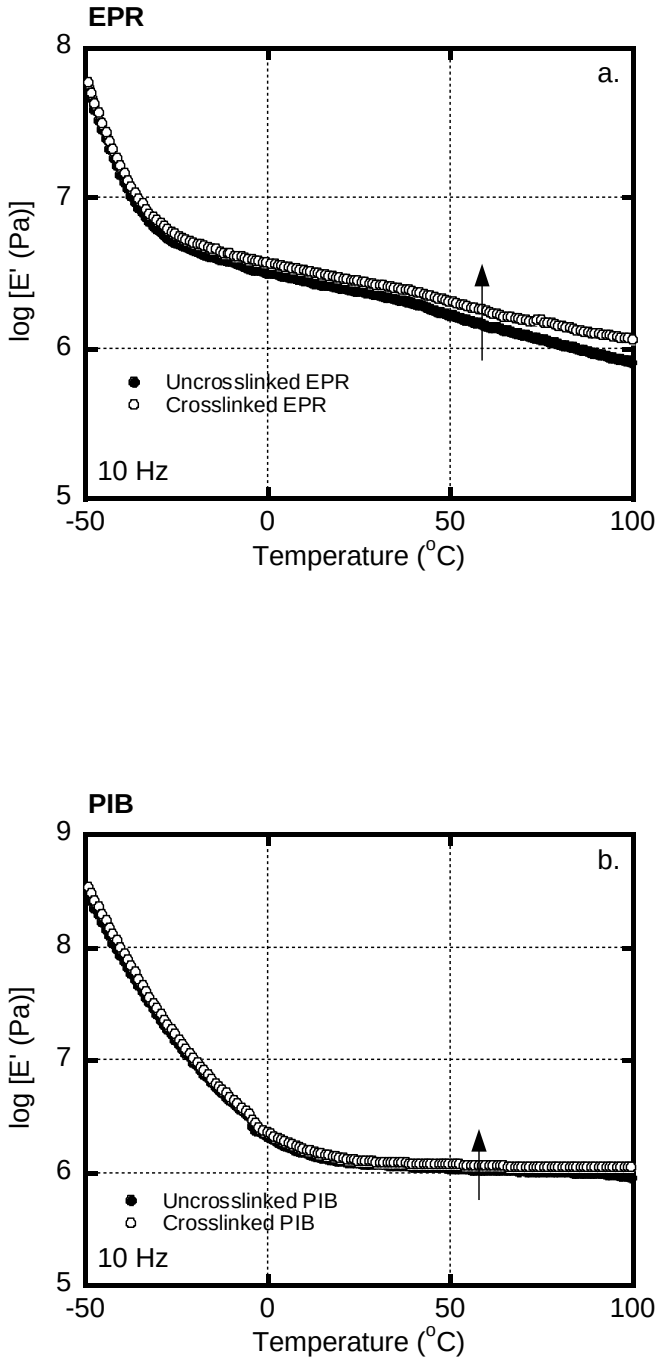

Figure 2.9 Temperature dependence of tensile loss modulus *E'* for the (closed symbols) uncrosslinked samples and (open symbols) crosslinked samples; (a) EPR and (b) PIB.

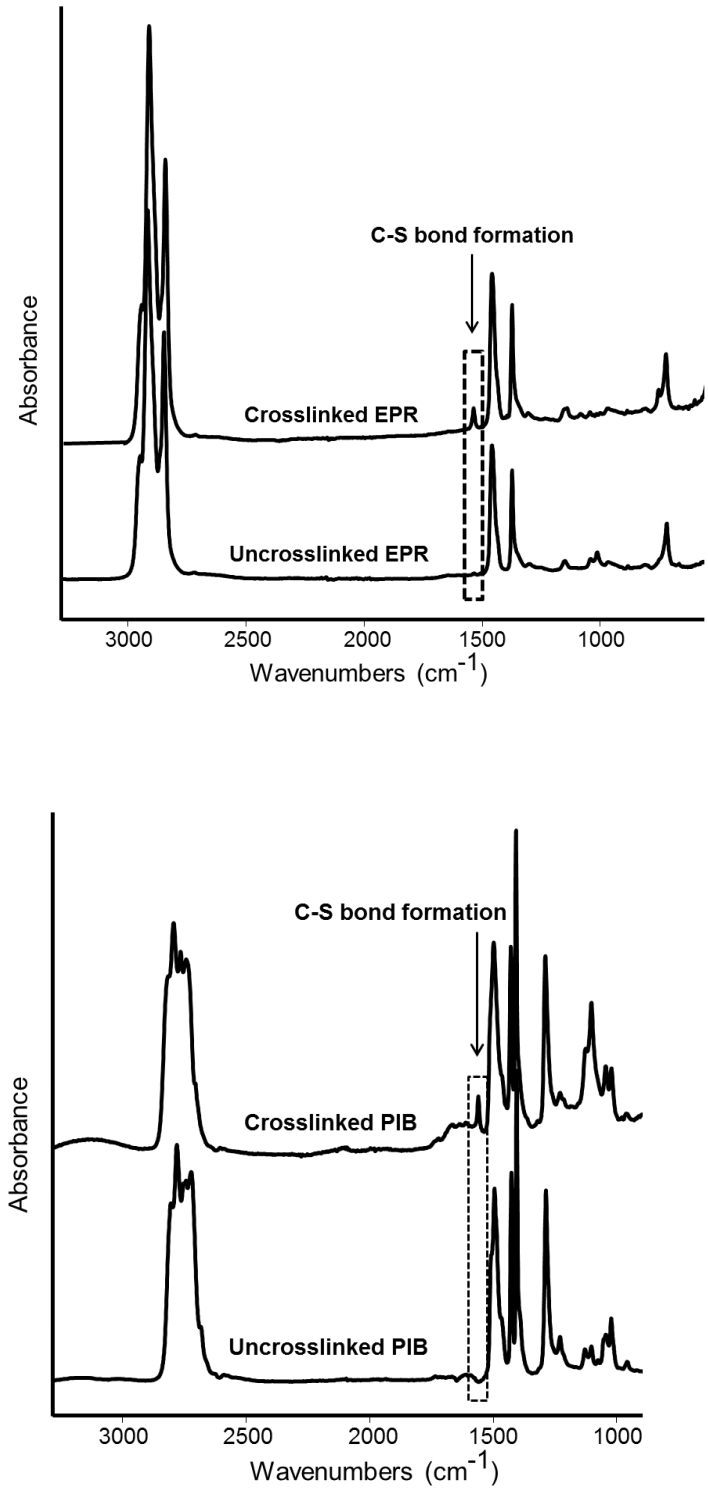

Figure 2.10 ATR-FT-IR spectra of the uncrosslinked and crosslink samples for (top) EPR and (bottom) PIB using sulfur as curing agent

The obtained interaction parameter between each crosslinked rubber and toluene at room temperature was applied to evaluate the crosslink density, i.e., 0.49 for EPR-toluene and 0.557 for PIB-toluene [23, 24]. Therefore, the crosslink densities can be calculated as follows; 6.3 x 10^{-11} [mol/m^3] for EPR and 2.0 x 10^{-11} [mol/m^3] for PIB.

Furthermore, they were immersed in DOA at -20 or 40 ^oC for 5 days, to measure the the weight of the swellen gel W_s. Then they were dipped in ethanol several times to remove the DOA excess perfectly. After drying in a vacuum oven, the dried samples were measured the weight of the dry gel W_d. The swell ratio q was defined by the following equation.

$$q = \frac{W_s}{W_d} \tag{2.3}$$

The swell ratios of the crosslinked rubbers after 5 days immersion in DOA at various temperatures, i.e., -20 ^oC, room temperature, and 40 ^oC, were measured. The temperature effect on the swelling behavior of the swollen samples after immersion is shown in Figure 2.11. It is obviously seen that the swollen samples for both crossilnked EPR and PIB are larger than that of the original dried sample, i.e., the crosslinked samples without immersion. Moreover, the swollen PIB is obviously larger than the swollen EPR after immersion at 40 ^oC due to the more preferable state of DOA to PIB. The results indicated that the swell ratio is affected by the temperature, i.e., -20 and 40 ^oC, which correspond to the results of the laminate system. The gel fraction and swell ratio values of the crosslinked rubber in DOA at various temperatures are listed in Table 2.1.

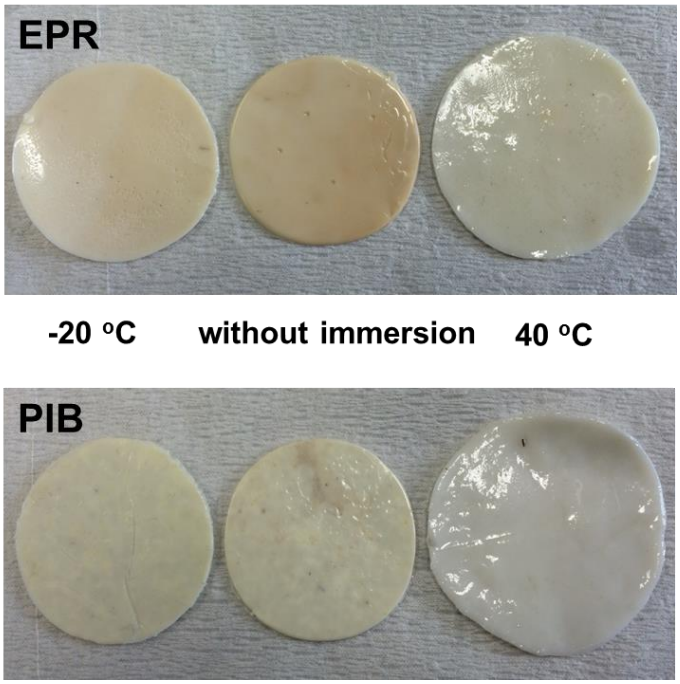

Figure 2.11 Photographs of the swollen crosslinked samples with/without immersion in DOA at various temperatures; (upper) EPR and (lower) PIB.

Table 2.1 The gel fraction and swell ration of the crosslinked rubbers in DOA

Temperature (^{o}C)	**Gel fraction**	**Swell ratio *q***
Crosslinked EPR		
-20	1.017	1.349
25	1.080	1.457
40	1.228	1.478
Crosslinked PIB		
-20	1.056	1.046
25	1.092	1.508
40	1.222	1.694

The interaction parameter between DOA and each rubber at various temperatures of immersion can be theoretically calculated from the obtained crosslink density as expressed in Figure 2.12.

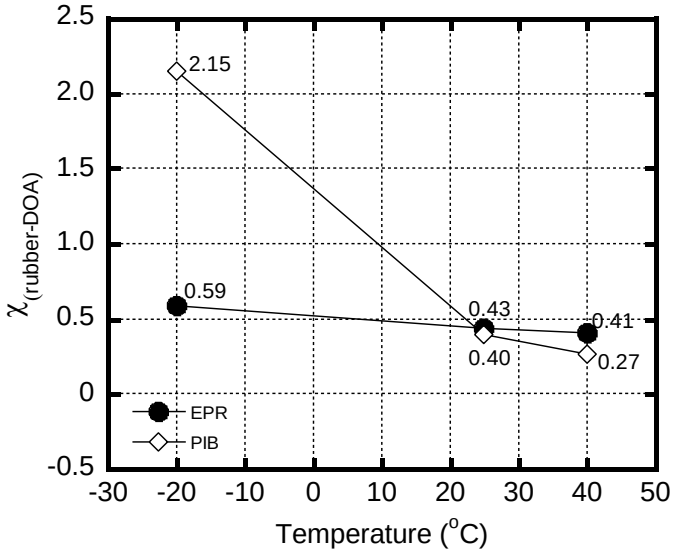

Figure 2.12 Temperature dependence of the Flory-Huggins interaction parameter between rubber and DOA; (closed circles) EPR and (open diamonds) PIB.

From the figure, the interaction parameter between DOA and EPR is smaller than that between DOA and PIB at -20 ^{o}C and vice versa at 40 ^{o}C. The results agree with the DOA transfer phenomenon observed in the laminated sheets.

2.4 Conclusion

The temperature dependence of the interaction parameter between a rubber and a plasticizer in an immiscible blend is found to be a driving force for the plasticizer transfer through the phase boundary, which is a function of ambient temperature. In this study, DOA is mixed in a rubber such as EPR and PIB. It is revealed that more DOA resides in EPR at -20 ^{o}C and vice versa at 40 ^{o}C. The DOA amount qualitatively corresponds with the difference in the interaction parameter, which is evaluated by the swollen experiment based on the Flory-Rhener theory.

The transfer is also expected even in the sea-island structure of the EPR/PIB blend. When the EPR is a matrix phase, the blend shows an interesting property needed for all-season tire, because T_g of the matrix is low at low temperature, i.e., winter, and high in summer season.

References

1. Sumita, M.; Sakata, K.; Hayakawa, Y.; Asai, S.; Miyasaka, K.; Tanemura, M., *Colloid and Polymer Science* **1992,** *270* (2), 134-139.
2. Moussaif, N.; Jérôme, R., *Polymer* **1999,** *40* (14), 3919-3932.
3. Sunil Jose, T.; Anoop Anand, K.; Joseph, R., *International Journal of Polymeric Materials* **2010,** *59* (7), 488-497.
4. Das, A.; Mahaling, R. N.; Stöckelhuber, K. W.; Heinrich, G., *Composites Science and Technology* **2011,** *71* (3), 276-281.
5. Göldel, A.; Marmur, A.; Kasaliwal, G. R.; Pötschke, P.; Heinrich, G., *Macromolecules* **2011,** *44* (15), 6094-6102.
6. Flory, P. J., *The Journal of Chemical Physics* **1942,** *10* (1), 51-61.
7. Huggins, M. L., *The Journal of Physical Chemistry* **1942,** *46* (1), 151-158.
8. Graessley, W. W.; Krishnamoorti, R.; Reichart, G. C.; Balsara, N. P.; Fetters, L. J.; Lohse, D. J., *Macromolecules* **1995,** *28* (4), 1260-1270.
9. Tambasco, M.; Lipson, J.; Higgins, J. S., *Macromolecules* **2006,** *39* (14), 4860-4868.
10. Nedoma, A. J.; Robertson, M. L.; Wanakule, N. S.; Balsara, N. P., *Industrial & Engineering Chemistry Research* **2008,** *47* (10), 3551-3553.
11. Gardiner, J. B., *Rubber Chemistry and Technology* **1968,** *41* (5), 1312-1328.
12. Zaikin, A.; Zharinova, E.; Bikmullin, R., *Polymer Science Series A* **2007,** *49* (3), 328-336.
13. Yoon, H.; Okamoto, K.; Yamaguchi, M., *Carbon* **2009,** *47* (12), 2840-2846.
14. Im, S.-H.; Choi, S.-S., *Elastomers and Composites* **2009,** *44* (4), 397-400.

15. Le, H. H.; Ilisch, S.; Heidenreich, D.; Wutzler, A.; Radusch, H.-J., *Polymer Composites* **2010,** *31* (10), 1701-1711.

16. Doan, V. A.; Nobukawa, S.; Ohtsubo, S.; Tada, T.; Yamaguchi, M., *Journal of Materials Science* **2012,** *48* (5), 2046-2052.

17. Freed, K. F.; Dudowicz, J., *Macromolecules* **1996,** *29* (2), 625-636.

18. White, R. P.; Lipson, J. E.; Higgins, J. S., *Macromolecules* **2012,** *45* (21), 8861-8871.

19. Tadmor, Z.; Gogos, C. G., *Principles of polymer processing*. John Wiley & Sons: New Jersey, 1979.

20. Helfand, E.; Tagami, Y., *Journal of Polymer Science Part B: Polymer Letters* **1971,** *9* (10), 741-746.

21. Helfand, E.; Tagami, Y., *The Journal of Chemical Physics* **1972,** *56* (7), 3592-3601.

22. R. Krishnamoorti; W. W. Graessley; L. J. Fetters; R. T. Garner; Lohse, D. J., *Macromolecules* **1995,** *28*, 1252-1259.

23. Treloar, L. R. G., *The physics of rubber elasticity*. Oxford University Press: New York, 1975.

24. Dudek, T.; Bueche, F., *Journal of Polymer Science Part A: General Papers* **1964,** *2* (2), 811-822.

Chapter 3

Interphase Transfer of Tackifier between Immiscible Rubbers

3.1 Introduction

As explained in detail in the previous chapter, such a third component is not distributed homogeneously in general. Therefore, the possible uneven distribution of a third component in a phase-separated polymer blend should be investigated greatly. This is critically important to enhance properties of a final products [1-4]. The distribution state of a low-molecular-weight compound in an immiscible polymer blend is generally determined by the interaction parameter between the components [5-7] as demonstrated in the previous chapter. Besides oil and plasticizer, a tackifier is also an important component for rubber compounds.

A tackifier is a fundamentally low-molecular-weight “glue” substance that generally adds an elastomer compound to provide the tackiness between layers during processing operation. There have been classified into three types; hydrocarbons, petroleum, and phenolic resins. A tackifier is primarily applied in pressure-sensitive-adhesives (PSAs) materials, in which a strong adhesion is developed at low pressure and short contact times [8-10].

In this study, the tackifier content in each phase of an immiscible rubber blend is focused. In particular, the effect of the ambient temperature is examined in order to control the viscoelastic properties, including the glass transition temperature.

3.2 Experimental

3.2.1 Materials

In this study, natural rubber NR (TSR) and poly(isobutylene) PIB were used. PIB was purchased from Sigma Aldrich Corp., USA. A coumarone-indene random copolymer (Nitto Chemical Industry Co., Ltd., Nitto resin L-5, Japan) was employed as a tackifier. The chemical structures of coumarone and indene are shown in Figure 3.1. The tackifier is in the liquid state at room temperature. The viscosity at 23 ^{o}C was 0.5 Pa s. The average molecular weights were measured by gel permeation chromatography (Tosoh Corp., HLC-8020, Japan) using chloroform as a solvent, which are summarized in Table 3.1, with their glass transition temperatures, T_g, evaluated by a differential scanning calorimeter at a heating rate of 10 ^{o}C/min.

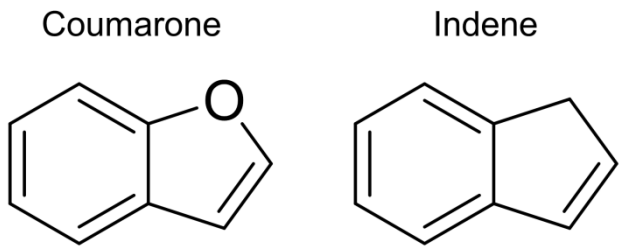

Figure 3.1 Chemical structures of coumarone and indene.

Table 3.1 Characteristics of the materials

Materials	T_g (°C)[a]	M_n[b]	M_w[b]	M_w/M_n
NR	-59.6	7.8×10^6	2.3×10^7	2.9
PIB	-57.3	5.6×10^6	7.5×10^6	1.3
Tackifer	-25.8	660	810	1.2

[a]Evaluated by DSC at 10 °C/min
[b]Polystyrene standard

3.2.2 Sample preparation

One of the rubbers and various amounts of the tackifier were put into a mixed solvent of dichoromethane and toluene (80 wt.% / 20 wt.%) at room temperature. The solution was poured onto a PTFE plate and exposed to the atmosphere to evaporate the solvent. After drying, the obtained blends, were compressed into flat sheets with 1 mm thickness using a compression-molding machine at 100 °C under 20 MPa.

One NR sheet and one PIB sheet, each containing 10 phr of the tackifier, were laminated together. After making a complete contact of two sheets under an applied slight pressure by manual operation, the laminated samples were annealed without pressure at -20 °C or 40 °C for 5 days, which was originally developed for the filler transfer experiments [11-14].

3.2.3 Measurements

The temperature dependence of storage modulus *E′* and loss modulus *E″* was measured by a dynamic mechanical analyzer (UBM Co., Ltd., DVE4, Japan) using a rectangular specimen (5 mm in width and 20 mm in length). The sample was heated from -100 to 100 ^{o}C at a heating rate of 2 ^{o}C/min. The frequency applied was 10 Hz.

Thermal properties were evaluated by a differential scanning calorimeter (DSC) (PerkinElmer Inc., DSC 8500, USA). After cooling to -100 ^{o}C, the samples were heated at a rate of 10 ^{o}C/min.

Fourier–transform infrared spectroscopy (FT-IR) analyzer (PerkinElmer Inc., Spectrum 100, USA) was used to evaluate the amount of the tackifier. The film was perfectly attached to the ATR plate made of diamond, and measured its ATR spectra. The absorbance at 750 cm^{-1}, which is ascribed to the C-O-C stretching [15], was employed to determine the tackifier content. For the purpose, the calibration curve was prepared using NR sheets containing 0, 5, 10, and 15 phr of the tackifier.

3.3 Results and Discussion

3.3.1 Characteristics of rubbers containing tackifier

Prior to the transfer experiments, the dynamic mechanical properties of a rubber with the tackifier were studied. Figures 3.2 and 3.3 show the temperature dependence of the dynamic tensile moduli for the pure rubbers and the rubbers containing 10 phr of the

tackifier. The samples were cooled down from room temperature to -120 ^{o}C before the measurement. It is found that the peak temperature of *E''*, i.e., T_g, is shifted to higher temperature by mixing the tackifier for both rubbers. T_g's of pure rubbers are -73.3 ^{o}C for NR and -64.3 ^{o}C for PIB, while those of the rubbers containing 10 phr of the takifier are -64.3 ^{o}C for NR and -62.3 ^{o}C for PIB. It should be noted that there is no peak in the *E''* curve that could be due to T_g of the pure tackifier. These results demonstrate that the tackifier is miscible with each rubber. In fact, the sample sheets containing the tackifier are transparent, i.e., no light scattering that could be ascribed to the tackifier dispersion as a different phase. Irrespective of the blend ratio, the miscibility is detected. Therefore, at least 15 phr of the tackifier is dissolved into each rubber.

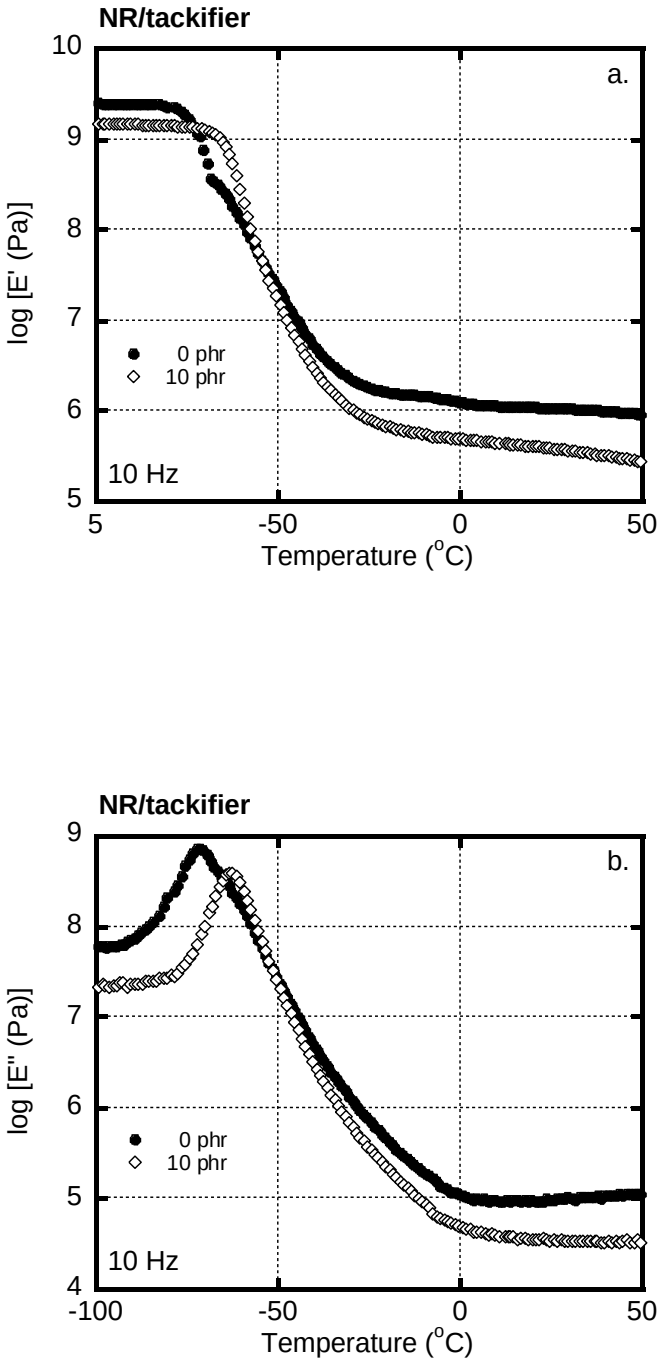

Figure 3.2 Temperature dependence of the (a) storage modulus *E'* and (b) loss modulus *E''*, for (closed circles) pure NR and (open diamonds) NR containing 10 phr of the tackifier.

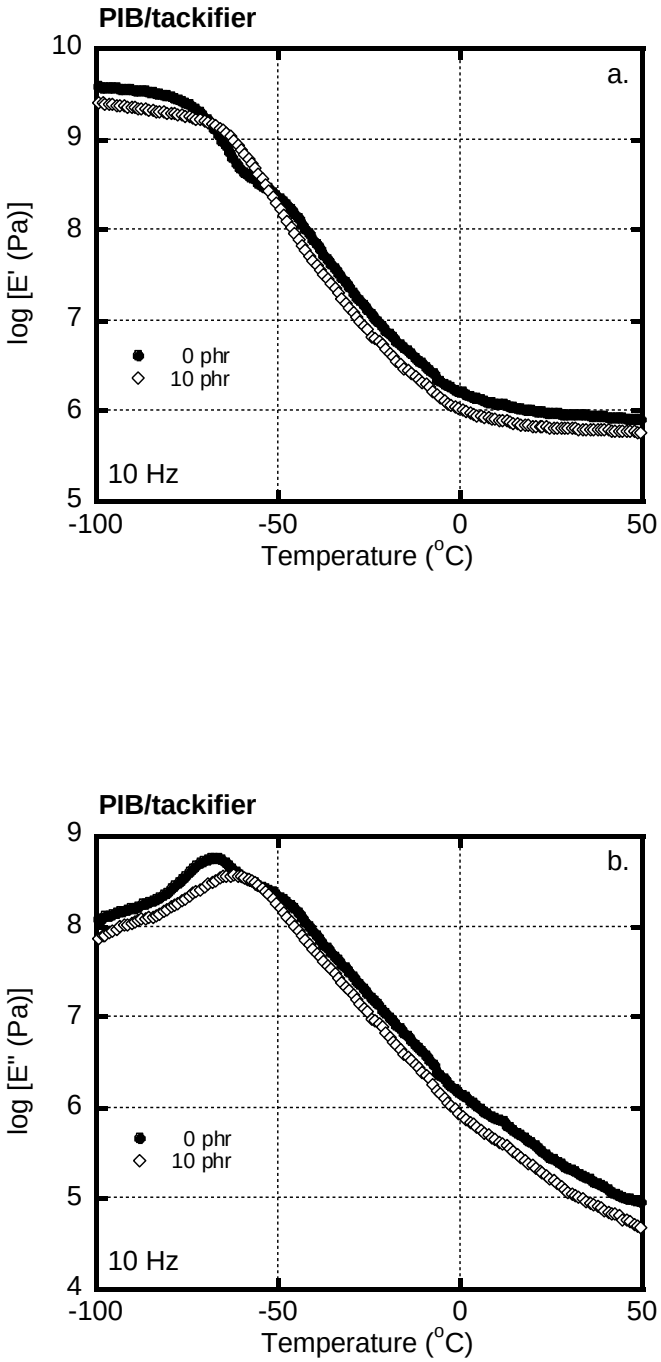

Figure 3.3 Temperature dependence of the (a) storage modulus *E'* and (b) loss modulus *E''*, for (closed circles) pure PIB and (open diamonds) PIB containing 10 phr of the tackifier.

The ATR spectra for the NR sheets containing various amounts of the tackifier are shown in Figure 3.4. In the figure, the peak absorption at 750 cm^{-1} (arrow) refers to the stretching vibration of C-O-C of the coumarone component in the tackifier, which is not detected in the pure NR. It is obviously seen that the peak absorbances increase with increasing the tackifier content. A straight line is obtained when the 750 cm^{-1} peak intensities are plotted against the weight ratio of the tackifier in Figure 3.5. This will be used as a calibration curve to evaluate the amount of the tackifier in the separated NR sheets after annealing. Moreover, the addition of 10 phr of the tackifier into the PIB also affects the peak absorption at 750 cm^{-1} as shown in Figure 3.6.

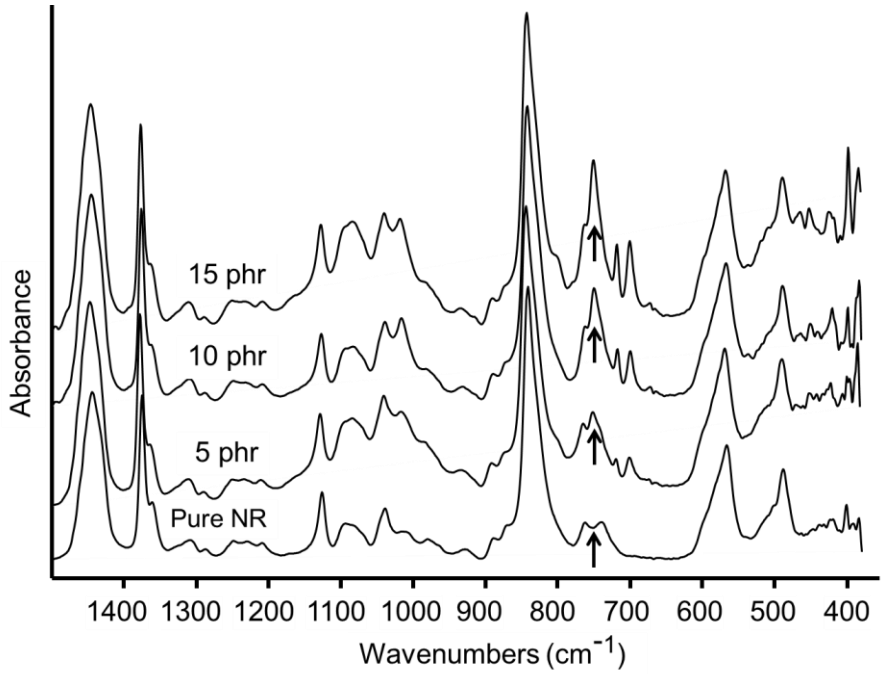

Figure 3.4 ATR-FT-IR spectra of NR with various amounts of the tackifier.

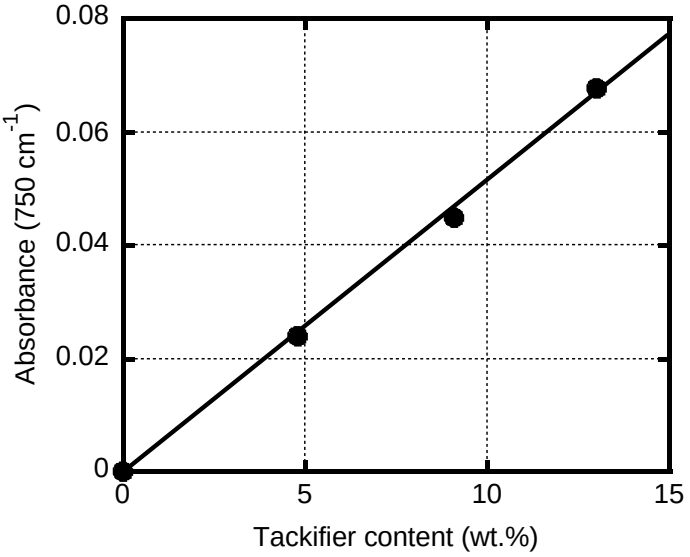

Figure 3.5 Absorbances at 750 cm^{-1} for NR containing various amounts of the tackifier.

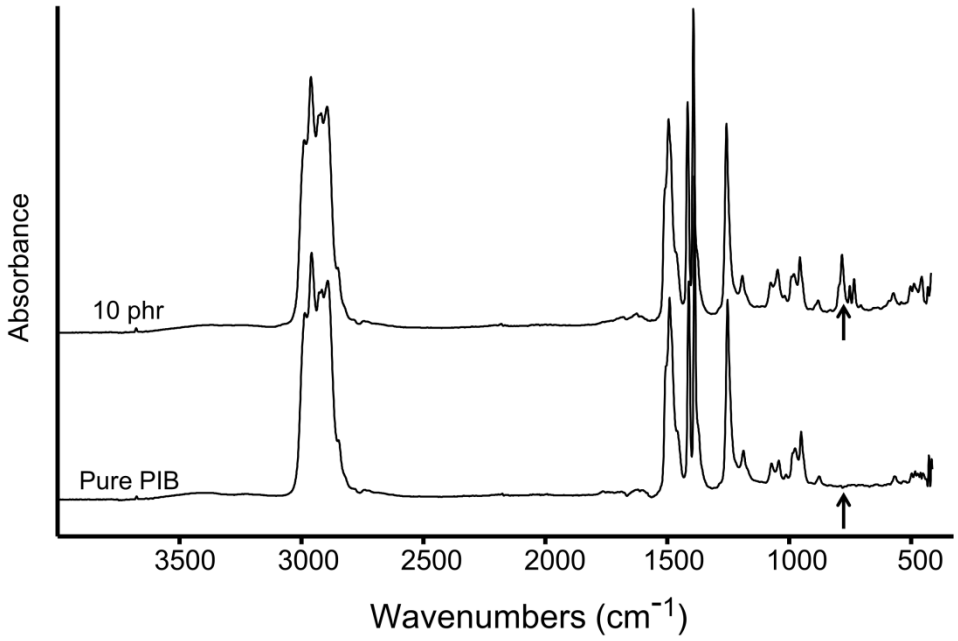

Figure 3.6 ATR-FT-IR spectra of the pure PIB and PIB containing 10 phr of the tackifier.

3.3.2 Interphase transfer of the tackifier

The ATR spectra of the separated NR sheets, which were originally mixed with 10 phr of the tackifier, after exposure to the annealing procedure at -20 ^{o}C or 40 ^{o}C are measured as shown in Figure 3.7. It is revealed that the peak intensity at 750 cm^{-1} is affected by the annealing temperature; a strong peak after annealing at 40 ^{o}C and a weak one after annealing at -20 ^{o}C. From the results, it can be explained that some amounts of the tackifier are migrated from NR to PIB at -20 ^{o}C, whereas the tackifier transfers to NR when annealing at 40 ^{o}C.

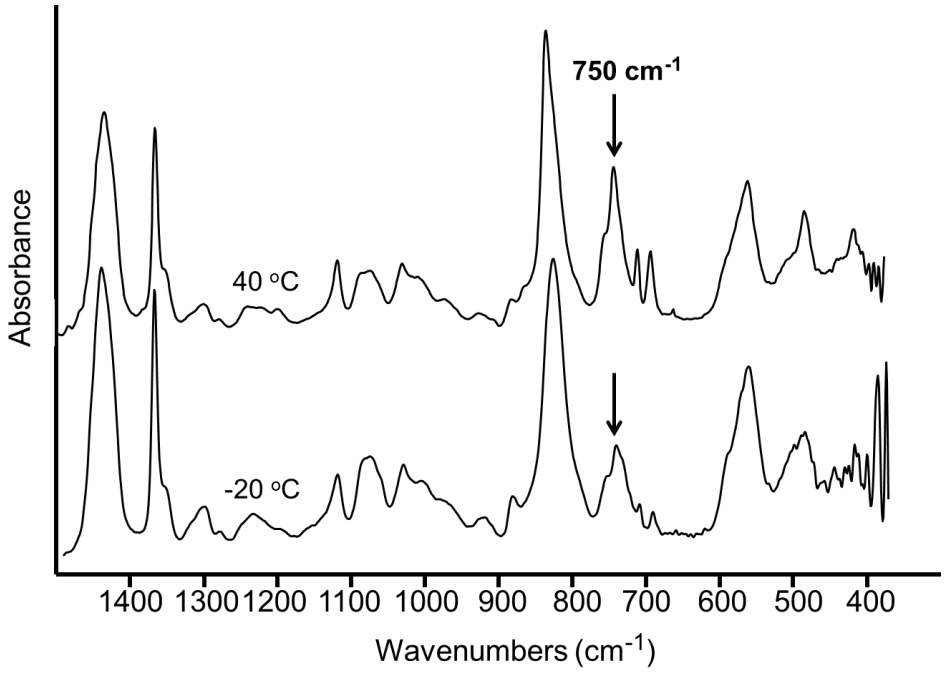

Figure 3.7 ATR-FT-IR spectra of the NR sheets after annealing for 5 days at (bottom) -20 ^{o}C and (top) 40 ^{o}C

The amount of the tackifier transfer in the separated NR sheets is estimated based on the calibration curve obtained from the FT-IR measurements. From the results, 2.1 phr of the tackifier transfers from NR to PIB during annealing at -20 ^{o}C. In other words, NR contains 7.9 phr of the tackifier while PIB has 12.1 phr at this temperature. In contrast, at 40 ^{o}C, the transfer in the opposite direction is detected, in which 2.0 phr of the tackifier moves from PIB to NR.

The distribution state of the tackifier in this experiments is assumed to be in the equilibrium condition because the peak intensity of the separated sheets after exposure to the annealing procedure for 10 days is similar to the results in Figure 3.7, i.e., the samples annealed for 5 days. This is because the diffusion constant D_t of a low-molecular-weight compound in a rubber is assumed to be 10^{-11} m^2/s. The diffusion time t_D is given by the following equation [16].

$$t_D = \frac{r^2}{D_t} \tag{3.1}$$

Considering that the diffusion distance r in eq. (3.1) is the film thickness, i.e., 1 mm, the diffusion time is estimated to be 1 day. This is much shorter than the annealing time. Since the amount of the tackifier in each sheet is affected by the ambient temperature, i.e., the annealing temperature, each separated sheet must has a different T_g. Figure 3.8 shows the temperature dependence of the tensile loss modulus E'' for the separated sheets after annealing. As seen in the figure, T_g's of NR and PIB after the -20 ^{o}C annealing shift to lower and higher temperature, respectively. This is reasonable because the tackifier transfers from NR to PIB during annealing. Furthermore, the annealing at 40 ^{o}C makes NR contain a larger amount of the tackifier than PIB, leading to higher T_g for separated NR and vice versa.

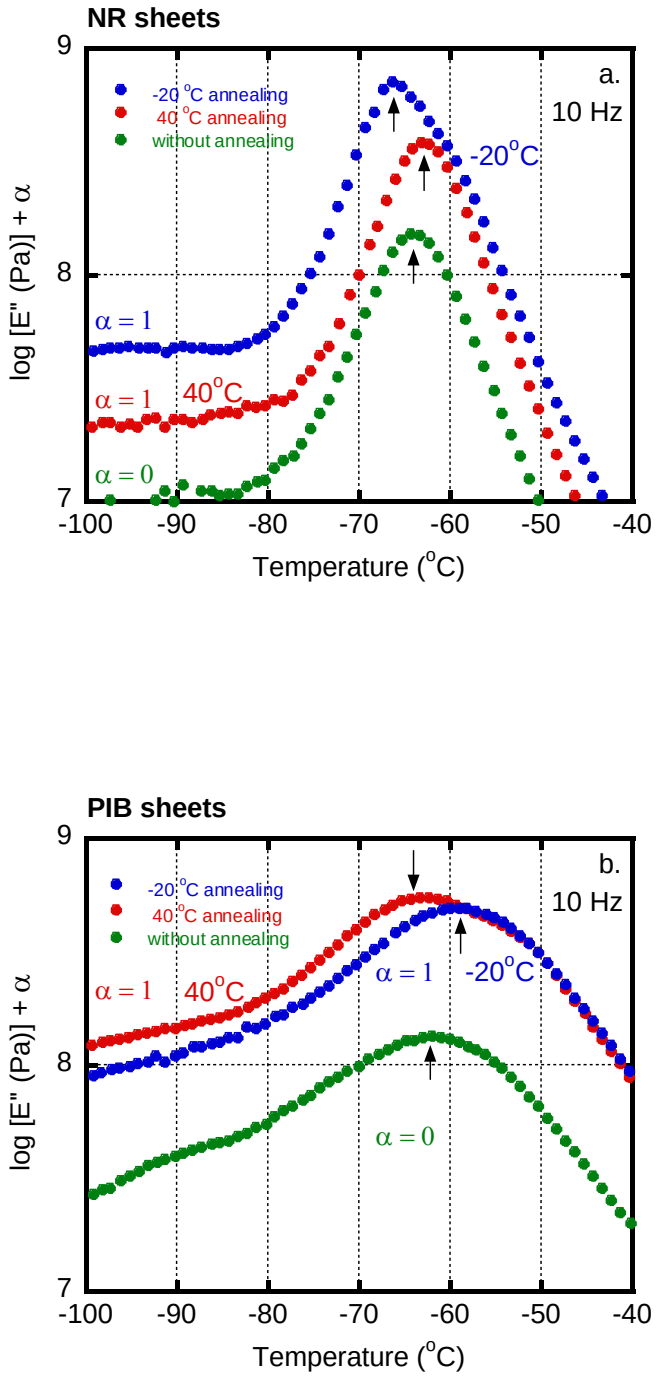

Figure 3.8 Temperature dependence of tensile loss modulus *E"* for the samples after annealing at (blue) -20 °C, (red) 40 °C, and (green) rubber containing 10 phr of the tackifier; (a) NR and (b) PIB.

The results in the figure correspond well with the FT-IR spectra and therefore demonstrate that the T_g shift occurs by the tackifier transfer. The mechanism of the tackifier transfer is investigated by the DSC measurement using the original NR sheet containing 10 phr of the tackifier (not laminated). The sample which was encapsulated in an Aluminum pan was preserved at the annealing temperature of the laminate sheets, i.e., at -20 ^{o}C for 5 days. Then, it was quenched to -120 ^{o}C immediately after setting into the DSC machine before starting the measurement.

It is found from the DSC heating curve in Figure 3.9 that the endothermal peak, defined as the melting point of the NR crystals, is obviously detected at 0 ^{o}C and the heat of fusion is calculated to be 9.37 J g^{-1}. Since the heat of fusion of a perfect NR crystal was reported to be 67.3 J g^{-1} [17], the NR crystallinity of this sample is 13.9 wt.%. There is no crytals at room temperature because its low melting point. The presence of the NR crystallization at low temperature decreases the amorphous regions, which is responsible for the tackifier transfer. This is plausible because the tackifier can be dissolved only in the amorphous regions, not in the crystalline ones. It is known that the NR crystals can restrict the motion of the amorphous chain, which may also increase T_g of the rubber sheet. Moreover, T_g of NR was observed at around -60 ^{o}C with a small peak of enthalpy relaxation for the conditions used.

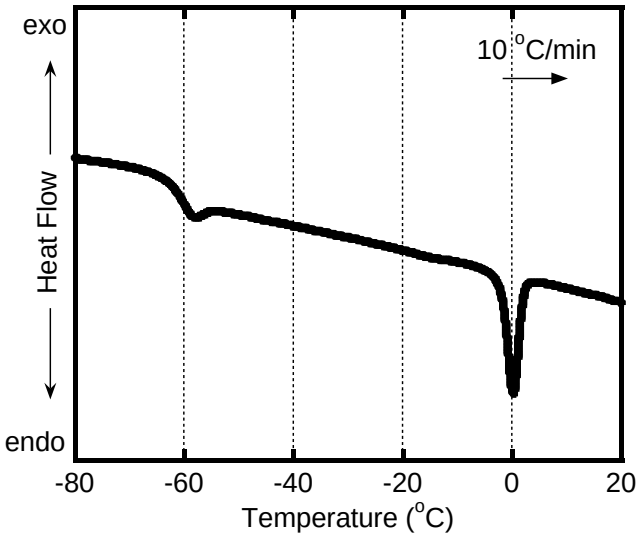

Figure 3.9 DSC heating curve of the NR sheet containing 10 phr of the tackifier after annealing at -20 °C

The interphase transfer of the tackifier due to the crystallization of NR is also observed when the amount of the tackifier is 20 phr. The transfer direction is similar to those of 10 phr of the tackifier. The T_g's of separated sheets, evaluated by the dynamic mechanical measurement, are summarized in Table 3.2.

Table 3.2 T_g change in the laminated NR and PIB with 20 phr of the tackifier

Sample	**T_g of NR (°C)**	**T_g of PIB (°C)**
Pure rubber	-73.3	-64.3
rubber/20 phr tackifier	-58.1	-60.3
-20 °C annealing	-60.3	-56.2
40 °C annealing	-55.3	-62.8

Although the interphase transfer of the tackifier occurs by the different mechanism from that in the previous chapter, the tackifier transfer is also expected to occur in the blend with a sea-island morphology. When the matrix is NR, the blend shows good mechanical properties as a rubber in winter season due to the low T_g and vice versa in summer season. This will be used as an alternative method to develop a new material of an immiscible rubber blend, especially for tire application in near future.

3.4 Conclusion

Dynamic mechanical analysis and FT-IR measurements are conducted to confirm the transfer of the tackifier between NR and PIB using the separated sheet samples after annealing treatment. It is revealed that the direction of the tackifier transfer is a function of annealing temperature. The tackifier migrates from NR to PIB at -20 ^{o}C, whereas it moves to NR at 40 ^{o}C. In this study, the crystallization of NR is responsible for the tackifier transfer. The crystallization growth decreases the amount of amorphous regions of NR, leading to the tackifier transfer to PIB at -20 ^{o}C. On the contrary, the amorphous region increases when the crystals are melted beyond the melting point, the tackifier moves from PIB to NR at 40 ^{o}C. The amount of the tackifier in each component is expected to change with the ambient temperature even in the blend, i.e., T_g of each component could also be changed. The transfer phenomenon from is applicable to the development of a new high-performance rubber material.

References

1. Sircar, A., *Rubber Chemistry and Technology* **1981,** *54* (4), 820-834.
2. Karasek, L.; Meissner, B.; Asai, S.; Sumita, M., *Polym J* **1996,** *28* (2), 121-126.
3. Sau, K.; Chaki, T.; Khastgir, D., *Polymer* **1998,** *39* (25), 6461-6471.
4. Ziegler, J.; Schuster, R., *KGK. Kautschuk, Gummi, Kunststoffe* **2008,** *61* (10), 510-517.
5. Hobbs, S.; Dekkers, M.; Watkins, V., *Polymer* **1988,** *29* (9), 1598-1602.
6. Mamunya, Y. P., *Journal of Macromolecular Science—Physics* **1999,** *38* (5-6), 615-622.
7. Kuhakongkiat, N.; Wachteng, V.; Nobukawa, S.; Yamaguchi, M., *Polymer* **2015,** *78*, 208-211.
8. Kumar, K. D.; Tsou, A. H.; Bhowmick, A. K., *Journal of Polymer Science Part B: Polymer Physics* **2010,** *48* (9), 972-982.
9. Khan, I.; Poh, B., *Journal of Polymers and the Environment* **2011,** *19* (3), 793-811.
10. Poh, B.; Chee, C., *International Journal of Polymeric Materials* **2007,** *56* (3), 247-255.
11. Yoon, H.; Okamoto, K.; Yamaguchi, M., *Carbon* **2009,** *47* (12), 2840-2846.
12. Doan, V. A.; Nobukawa, S.; Yamaguchi, M., *Composites Part B: Engineering* **2012,** *43* (3), 1218-1223.
13. Doan, V. A.; Nobukawa, S.; Ohtsubo, S.; Tada, T.; Yamaguchi, M., *Journal of Polymer Research* **2013,** *20* (5), 1-6.
14. Wiwattananukul, R.; Hachiya, Y.; Endo, T.; Nobukawa, S.; Yamaguchi, M., *Composites Part B: Engineering* **2015,** *78*, 409-414.

15. Noskov, A., *Journal of Applied Spectroscopy* **1969,** *10* (4), 403-406.

16. Tadmor, Z.; Gogos, C. G., *Principles of polymer processing*. John Wiley & Sons: New Jersey, 1979.

17. Brandrup, J.; Immergut, H. E.; Grulke, A. E., *Polymer Handbook Vol. 1*. Wiley: New York, 1999.

Chapter 4

Thermochromic Immiscible Polymer Blend by Interphase Transfer of Plasticizer

4.1 Introduction

Over the last decade, the demand of "smart materials" has been increasingly developed including thermochromic materials. The change of the light scattering properties according to the temperature change can be utilized for this application [1-3]. Takahashi et al. [4] developed a thermochromic polymer blend using a binary blend of ethylene-vinyl acetate copolymer (EVA) and poly(methyl methacrylate) (PMMA). This is attributed to the difference in the temperature dependence of refractive index between both polymers. The refractive index of PMMA is less sensitive to the temperature because it shows smaller thermal expansion than EVA. As a result, although PMMA and EVA have similar refractive indices at room temperature, leading to good transparency of the blend, the blend becomes opaque at high temperature. Errico et al. [5] also found that the transparency changes from transparent to opaque at high temperature. However, the magnitude of the change in the light transmittance is not good enough for the industrial application. This is owing to the weak temperature dependence of the refractive index difference.

Here, a new material design for the thermochromic immiscible polymer blend composed of EVA and poly(vinyl butyral) PVB is proposed. Although both of them are used

in the laminated safety glasses at present, the blend has never been employed in this application to the best of my knowledge [6-9]. In this study, light scattering originated from the refractive index difference is applied to provide thermochromic property. Furthermore, the interphase transfer of a low-molecular-weight compound having a different refractive index is utilized to enhance the temperature dependence of the refractive index difference between the polymers

4.2 Experimental

4.2.1 Materials

In this work, ethylene-vinyl acetate copolymer (EVA) (EV360, Mitsui-Dupont Fluorochemical, Japan) was used. The vinyl acetate content is 25 wt.% and the melt flow rate is 2 [g/10 min at 190 °C]. The other polymer was a terpolymer of vinyl butyral, vinyl alcohol, and vinyl acetate (Denka PVB4000-4, Denki Kagaku Kogyo, Japan), denoted as PVB. The weight fraction of the monomers is as follows; vinyl butyral : vinyl alcohol : vinyl acetate = 80 : 18 : 2. The DSC measurement carried out at 10 ^{o}C/min of a scanning rate shows that the glass transition temperature T_g, crystallization temperature T_c, and melting point T_m are -31 ^{o}C, 60 ^{o}C, and 81 ^{o}C, respectively. The chemical structure of both EVA and PVB are illustrated in Figure 4.1. The number- and weight-average molecular weights of PVB, measured by a gel permeation chromatography (HLC-8020, Tosoh, Japan) in chloroform with a polystyrene standard, are $M_n = 1.8 \times 10^5$ and $M_w = 3.1 \times 10^5$. Furthermore, di-2-ethylhexyl adipate (DOA) (New Japan Chemical) was employed without further purification, because it has low refractive index.

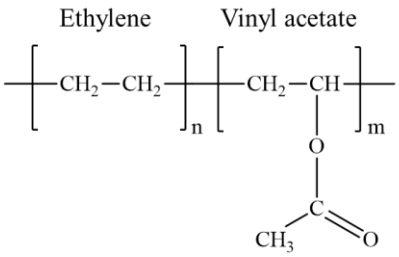

Ethylene-vinyl acetate (EVA)

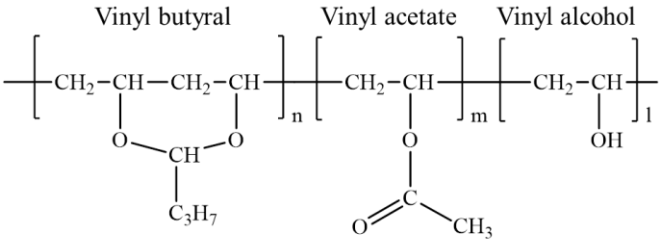

Poly(vinyl butyral) (PVB)

Figure 4.1 Chemical structure of plastics used in this research

4.2.2 Sample preparation

Various blends such as EVA/DOA, PVB/DOA, EVA/PVB, and EVA/PVB/DOA, were prepared by melt-mixing using an internal batch mixer (Labo-Plastomill, Toyoseiki, Japan) with a blade rotation of 30 rpm for 5 min at 120 °C. The blends obtained were compressed into flat films with 0.3 and 1 mm thickness using a compression-molding machine (Tester Sangyo, Table-type test-press, Japan) at 120 °C under 30 MPa for 3 min. They were subsequently cooled down at 25 °C for 3 min.

The films of EVA/DOA (100/10) and PVB/DOA (100/10) were laminated together by manual operation under a slight pressure to make them contact perfectly. Then the

samples were annealed without pressure at 0, 25, 40, and 60 °C for 5 days in a temperature controlled chamber.

4.2.3 Measurements

Refractive index in the wavelength from 450 to 680 nm was measured at various temperatures by an Abbe refractometer with a temperature controller (DR-M2, Atago, Japan). 1-Bromonaphthalene (Sigma Aldrich Corp., USA) was used as a contact liquid.

The temperature dependence of the light transmittance was evaluated at various temperatures using an ultraviolet-visible spectrometer (Lamba 25, PerkinElmer, USA) equipped with a temperature controller. The measurement was performed in the wavelength region from 200 to 1100 nm using a film with 1 mm thickness. The light transmittance T was determined by the following relation:

$$T(\%) = T_I / T_0 \times 100 \qquad (4.1)$$

where T_I is the intensity of the transmittance light and T_0 is that of the incident light.

The temperature dependence of oscillatory tensile moduli such as storage modulus E' and loss modulus E'' was measured by a dynamic mechanical analyzer (DVE4000, UBM, Japan) at 10 Hz. Rectangular specimens with the dimensions of 5 mm in width and 20 mm in length were cut out from the compressed sheets with 0.3 mm thickness. The heating rate was 2 ^{o}C/min.

The morphology was investigated by scanning electron microscope (SEM) (S4100, Hitachi, Japan). The surface of cryogenically fractured sample was coated with Pt-Pd by a sputter coating machine prior to the observation.

The linear coefficient of thermal expansion was measured by a thermo-mechanical analyzer (TMA) (TMA4000SA, Bruker AXS, USA) in a tensile mode in the temperature range from 0 ^{o}C to 60 ^{o}C at a heating rate of 2 ^{o}C /min. A constant load, 10 g, was applied in tensile mode. The rectangular specimens with the dimension of 5 mm x 0.3 mm x 20 mm (length) were employed.

4.3 Results and Discussion

4.3.1 Effect of the plasticizer addition

The wavelength dispersion of the refractive indices of EVA, PVB, and DOA, measured at 20 °C is shown in Figure 4.2. The figure demonstrates that the refractive index of EVA is slightly higher than that of PVB, although the difference in the long wavelength region is pronounced. As well known, the refractive index of a conventional polymer decreases with the wavelength, i.e., so called ordinary wavelength dispersion. The phenomenon can be expressed by the following Sellmeier relation [10-12].

$$n(\lambda) = A + \frac{B}{\lambda^2 - \lambda_{ab}^2} \tag{4.2}$$

where λ and $n(\lambda)$ are the wavelength of light and the refractive index at λ, respectively, λ_{ab} is the coefficient having the relation with the wavelength of a strong vibrational absorption peak in ultraviolet region, and A and B are the Sellmeier coefficients.

Since EVA has a lot of carbonyl groups in the chemical structure that show strong absorbance near the visible light region, the wavelength dispersion is stronger than that of PVB. Figure 4.2 shows that DOA has significantly lower refractive index in the wide range of wavelength. Considering that the refractive index of a mixture is basically provided by the simple addition rule, the DOA addition greatly decreases the refractive index of the polymer used in this study.

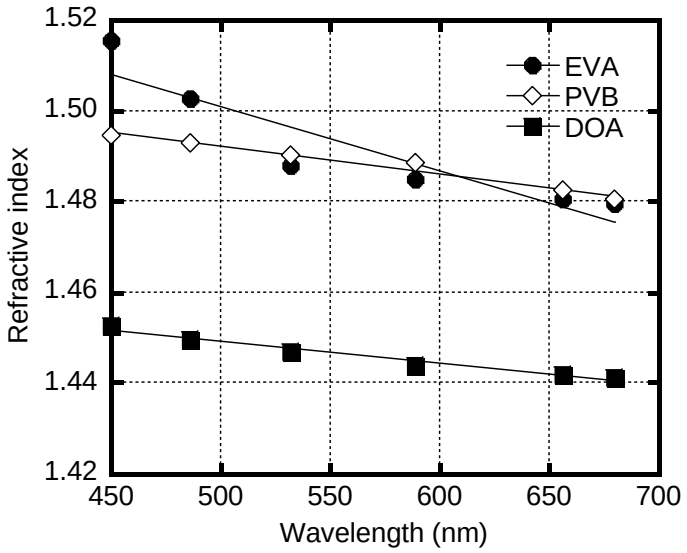

Figure 4.2 Wavelength dispersion of refractive indices at room temperature; (closed circles) EVA, (open diamonds) PVB, and (closed squares) DOA

The refractive indices at 589 nm of EVA/DOA and PVB/DOA, measured at 20 °C, are shown in Figure 4.3. Since the refractive index of DOA, 1.444, is significantly lower than those of the polymers (1.4865 for EVA and 1.4883 for PVB), the values of the blends decrease with the DOA content.

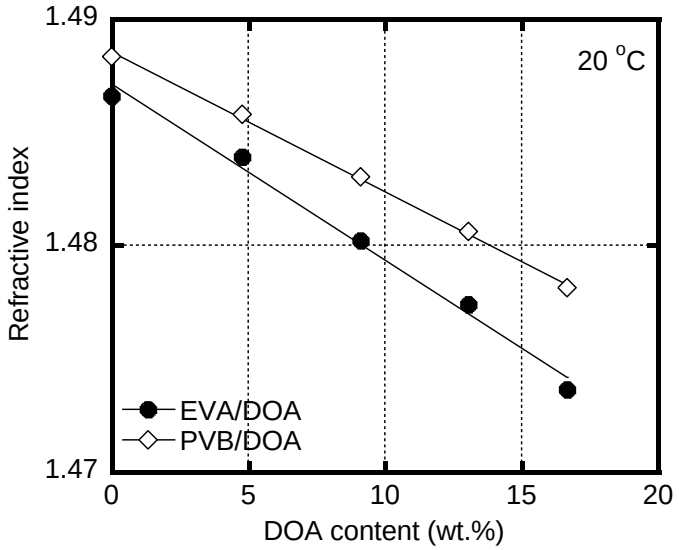

Figure 4.3 Relation between the DOA content and refractive index for (circles) EVA/DOA and (diamond) PVB/DOA at 20 °C. The refractive index was measured at 589 nm.

The temperature dependence of the tensile storage modulus *E′* and loss modulus *E″* is shown in Figures 4.4 and 4.5. The peak temperature of *E″*, ascribed to the glass-to-rubber transition, shifts to lower temperature by the DOA addition, suggesting that DOA is miscible with each polymer and acts as a plasticizer. In fact, the binary blends with DOA exhibit good transparency.

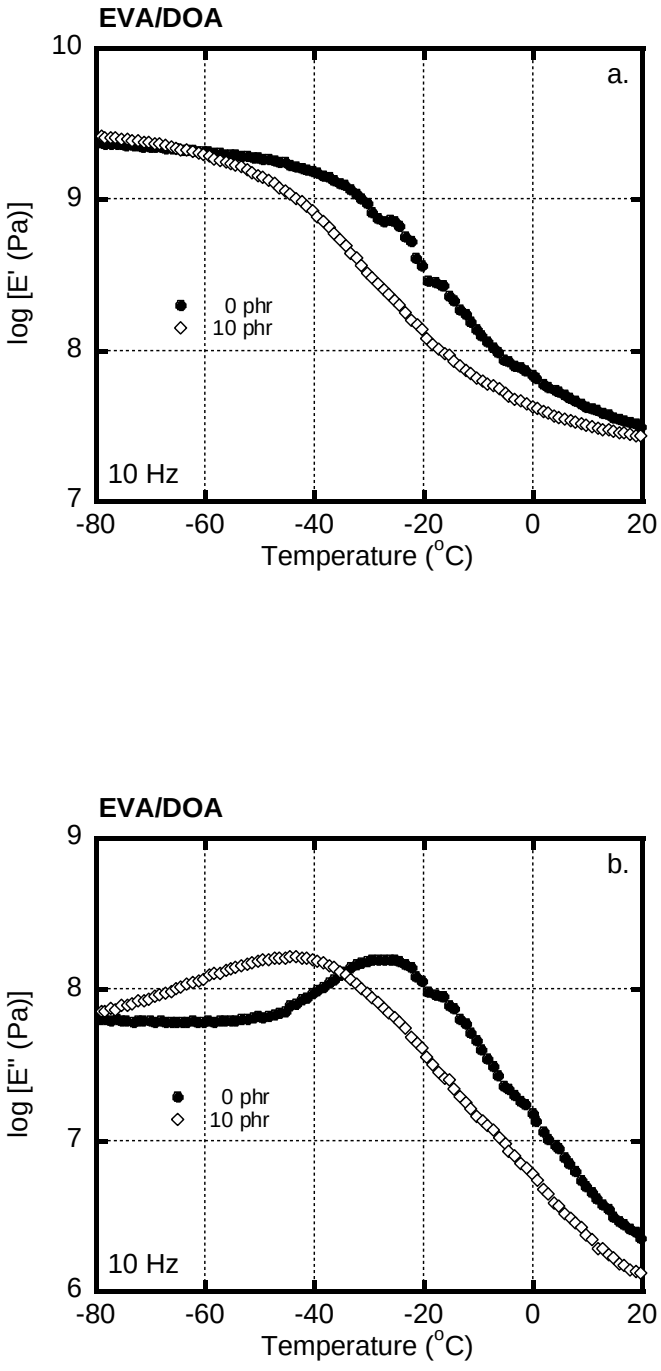

Figure 4.4 Temperature dependence of (a) storage modulus *E'* and (b) loss modulus *E''* for (closed circles) pure EVA and (open diamonds) EVA containing 10 phr of DOA

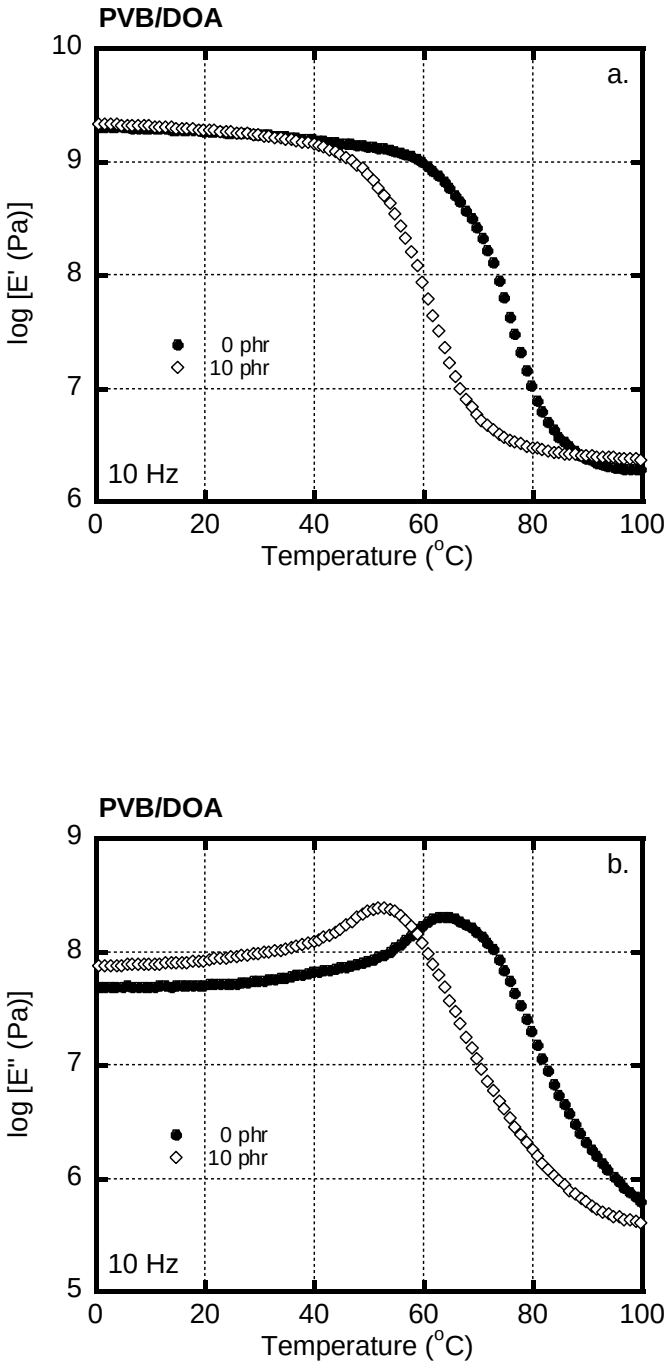

Figure 4.5 Temperature dependence of (a) storage modulus *E'* and (b) loss modulus *E''* for (closed circles) pure PVB and (open diamonds) PVB containing 10 phr of DOA

4.3.2 Interphase transfer of DOA

After the laminated films of EVA/DOA (90/10) and PVB/DOA (90/10) were annealed at various temperatures for 5 days, they were separated. The separation was performed without any difficulty. Then the refractive index of the separated films was measured at 20 °C to evaluate the DOA amount using the calibration curve shown in Figure 4.6. Prior to the measurements, the films were kept at 20 °C for one night to homogenize the DOA distribution. It is found that the refractive index of the separated EVA film after annealing at 60 °C is lower than that of EVA/DOA (90/10), i.e., the film prior to the laminating, suggesting that DOA moves from PVB to EVA during the annealing procedure. In contrast, the refractive index of the separated PVB film is higher than that of PVB/DOA (90/10). Moreover, the trend is opposite after annealing at 0 °C; i.e., the refractive index of the separated EVA is higher than that of EVA/DOA (90/10) and vice versa.

These results demonstrate that the amount and direction of the DOA transfer depend on the annealing temperature, that is summarized in Table 4.1.

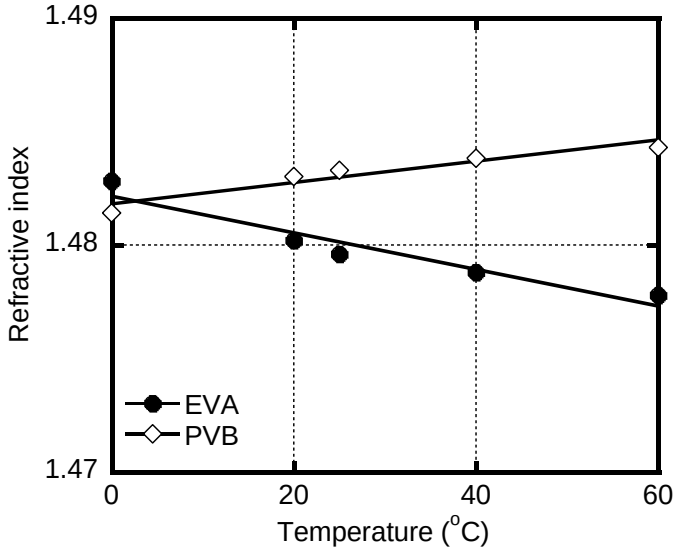

Figure 4.6 Refractive indices at 20 °C of the films separated after annealing at various temperatures. The wavelength was 589 nm.

Table 4.1 Amount of DOA transfer during annealing

Annealing Temperature	**Amount of DOA transfer (phr)**	**Transfer direction**
60 °C	2.5	from PVB to EVA
40 °C	1.2	from PVB to EVA
25 °C	0.1	from PVB to EVA
0 °C	3.2	from EVA to PVB

* Initial films contain 10 phr of DOA.

Light scattering intensity is determined by the refractive index difference and size of phase separation. In other words, the light transmittance is affected by the refractive index difference at the ambient temperature because the size of phase separation does not change by the temperature. Therefore, the refractive indices at the annealing temperature, not room temperature, were also measured using the separated films. As shown in Figure 4.7, the refractive index difference increases with increasing the temperature and is the lowest around at 0 °C.

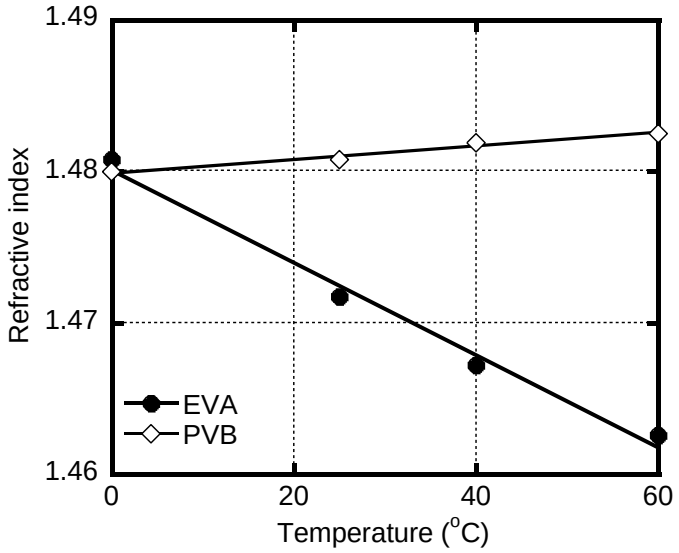

Figure 4.7 Refractive index of the films separated after annealing. The refractive index measurements were performed at the annealing temperature.

4.3.3 Structure and properties of blends

The temperature dependence of the tensile storage modulus *E′* and loss modulus *E″* for EVA/PVB (50/50) is shown in Figure 4.8. The *E”* curves around at the glass-to-rubber transition region for the individual pure components are also shown in the figure with a vertical shift. The dynamic mechanical properties are typical ones for immiscible polymer blends; double peaks ascribed to the glass-to-rubber transition are clearly detected in the blend. Furthermore, the peak temperatures in the blend correspond with those of pure EVA and PVB.

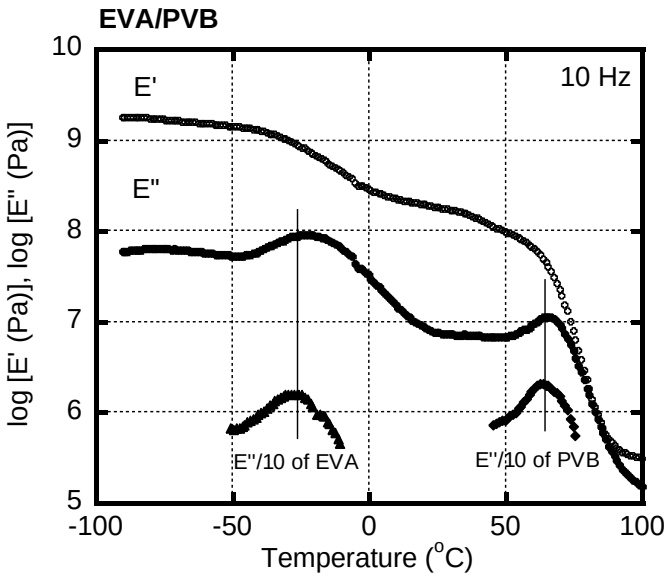

Figure 4.8 Temperature dependence of (open circles) tensile storage modulus *E′* and (closed circles) loss modulus *E″* for EVA/PVB. The *E″* curves of the pure (triangles) EVA and (diamonds) PVB are also shown in the figure with a vertical shift.

The dynamic mechanical properties for EVA/PVB/DOA (50/50/10) are shown in Figure 4.9 with an SEM image of the fractured surface. As similar to the blend without DOA, double peaks are detected in the *E"* curve. The peak temperatures of *E"* are -44 °C and 52 °C, which are ascribed to T_g's of EVA and PVB phases, respectively. The result demonstrates that DOA cannot act as a compatibilizer for the blend, but is dissolved into EVA and PVB. This is reasonable because DOA is a plasticizer for both EVA and PVB. Moreover, it is found from the SEM picture that the cord length, i.e., the size of phase separation, is around 1-5 μm.

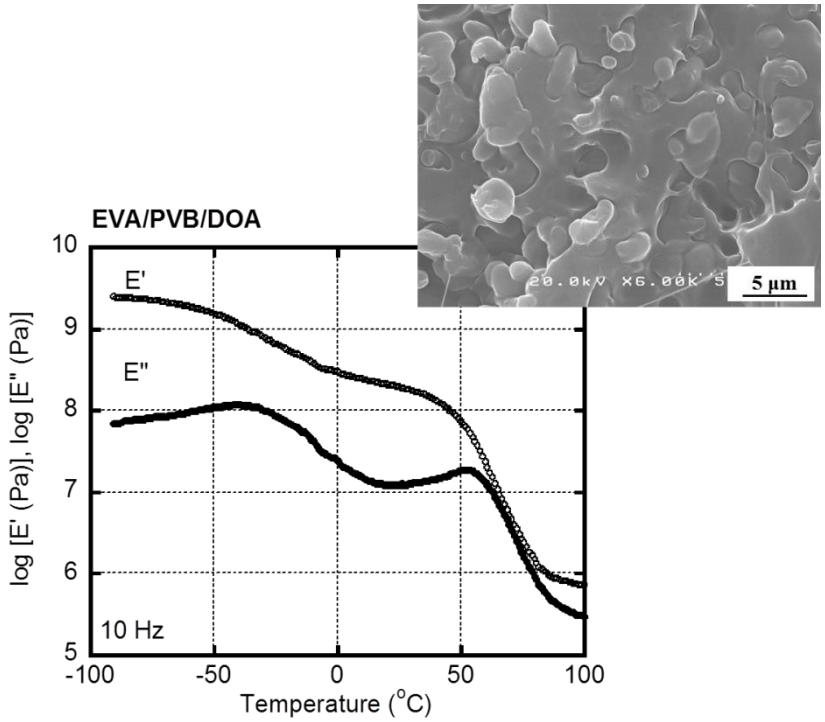

Figure 4.9 Temperature dependence of (open circles) tensile storage modulus *E'* and (closed circles) loss modulus *E"* at 10 Hz for EVA/PVB/DOA (50/50/10)

The temperature dependence of the light transmittance for the ternary blend, i.e., EVA/PVB/DOA (50/50/10), is shown in Figure 4.10. It is demonstrated that the transparency changes with the ambient temperature. Furthermore, the light transmittance in the short wavelength is lower than that in the long wavelength. These results are explained by the difference in the refractive indices of both phases. Therefore, the DOA transfer plays an important role in the abrupt change of light transmittance as a function of the ambient temperature.

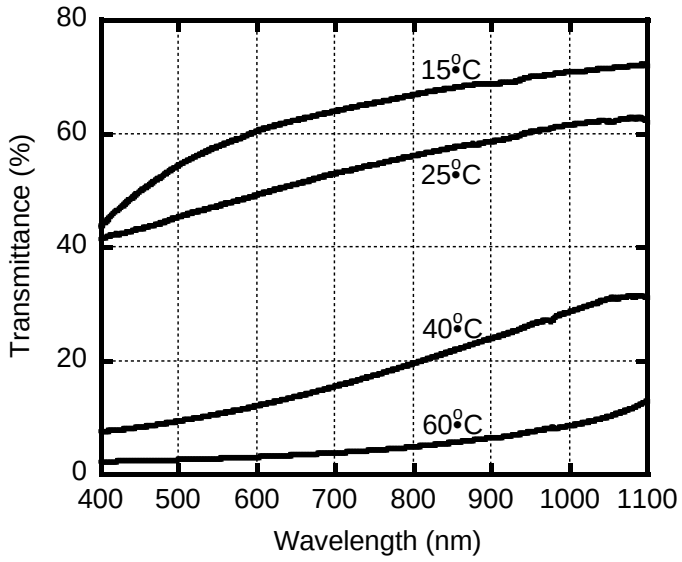

Figure 4.10 Temperature dependence of light transmittance for EVA/PVB/DOA (50/50/10) The thickness of the film was 1 mm.

The temperature dependence of the refractive index can be expressed by the Lorentz-Lorenz equation by the following equations [13, 14];

$$\frac{\partial n}{\partial T} = (n-1)\left[\frac{1}{\rho}\frac{\partial \rho}{\partial T} + \frac{1}{[R]}\frac{\partial [R]}{\partial T}\right] \cong (n-1)\frac{1}{\rho}\frac{\partial \rho}{\partial T} \tag{4.3}$$

$$\frac{1}{\rho}\frac{\partial \rho}{\partial T} = -3\beta \tag{4.4}$$

where ρ is the density, $[R]$ is the molecular refractive, and β is the linear coefficient of thermal expansion.

As explained in the introduction of this chapter, the difference in the thermal expansion contributes to the temperature dependence of the light scattering intensity. Therefore, the linear coefficient of thermal expansion β, defined by eq. (4.4), was evaluated using PVB, PVB/DOA, EVA, and EVA/DOA.

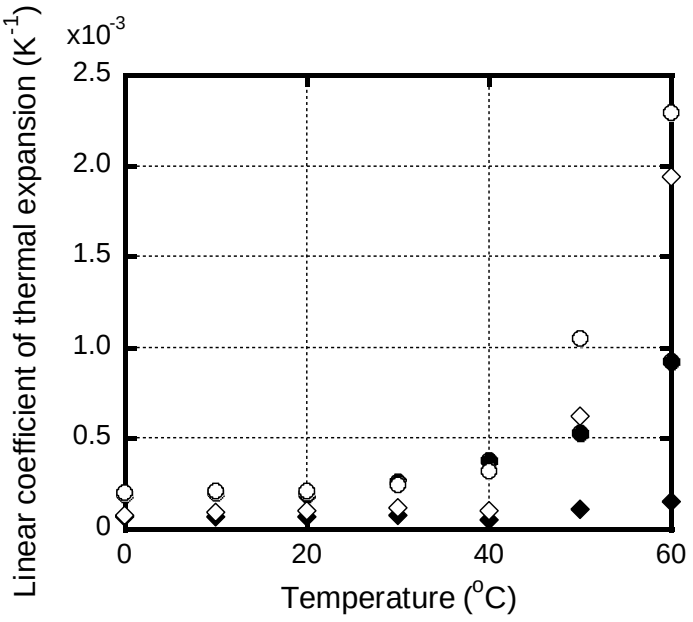

Figure 4.11 Linear coefficient of thermal expansion for (closed symbols) pure plastic and (open symbols) plastic containing 10 phr of DOA; (circles) EVA and (diamonds) PVB

It is found from Figure 4.11 that the linear coefficients of thermal expansion of both EVA and PVB are increased by the addition of DOA. This is reasonable because the plasticizer tends to loosen the molecular packing and enlarges the free volume. Furthermore, the value becomes large at high temperature. Consequently, thermal expansion of plasticized EVA is significantly larger at high temperature owing to the T_g shift to lower temperature. It is well known that the refractive index of a polymer decreases with temperature. For the material design, therefore, the contribution of the thermal expansion has to be also taken into consideration.

4.4 Conclusion

The temperature dependence of the transparency for immiscible blends composed of EVA and PVB was studied considering the effect of the DOA addition. It is found that the ternary blend shows the strong temperature dependence of the light transmittance, i.e., from transparent to opaque. This is because the difference in the refractive index between two phases is greatly affected by the ambient temperature. Furthermore, the DOA transfer is also observed between EVA and PVB in the laminated sheets as a function of temperature. At high temperature, the DOA migrates from PVB to EVA. Consequently, the refractive index of EVA becomes lower than that of PVB.

In the blend, therefore, the temperature dependence of the refractive index difference between phases is enhanced by the DOA transfer since DOA has a low refractive index. This can be a novel material design for a thermochromic material.

References

1. Ritter, A., *Smart Materials in Architecture, Interior Architecture and Design*. Walter de Gruyter: 2007.
2. Seeboth, A.; Lötzsch, D.; Ruhmann, R.; Muehling, O., *Chemical Reviews* **2014,** *114* (5), 3037-3068.
3. Jochum, F. D.; Theato, P., *Chemical Society Reviews* **2013,** *42* (17), 7468-7483.
4. Takahashi, S.; Okada, H.; Nobukawa, S.; Yamaguchi, M., *European Polymer Journal* **2012,** *48* (5), 974-980.
5. Errico, M.; Greco, R.; Laurienzo, P.; Malinconico, M.; Viscardo, D., *Journal of Applied Polymer Science* **2006,** *99* (6), 2926-2935.
6. Jalham, I. S.; Alsaed, O., *New Journal of Glass and Ceramics* **2011,** *1* (02), 40.
7. Alsaed, O.; Jalham, I., *Jordan Journal of Mechanical and Industrial Engineering* **2012,** *6* (2), 127-133.
8. Zang, M.; Chen, S., *Wiley Encyclopedia of Composites* **2012**.
9. Juozapaitis, A.; Vainiūnas, P.; Zavadskas, E. K.; Serafinavičius, T.; Lebet, J.-P.; Louter, C.; Lenkimas, T.; Kuranovas, A., *Procedia Engineering* **2013,** *57*, 996-1004.
10. Harding, G. F., *Optical Properties of Polymers*. Elsevier Applied Science: London, 1986.
11. Ghosh, G., *Optics Communications* **1999,** *163* (1), 95-102.
12. Scharf, T., *Polarized Light in Liquid Crystals and Polymers*. John Wiley & Sons: 2007.
13. Lorentz, H., *Annalen der Physik* **1880,** *245* (4), 641-665.
14. Lorenz, L., *Annalen der Physik* **1880,** *247* (9), 70-103.

Chapter 5

General Conclusion

In order to provide high-performance properties and/or novel functions for a polymer blend, a low-molecular-weight compound is often added as a third component. In the case of an immiscible polymer blend with a third component, the overall morphology affecting final properties is controlled by not only the characteristics of individual components, but also the morphology including the distribution state of a third component. Since a third component with low molecular weight is usually dissolved into polymers due to the contribution of mixing entropy, it is expected not to form another phase but distribute within polymers. Furthermore, they show uneven distribution because the miscibility of a third component with each polymer is different in general. Moreover, it has been reported that the transfer of this third component through interphase boundary can occur when it is not in the equilibrium state.

Most researches on the interphase transfer phenomenon of a third component in an immiscible blend have been studied under flow field at the mixing process. Although less attention has been focused on the transfer without flow field, it is very important to understand the change in various properties during storage or usage. Furthermore, the interaction parameter is dependent upon the temperature, suggesting that the temperature change during usage will lead to the interphase transfer of a third component. In this thesis, the uneven distribution of a low-molecular-weight component, i.e., liquid compound, in

immiscible blends is demonstrated with the interphase transfer behavior. Furthermore, the effect of the ambient temperature on the distribution state is focused to propose a novel polymer blend with high performance and/or function, which is significantly different from previous researches.

In Chapter 2, the interphase transfer of di-2-ethylhexyl adipate (DOA), known as plasticizer, is studied using immiscible amorphous polyolefins such as ethylene-propylene copolymer (EPR) and poly(isobutylene) (PIB). The temperature dependence of the interaction parameter between DOA and each polymer is found to be responsible for the DOA transfer. The experimental results revealed that more DOA favorably localizes in EPR phase when the annealing was performed at low temperature, i.e., -20 ^{o}C, and vice versa at 40 ^{o}C. The remarkable DOA transfer corresponds to the temperature dependence of the interaction parameter which is evaluated from the swell ratio in DOA based on the Flory-Rhener theory; The interaction parameter of DOA with EPR is lower than that of the DOA with PIB at -20 ^{o}C and vice versa at 40 ^{o}C. Since DOA greatly affects T_g of each phase, the interphase transfer phenomenon is applicable to develop an attractive tire, in which the EPR matrix shows low T_g at low temperature or winter and vice versa in summer season.

In Chapter 3, the interphase transfer behavior between natural rubber (NR) and PIB is investigated using a coumarone-indene copolymer with low molecular weight, known as a tackifier, which increases T_g for both rubbers. It is revealed that the tackifier transfer occurs between the rubbers, which is affected by the annealing temperature. For example, more tackifier is detected in PIB in the laminated sheets at -20 ^{o}C. Consequently, T_g of NR shifts to lower temperature, whereas T_g of PIB is found at higher temperature. The driving force of

the tackifier transfer is the crystallization of NR. This is reasonable because the tackifier can be dissolved only in the amorphous region, not in the crystals. On the contrary, after the crystals is melted beyond T_m, i.e., 0 ^oC, the tackifier migrated from PIB to NR. It is expected to apply this behavior to a new material, in which the tackifier is employed as one component in the blend.

In Chapter 4, the transparency and its temperature dependence are studied for the immiscible polymer blend of a copolymer composed of ethylene and vinyl acetate (EVA) and a terpolymer of vinyl butyral, vinyl alcohol, and vinyl acetate (PVB) with DOA. It is found that the appearance of the blend changes from transparent to opaque with increasing the temperature. In addition, the interphase transfer of DOA in the laminated systems is also observed, which is greatly affected by the ambient temperature. Since the DOA has the lowest the refractive index, the migration into one phase reduces the refractive index of the phase. As a result, the mismatch of the refractive indices of both phases occurs, leading to light scattering. It is found that the DOA moves from PVB to EVA at high temperature, resulting in the lower refractive index of EVA phase, and vice versa at low temperature.

This research demonstrated that the distribution state of a low-molecular-weight compound as a third component in an immiscible blend is greatly affected by the ambient temperature via the interphase transfer phenomenon. This phenomenon will be applicable to a novel material design, which has not been reported to the best of my knowledge. Since most tires are composed of immiscible rubber blends containing low-molecular-weight liquid compounds, this technique should be considered in the tire industry. For example, all-season tire is an attractive application, in which a matrix shows low T_g in winter and high

T_g in summer owing to the change of a liquid content in a matrix through the interphase transfer. The difference in the refractive index between phases can be also controlled using this phenomenon, which will be applicable to a thermochromic material. Furthermore, the change in the viscoelastic properties is expected to be used for a damping material.

Finally, I wish that the industrial development will be accelerated by the concept of the material design proposed in this thesis.

Achievements

Publications

1. **Nawaphorn Kuhakongkiat,** Viyada Wachteng, Shogo Nobukawa, and Masayuki Yamaguchi
   "Interphase Transfer of Plasticizer between Immiscible Rubbers"
   Polymer **2015,** 78, 208-211

2. **Nawaphorn Kuhakongkiat,** Shogo Nobukawa, and Masayuki Yamaguchi
   "Interphase Transfer of Tackifier between Immiscible Rubbers"
   Journal of Macromolecular Science Part B. Physics **2016**, 55(3), 262-271l

3. **Nawaphorn Kuhakongkiat,** Kento Yoshida, Guesnier Mathieu Serge Rene, Mitsunari Sugiyama, and Masayuki Yamaguchi
   "Design of Thermochromic Polymer Blend by Interphase Transfer of Low-Molecular-Weight Compound"
   to be submitted

Presentations

International conference

1. **Nawaphorn Kuhakongkiat,** Kento Yoshida, and Masayuki Yamaguchi
   "Temperature Dependence of Plasticizer Transfer between Immiscible Rubbers"
   The XVIIth International Congress on Rheology (ICR2016), August 8-13, 2016, Kyoto, Japan

2. **Nawaphorn Kuhakongkiat,** Kento Yoshida, and Masayuki Yamaguchi
"Material Design of Functional Rubber Blends by Interphase Transfer of Liquid Components"
Global Rubber Research Fair (GRRF2016), March 9-11, 2016, Bangkok, Thailand

3. **Nawaphorn Kuhakongkiat,** Kento Yoshida, and Masayuki Yamaguchi
"Mutual Diffusion of Plasticizer in Immiscible Rubber Blends"
The 3rd International Symposium for Green-Innovation Polymers (GRIP2016), March 4-7, 2016, Ishikawa, Japan

4. **Nawaphorn Kuhakongkiat,** Kento Yoshida, Shogo Nobukawa, and Masayuki Yamaguchi
"Control of Glass Transition Temperature in Immiscible Rubber Blend"
Asian Workshop on Polymer Processing (AWPP2015), December 1-4, 2015, National University of Singapore, Singapore

5. **Nawaphorn Kuhakongkiat,** Shogo Nobukawa, and Masayuki Yamaguchi
"Manipulated Control of Glass Transition Temperature for Immiscible Rubber Blends"
International Polymer Conference of Thailand (PCT-5), June 18-19, 2015, Bangkok, Thailand

6. **Nawaphorn Kuhakongkiat,** Shogo Nobukawa, and Masayuki Yamaguchi
"Transfer Phenomenon of Tackifier between Immiscible Rubber Pair"
31st International Conference of the Polymer Processing Society (PPS-31), June 7-11, 2015, Jeju Island, Korea

7. **Nawaphorn Kuhakongkiat,** Shogo Nobukawa, Masayuki Yamaguchi
"Study on Interphase Transfer of the Tackifier between Immiscible Rubber Pair"
ANTEC Annual Meeting of Society of Plastic Engineering, March 23-25, 2015, Florida, USA

Domestic conference

1. **Nawaphorn Kuhakongkiat,** Shogo Nobukawa, Masayuki Yamaguchi
   "Study on Interphase Transfer of Tackifier between Immiscible Rubber Blends"
   63rd SPSJ Symposium on Macromolecules, September 24-26, 2014, Nagasaki, Japan

Award

1. JAIST Research Grant for Student Attending International Conferences
   Asian Workshop on Polymer Processing (AWPP2015), December 1-4, 2015,
   National University of Singapore, Singapore

2. JAIST Doctoral Research Fellowship (DRF), October 2013 – September 2016

^{1}H Nuclear Magnetic Resonance Spectroscopy for Chemical Structure Determination of Synthetic Rubbers

1. Introduction

Nuclear **M**agnetic **R**esonance spectroscopy or NMR is one of the most powerful techniques for confirmation of the structural elucidation of unknown compounds. The word "Nuclear" refers to the properties of nucleus, in which the spin nuclei were determined. Next, the "Magnetic", which involves magnetic field with magnitude and direction. And the "Resonance" refers to the magnet and radio wave was met at the right direction. The extremely important experimental technique is based on the nuclear spin of ^{1}H, ^{13}C, ^{15}N, ^{19}F, ^{31}P, and so forth.

1.1 Properties of nucleus

The simplet atom, hydrogen, is found in almost organic compounds, in which composed of a single proton and a single electron. The 1H is denoted for hydrogen atom which superscript signifies the sum of the atom's protons and neutrons. For the purpose of NMR, the magnetic properties of hydrogen nucleus possesses with angular momentum properties called "*spin*". The concept of nuclear spin describes the intrinsic angular momentum associated with the magnetic nucleus. The hydrogen spin is positively charged, which can generate a magnetic field and possess a *magnetic moment*, μ as shown in Figure 1. This magnetic moment is a vector and has values. Since the classical physics mentions that any kind of spinning body has an angular momentum P with behaves as parallel vectors, the relation between these two quantities is expressed by the following equation;

$$\mu = \gamma P \qquad (1)$$

where γ is a gyromagnetic ratio, which is a constant characteristic of the particular nucleus.

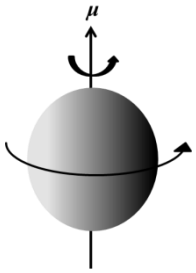

Figure 1 ^{1}H with intrinsic angular momentum moving in a circle called "*spin*"

There are three classes of nuclear spin which is an overall of the protons and neutrons in the spin angular momentum, Figure 2. When both the atomic number and atomic mass are even, the nucleus has no spin, signified as I=0 of carbon (^{12}C) and oxygen (^{16}O). These two nuclei are invisible for the NMR experiment. For the nucleus with the atomic number or atomic mass is odd, or both are odd, the nucleus has to be spinning. ^{1}H, ^{13}C, ^{15}N, ^{19}F, and ^{31}P have a spin of 1/2, in which those nuclei possess in the spherical spinning shape and easily examined by the NMR experiment. And the last with those of nuclei with I>1/2 are ^{1}H(D), ^{10}B, ^{14}N, ^{17}O, and ^{33}S, quadrupolar or ellipsoid spinning shape.

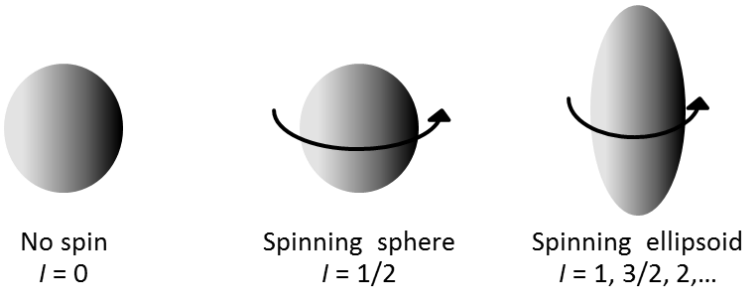

Figure 2 Three classes of spinning nuclei

The nuclear spin angular momentum is described in terms of its nuclear spin momentum quantum number I, which is dependent upon the mass number and atomic number in natural abundance. Some of the element isotopes show the spin quantum number as expressed in Table 1.

Table 1 Spin quantum number and natural abundance (%) of some useful nuclei

Nucleus	Spin quantum number, *I*	Abundance (%)
^{1}H	1/2	99.98
^{1}H (D)	1	0.016
^{10}B	3	18.83
^{11}B	3/2	81.17
^{13}C	1/2	1.108
^{14}N	1	99.635
^{15}N	1/2	0.365
^{17}O	5/2	0.037
^{19}F	1/2	100.00
^{29}Si	3/2	4.70
^{31}P	1/2	100.00
^{33}S	3/2	0.74

1.2 Magnetic properties

As discussed that the nuclei is associated with the angular momentum with intrinsic spin. The angular momentum can be defined in quantum physics by the following relation;

$$P = \frac{h}{2\pi} m \qquad (2)$$

where *h* is Planck's constant and *m* is the magnetic quantum number.

From the equation, the angular momentum *P* depends directly on the magnetic quantum number. It is found that the magnetic quantum number of any element is related to the nuclear spin quantum number *I* by the following equation;

$$m = (2I + 1) \qquad (3)$$

For the proton, the spin quantum number is $I = 1/2$, we can obtain $m = 2$. The two difference magnetic quantum number of a proton will be evaluated as follows;

$$m = +\frac{1}{2} \quad \text{and} \quad m = -\frac{1}{2}$$

Regarding to the eq. (1) and (2), we obtain a new eq. (eq. 4), which shows that the magnetic moment of a given element depends only on the magnetic quantum number by the following equation;

$$\mu = \gamma \frac{h}{2\pi} m \tag{4}$$

For the nuclei spin 1/2, the experimentalist subjects nuclei to an external strong laboratory magnetic field B_0, whose units are tesla, or T (1 Tesla = 10^4 gauss). The splitting of spins was affected when the B_0 turned along the direction as the z-axis. This makes the tendency for magnetic moment to align in the direction of $B_0(+z)$ over the opposite direction ($-z$) in accordance with the Boltzmann distribution. This phenomenon of the splitting into two specific groups has been called *"Zeeman effect"*, in which the interaction of the magnetic moment with a magnetic field is expressed in Figure 3.

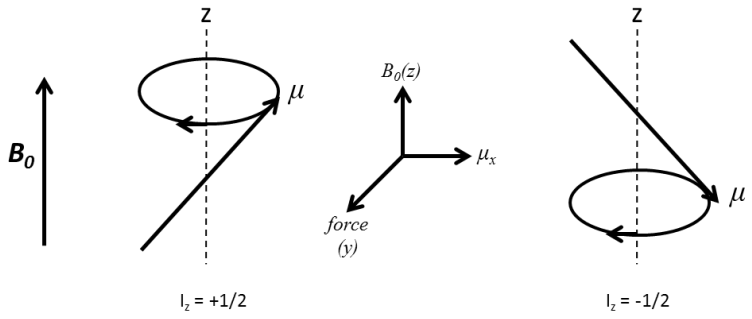

Figure 3 Interaction between the spinning nucleus and external field

Considering the spin in static magnetic field, we can obtain the potential energy E given by;

$$E = \mu B_0 \tag{5}$$

After we calculated the magnetic moment with the spin quantum number in eq. (4), we obtain a new equation relation, in which the energy levels are shown in Figure 4;

$$E = \frac{\gamma h B_0}{2\pi} m \qquad (6)$$

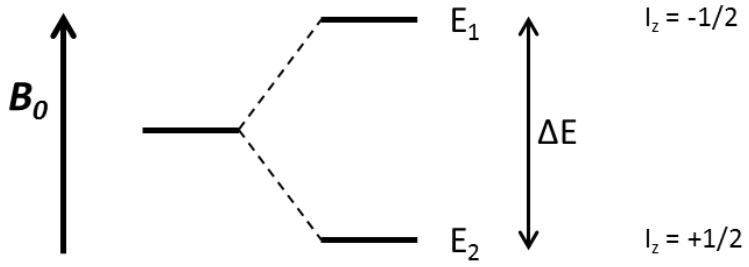

Figure 4 The energy levels difference between nuclei spin states as a function of the external magnetic field

1.3 Resonance phenomenon

As mentioned previous, the nucleus spin was move in circular motion in the static magnetic field along z-axis. This motion called "*precession*", which shows two precession for the nuclear spin with $I = 1/2$. From Figure 4, the transition from the lower energy state to the higher energy state can be brought by applying radiation of exactly the required frequency (in the radiofrequency range) to effect the transition between these energy levels in a static homogeneous magnetic field B_0. The introduced radiofrequency v is typically on the order of megahertz (MHz).

from $\Delta E = h\upsilon$ (7)

If we combine eq. (6), in which m is ripped off, with eq. (7), the frequency v at which the absorptions occur can readily be calculated;

$$\Delta E = \frac{\gamma h B_0}{2\pi} \qquad (8)$$

Modification of this equation, to include the gyromagnetic ratio γ, gives the following equation;

$$\upsilon = \frac{\gamma B_0}{2\pi} \qquad (9)$$

This equation is the fundamental NMR equation, in which the precessional motion of the nuclear magnetic moment around B_0 occurs with angular frequency. This equation has been known for "*Larmor frequency*" whose units are radians per second (rad s^{-1}).

In case of the basic experiment for a proton, a frequency of precession of 300 MHz is needed at a magnetic field of 7.05 tesla *T*, and the difference in energy between the spin energy states is 0.0286 cal mol^{-1}. At this condition, the frequency is the same as the Larmor frequency of the proton nucleus, the absorption and emission energies occur. The absorption energy occurs as +1/2 nuclei spin become -1/2 nuclei spin and emission occurs as -1/2 nuclei spin become +1/2 nuclei spin. This process is called "resonance" with the applied radiation.

1.4 Relaxation

The absorption energy results in the excitation of the nucleus from the lower to higher energy state, which results in resonance. After resonance, the tendency of nuclei of the difference energy levels will change. Of cause, the nuclei tendency at the lower energy state is reduced. In order to balance the resonance condition, some of the nuclei at the higher state must be able to lose their energy and return to the lower energy state. This process to the establishment and re-establishment at the original equilibrium of the nucleus spin magnetization is referred to as "relaxation phenomenon" as illustrated in Figure 5. The relaxation time is the time needed to relax the nuclei back to their equilibrium distribution state.

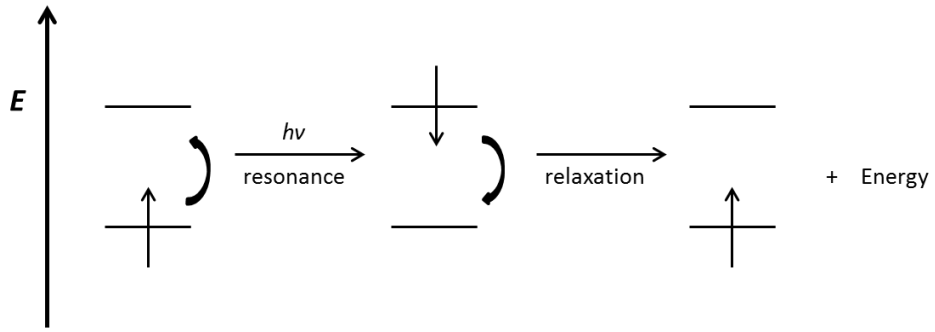

Figure 5 Simple presentation of resonance phenomenon and relaxation process

There are two main types of the relaxation process which will discuss;

1. Longitudinal spin relaxation, also known as spin-lattice relaxation, T_1

and 2. Transverse spin relaxation, also known as spin-spin relaxation, T_2

The terms of "lattice" are defined as all kinds of aggregates of atoms or molecules in the solution. The first spin-lattice relaxation involves the transfer of energy from the excited protons to the surrounding lattice. T_1 relaxation allows the nuclear spin magnetization vectors to re-establishment to the equilibrium according to the Boltzmann distribution. The magnitude of T_1 varies to a considerable extent depending on the nucleus and its environment. Therefore, T_1 typically determines how long the experiment must wait after the free induction decay FID repeating the process of applying the radiofrequency pulse. For many organic compounds, T_1 is less than 1 second.

In case of the spin-spin relaxation, involves the transfer of energy among the processing protons. T_2 causes the signal to decay exponentially to zero after applying radiofrequency pulse to the equilibrium. The most important feature of this spin-spin relaxation is to determine the natural width of the lines in the NR spectra. If the relaxation is very short, we will observe a broadening of the peaks and vice versa as simply illustrated in Figure 6.

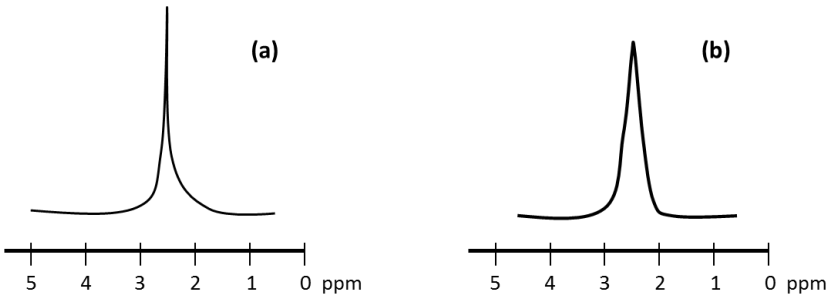

Figure 6 Influence of the spin-spin relaxation time T_2 on peak shape: (a) longer relaxation time; (b) short relaxation time

1.5 Chemical shift (δ)

When applying the protons with strong external magnetic field, the electron cloud that surrounding the nucleus also has charge, motion, and magnetic moment. The protons of a given compound can locate in different chemical environments under the difference of the influence of magnetic field with different resonance frequencies. Under the external magnetic field, the electrons generate their own magnetic fields, either increasing or decreasing the external magnetic field. This electronic modulation with the B_0 is termed "shielding", which depends on the nature of the surrounding electrons. Therefore the actual magnetic field B_{eff}, may be expressed as $B_0(1-\sigma)$, in which the electronic shielding σ normally is positive. The variation in the difference in resonance frequencies with shielding results has been termed "*chemical shift*". If two protons are located in the same chemical environment, they will be under the influence of the same magnetic field and then their resonance signals will overlap.

Chemical shifts are evaluated with reference to the absorptions of protons of reference compounds. The most generally used reference compounds for ^{1}H and ^{13}C NMR is tetramethylsilane, as expressed as TMS. It is chemically inert, symmetrical, volatile (b.p. 27 ^{o}C), and soluble in most organic solvents; it gives a single, intense, sharp, and its protons are more shield than almost organic compounds.

There are several reasons why TMS is used as a reference;

1. The TMS signal, which is at the right-hand side of the spectrum, is clearly distinguished from most other resonances. The methyl groups bonded are shielded more, in which resonate at the high field.

2. TMS is a cheap and readily available compound.

3. The low boiling point of TMS can be easily removed from the sample by evaporation after the spectrum recorded.

Figure 7 shows the NMR scale in ppm with the Larmor frequency in the experiment with 300 MHz. The term "shielded" is a relative one and means toward the right; "deshielded" means toward the left.

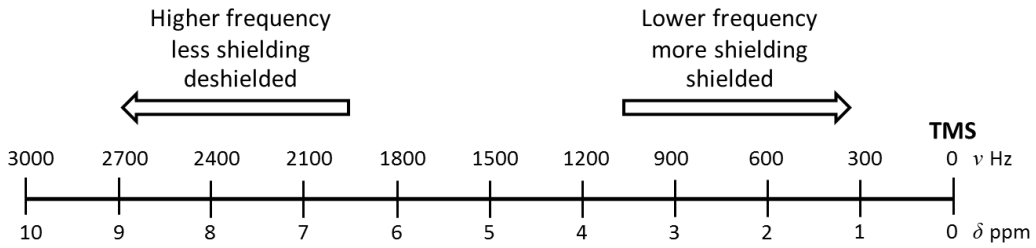

Figure 7 NMR scale for proton chemical shifts of organic compounds

Factors affecting the chemical shifts;

- *Paramagnetic*; from non-spherical electron distribution
- *Magnetic anisotropy of neighboring bonds and ring current effect*; usually causes from the π-electron of the triple bond and aromatic rings
- *Electronic field gradients*; results from the strong polar substituents of compounds
- *Hydrogen bonding*; this occurrence can decrease the electron density which will be observed the chemical shift in higher frequency
- *Solvent effect*; each solvent can interact with each specific electron portion of a molecules

1.6 Instrumentation and Sample preparation

The NMR spectrometer had been developed since 1953 for proton magnetic resonance using electromagnets with field of 1.4 T corresponding to 60 MHz frequency. The most powerful commercial NMR spectrometer is currently 1000 MHz. All of the instruments above 100 MHz are based on helium-cooled superconducting magnets or solenoids and operate in the pulsed Fourier-transform (FT) mode. The other basic requirements besides high field are frequency-field stability, field homogeneity, and a computer interface. The computer is used to acquire the data, carry out the FT, and further process and analyze the resulting spectra. The NMR spectrometer with schematic diagram is illustrated in Figure 8.

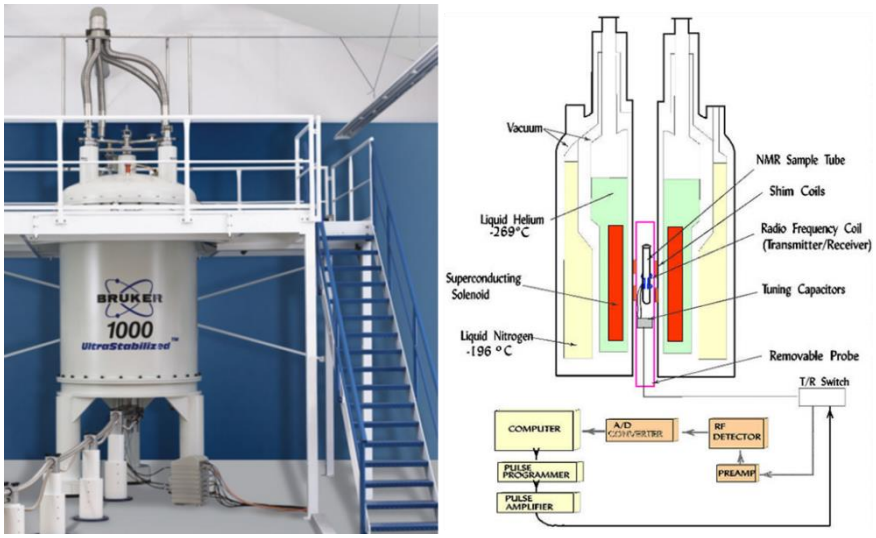

Figure 8 Schematic diagram of a Fourier-transform NMR spectrometer

From the figure, the basic requirements for all high-resolution NMR spectrometers are as follows:

1) a magnet capable of producing a very strong and homogeneous field
2) a stable radiofrequency generator
3) a radiofrequency receiver
4) a detector

The superconducting magnet part has a double Dewar-jacket arrangement, resembling a solid cylinder with a central axial hole. The outer Dewar is filled with liquid nitrogen at around -196 ^{o}C, while the inner Dewar with liquid helium at -269 ^{o}C. The solenoid coils are immersed in liquid helium. At the center tube, the shim solenoid coils are placed with diameter of 53 or 89 mm, which being considerably more expensive.

The preparation of the sample for NMR measurement is an important as recording the spectra. The sample must have good solubility in the chosen solvent, which has no resonances in the region of interest (Table 2). The most commonly used organic NMR solvent is chloroform-*d* ($CDCl_3$). In case of polar compounds, are likely soluble in $CDCl_3$, CD_3OD, and acetone-d_6. Moreover, DMSO-d_6 is an appropriate solvent for polar compounds and compounds containing hydroxyl groups. In a high-field magnetic field, 1 mg of sample in 0.5 ml of solvent is good enough for measurement, in which suspended dust or solid

undissolved should be avoided. It may affect the homogeneity of the magnetic field and causes the broadening of NMR lines. Thus, it is always recommended to filter the solution for NMR directly to the sample tube through a sintered glass or a small piece of tissue, such as a Kimwipe.

There are two additional approaches to increase the NMR signal of either small or relatively dilute samples; due to a high molecular weight.

1) Increasing the magnetic field strength because the sensitivity increases with the 3/2 power of B_0.

2) Construction of NMR probes for which the receiver coils or pre-amplifier is kept at very low temperature to minimize noise and, thereby, increase the signal-to-noise ratio.

An NMR tube is a cylindrical tube made of special glass with 18 cm in length and 5 mm in external diameter as shown in Figure 9. The solution should fill the NMR tube to a height of 4-5 cm, in which the signals from the finite volume of the detection coil in the NMR probe only will be received. That makes any sample outside this volume may well not be there. On the contrary, when is an excess of solvents, the concentration of the sample will be reduced, which will directly influence the intensity of lines, and expensive NMR solvent will be wasted. In addition, increased concentration and solvent volume will affect the spin rate of the NMR tubes. Thus, the choice of a suitable solvent for the determination of NMR spectra largely depends on solubility in the selected solvent of the compound to be studied.

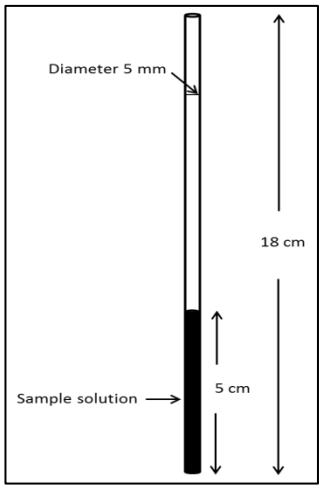

Figure 9 NMR sample tube for measurement

Table 2 List of solvents used for NMR measurement and its signal region

Solvent	Boiling point (^{o}C)	^{1}H signal (δ)
Acetone-d_6	55.5	2.05
Acetonitrile-d_3	80.7	1.95
Benzene-d_6	79.1	7.16
Chloroform-d	60.9	7.27
Cyclohexane-d_{12}	78.0	1.38
Dichloromethane-d_2	40.0	5.32
Dimethylsulfoxide-d_6	190.0	2.50
Nitromethane-d_3	100.0	4.33
Pyridine-d_5	114.0	7.19, 7.55, and 8.71
Tetrahydrofurane-d_8	65.0	1.73 and 3.58

1.7 ^{1}H chemical shift signals region

As mentioned earlier, the actual magnetic field B_{eff} expressed as $B_0(1-\sigma)$, in which the electronic shielding σ normally is positive. Variations in electron density surrounding at each non-equivalent nucleus in a molecule will therefore cause each nucleus to experience a different B_{eff}. The difference in resonance frequency phenomenon with shielding results has been termed "*chemical shift*" and reported in "ppm" as unit.

In case of the internal standard reference, tetramethylsilane $Si(CH_3)_4$,TMS, which is often carried out and represented the chemical shift at 0 ppm in spectra scale. A short summary of the chemical shift regions of some characteristic functional groups depending upon the hybridization of the carbons atoms is presented in Figure 10 and Table 3.

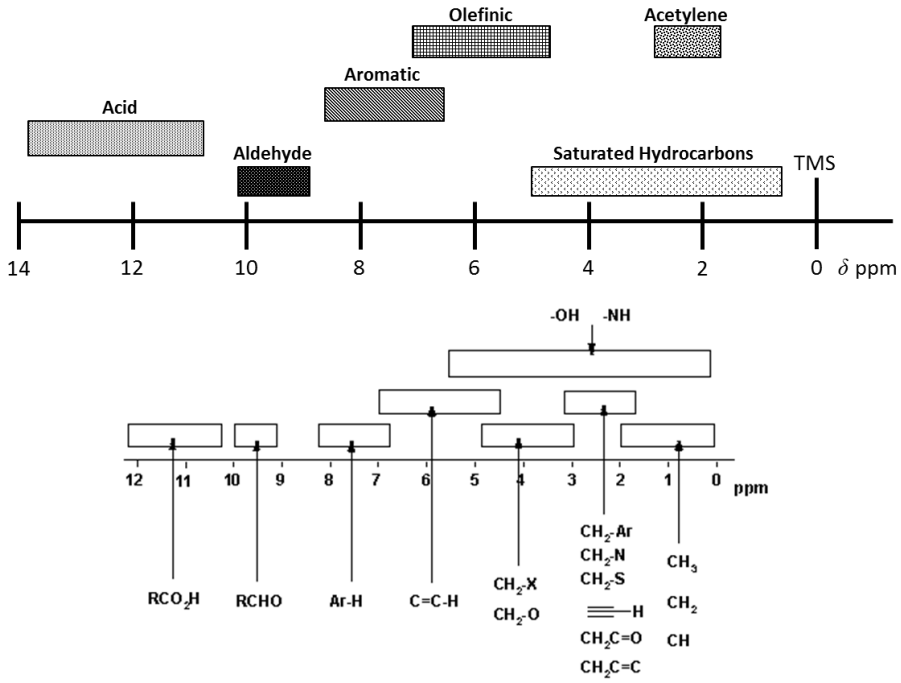

Figure 10 General chemical shift regions of different functional groups

Resonances outside these given ranges can be encountered depending upon the electronegativity and the number of the attached substituents. The values presented in table are the values for mono-substituted functional group. As an aromatic can resonate in the range of olefinic protons, so an olefinic proton resonate can also resonate in the range of aromatic protons.

Table 3 ^{1}H NMR chemical shifts of some characteristic functional groups

Functional group		**Chemical shift δ**
Cyclopropane		0.2
Primary hydrocarbons	R-CH_3	0.9
Secondary hydrocarbons	R_2-CH_2	1.3
Tertiary hydrocarbons	R_3-CH	1.5-1.6
Allylic	-C=C-CH_3	1.7
Amine	R-NH_2	1.0-5.0
Alcohol	R-OH	1.0-5.5
Carbonyl	-CO-CH-	2.0-2.7
Acetylene	-C≡CH-	2.0-3.0
Benzylic	Ar-CH-	2.2-3.0
I	-CH_2-I	2.0-4.0
Br	-CH_2-Br	2.5-4.0
Cl	-CH_2-Cl	3.0-4.0
F	-CH_2-F	4.0-4.5
Alcohol	-CH-OH	3.4-4.0
Ether	RO-CH-	3.3-4.0
Ester	R-COOCH-	3.7-4.1
Olefin	-C=CH-	4.5-6.5
Aromatic	Ar-H	6.0-8.5
Aldehyde	R-CHO	9.0-10.00
Acid	R-COOH	10.00-14.00

1.8 General detail of rubbers

The definition of rubber is a substance that can be stretched at room temperature to several times its original length and after release of the stretching force will recover quickly to approximately its original dimensions and shape. Rubber can be divided into two classes as follows;

1) Natural rubber and
2) Synthetic rubber

Almost 99 percent of world's natural rubber is produced by *Hevea brasiliensis*, the "Para Rubber" of international commerce. The name *Hevea* occupies the whole of Amazon River basin in Brazil. Natural rubber (NR), an industrial raw material of strategic importance, which is considered to be of the most versatile agricultural products. From an agro-ecological point of view, rubber is an ecofriendly tree species.

During the development of technologies necessary for the more effective use of natural rubber, i.e., vulcanization, chemists were actively searching for rubbery materials which could be manufactured artificially. By the end of 19th century, it begun the production of conjugated dienes could be converted into elastic materials by the polymerization process, known chemically as polybutadiene. Both USA and Europe were extremely attempted to produce other synthetic elastic materials. The success was initiated after the outbreak of the Second World War, in which the manufactured on a large scale of the copolymer styrene-butadiene, to be known as SBR, was improved. The SBR is today a one major material in rubber materials, subsequently, styrene-acrylonitrile, NBR.

The following lists are the commercially synthetic rubbers

1) Synthetic isoprene rubber, IR
2) Polybutadiene, Butadiene rubber, BR
3) Styrene-butadiene rubber, SBR
4) Acrylonitrile-butadiene rubber, Nitrile rubber, NBR
5) Chloroprene rubber, CR
6) Ethylene-propylene diene monomer, EPDM
7) Polyisobutylene-isoprene rubber, Butyl rubber, IIR
8) Silicone rubber, MQ
9) Polyurethane rubber, PU
10) Polyacrylate, ACM

1.9 Rubbers structure characterization

The structure of elastomers provides an important information to polymer researcher and technology, because it is closely related to the properties and hence the performance of the polymer. This would certainly contribute to an effective control in producing elastomers with certain desirable properties. Therefor, structural characterization of elastomers, whether natural or synthetic, is a subject importance in many research works.

For this aspect, high-resolution nuclear magnetic resonance NMR, i.e., more than 200 MHz, is one of the most powerful tools for the structural characterization. This is because of its high sensitivity, applicability for quantitative measurements without calibration, and versatility application to elastomers in soli, solution, latex, and swollen states. The NMR technique has been additional applied to the characterization of elastomers in many areas, such as chemical composition analysis, the extent of chemical modification, isomeric structure of diene monomer units, sequence distribution, small amounts of modified structure, end-groups, etc.

The combination using ^{1}H- and ^{13}C-NMR techniques can be done for the analysis of chemical composition of copolymer without difficulty, in which the signals of each component are assigned correctly. For example, diene monomers, which is composed in many rubbers such as butadiene, isoprene, and 2-chlorobutadiene, give rise to the following isomeric structure shown in Figure 11. It should be noted that the configurational sequences of 1,2 and 3,4 units reflect the arrangement of *R* and *S* configuration.

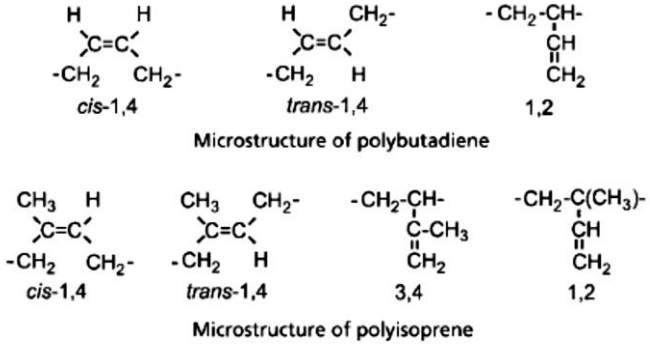

Figure 11 Microstructures of polybutadiene and polyisoprene

2. Experiment:

2.1 Materials

There are 4 types of synthetic rubbers used to be studied as follows;

1) Styrene-butadiene rubber, SBR
2) Acrylonitrile-butadiene rubber, NBR
3) Isobutylene-isoprene rubber, IIR
4) Ethylene-propylene diene monomer, EPDM

The general chemical structure of these rubbers is illustrated in Figure 12. The abbreviation of m, n, and o are represented the monomer contents in each rubber.

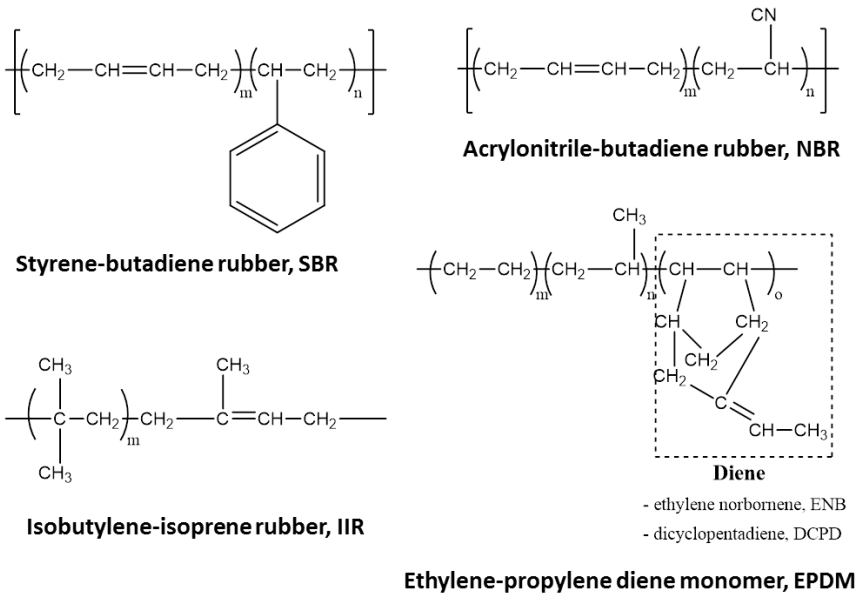

Figure 12 Chemical structure of rubbers used in this study

2.2 Sample preparation

About 5-10 mg of the sample was dissolved in chloroform-*d* ($CDCl_3$). After completely dissolving, the solution was transferred into a specific NMR tube with a height of 4 cm.

2.3 NMR spectrometer measurement

Proton nuclear magnetic resonance (^{1}H-NMR) 400 MHz spectra were recorded on a AVANCE III 400, Bruker Biospin spectrometer. Trimethylsilane (TMS) was used as internal standard reference with the number of scan at 16.

3. Results and Discussion

3.1 Styrene-butadiene rubber, SBR

A random synthetic copolymer which can be produced by both emulsion and solution polymerization technique. Nowadays, emulsion grades are being the most widely used, in which the "cold" polymerization temperature controlling yields a better superior properties than that of "hot" polymerization type. Both random emulsion and solution polymerized SBR contain about 23 wt.% of styrene content.

Butadiene rubber (BR) and pure polystyrene (PS) were prior recorded to determine the original proton characteristic, in which SBR was composed of these two monomers in the polymerization process as shown in Figure 13 and 14, respectively. In case of BR, there are two types of proton, i.e., secondary hydrocarbon and olefinic proton, represent with the symbol a and b, respectively, are detected. The results show that at 2.07 ppm, a, is the singlet peak of secondary hydrocarbon bearing 4 protons. Another at 5.23 ppm, b, is the doublet peak 2 protons of olefinic proton on the monomer structure. For the pure polystyrene sample, three proton signals were obtained. In the figure, secondary hydrocarbon proton, a, appears in a broad region 1.23-1.74 ppm. A singlet peak of a tertiary hydrocarbon proton, b, was next detected at 1.93 ppm. In addition, the 5 benzylic protons of the aromatic styrene were observed in a broad region 6.23-7.25 ppm.

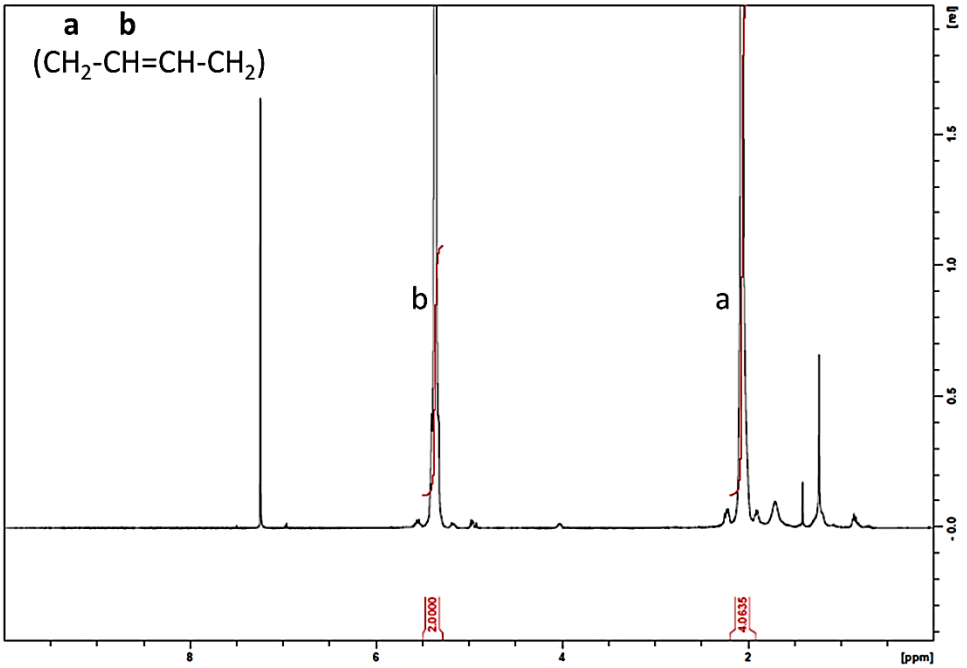

Figure 13 [1]H-NMR spectrum of butadiene rubber in $CDCl_3$

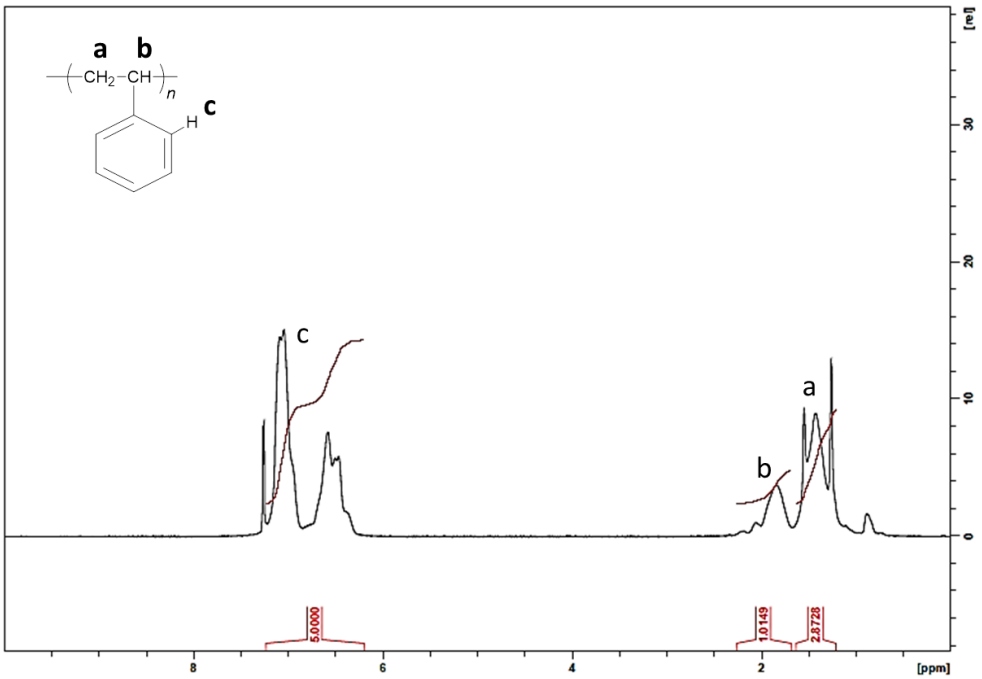

Figure 14 [1]H-NMR spectrum of pure polystyrene in $CDCl_3$

Figure 15 shows the ^{1}H-NMR spectrum for the SBR in $CDCl_3$, in which the proton signals were assigned. The results correspond with the result obtained of unmodified SBR, which was carried out by Khoee and Sorkhi.

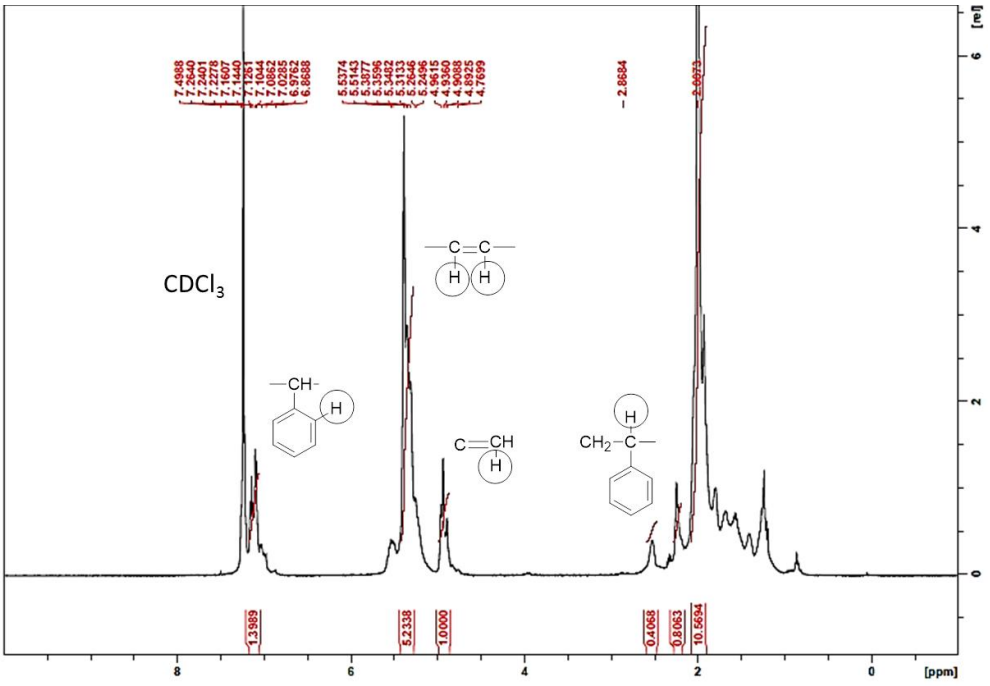

Figure 15 ^{1}H-NMR spectrum of SBR in $CDCl_3$

The following are the proton signals of the unmodified SBR in $CDCl_3$: δ 1.23 (doublet, 2H), 1.82-2.02 (singlet, aliphatic hydrogens), 4.91-5.03 (triplet, =C*H*$_2$), 5.35-5.40 (doublet, -C*H*=C*H*-), 5.51 (multiplet, -C*H*-CH$_2$), and 7.11-7.24 (multiplet, 5H) ppm. From the result in Figure 15, the proton signals are listed in Table 4.

Table 4 ^{1}H NMR chemical shifts of some characteristic functional groups

^{1}H chemical shift, ppm	**Description**
2.00	multiplet, aliphatic hydrocabon
2.43	singlet, tertiary hydrocarbon, -C*H*-
4.89-4.96	triplet, seconday hydrocarbon, =C*H*$_2$
5.34	doublet, olefinic, -C*H*=C*H*-
7.08-7.14	multiplet, benzylic proton

For the quantitative analysis, the peak integration of olefinic proton of butadiene mononor and benzylic proton of styrene monomer has to be applied. Nevertheless, the benzylic proton signals are close to the signal of $CDCl_3$ solvent at 7.24. Hence, the sample was measured by using methylene chloride-d_2 CD_2Cl_2, in which the solvent signal will be observed at 5.32 ppm. As seen in Figure 16, the singlet solvent signal was detected at 5.32 ppm. Moreover, the multiplet benzylic proton of the styrene monomer was significantly observed in a broad region 6.92-7.28 ppm.

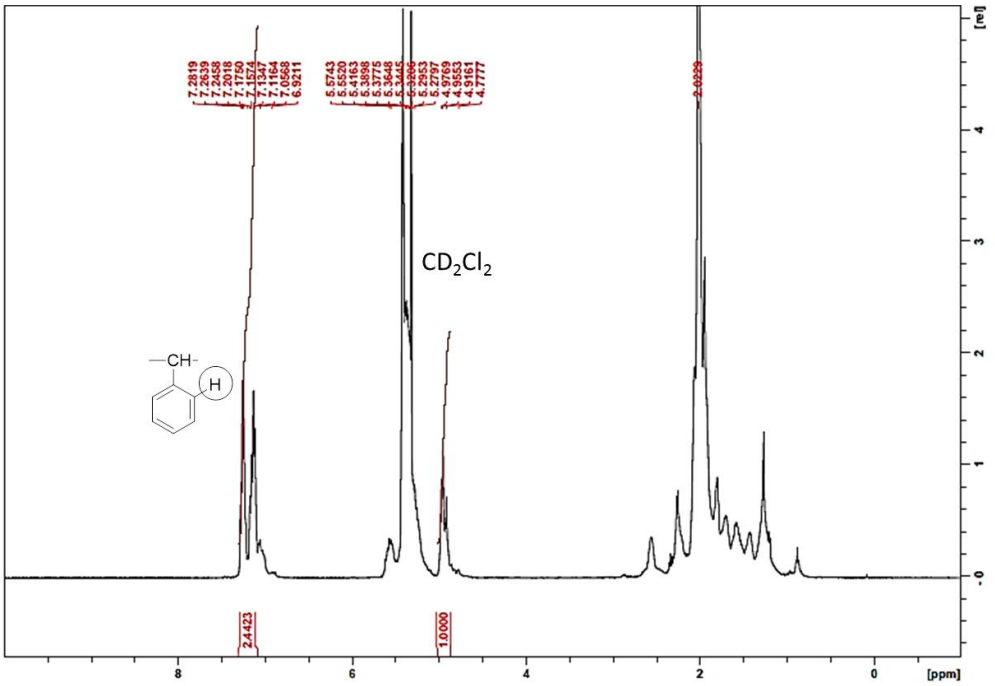

Figure 16 ^{1}H-NMR spectrum of SBR in CD_2Cl_2

3.1.1 Quantitative evaluation of monomer

The peak integration from the Figure 15 and 16 were applied to calculate the structure composition especially the styrene content.

The olefinic proton integration at 5.34 ppm is 5.2338, which composed of two proton from the double bond butadiene. Another six proton of benxylic styrene integration is 2.4423.

Olefinic; 2(H) = 5.2334 so, 1(H) = 2.6167

Benxylic; 5(H) = 2.4423 so, 1(H) = 0.4885

Butadiene	**:**	**Styrene**
2.6167 :		0.48885
~ 2.6	:	~ 0.49
~ 5.2	:	~ 1.00
~ 83.3 %	:	~ 16.7 %

From the [1]H-NMR calculation, the SBR in this study composed of 83 wt.% unsaturated butadiene and 16 wt.% of styrene monomer, respectively.

3.2 Acrylonitrile-butadiene rubber, NBR

A random copolymerization of butadiene and acrylonitrile, in which either cold or hot emulsion process can be produced. The introduction of acrylonitrile into the backbone is to increase the oil resistance property. Commercially available NBR has acrylonitrile (ACN) content from 18-50 wt.% grades, which is labeled as follows;

Low	18-24 % ACN
Medium low	26-28 % ACN
Medium	34 % ACN
Medium high	38-40 % ACN
High	50 % ACN

Pure polyacrylonitrile was prior observed the proton characteristic as shown in Figure 17. In the figure, there are two types of proton, i.e., secondary and tertiary hydrocarbon proton, represent with the symbol a and b, respectively, are detected. The peak, a, at 1.53 ppm is the aliphatic secondary proton and, b, at 1.28 ppm is the tertiary proton signal adjacent to the cyanide group.

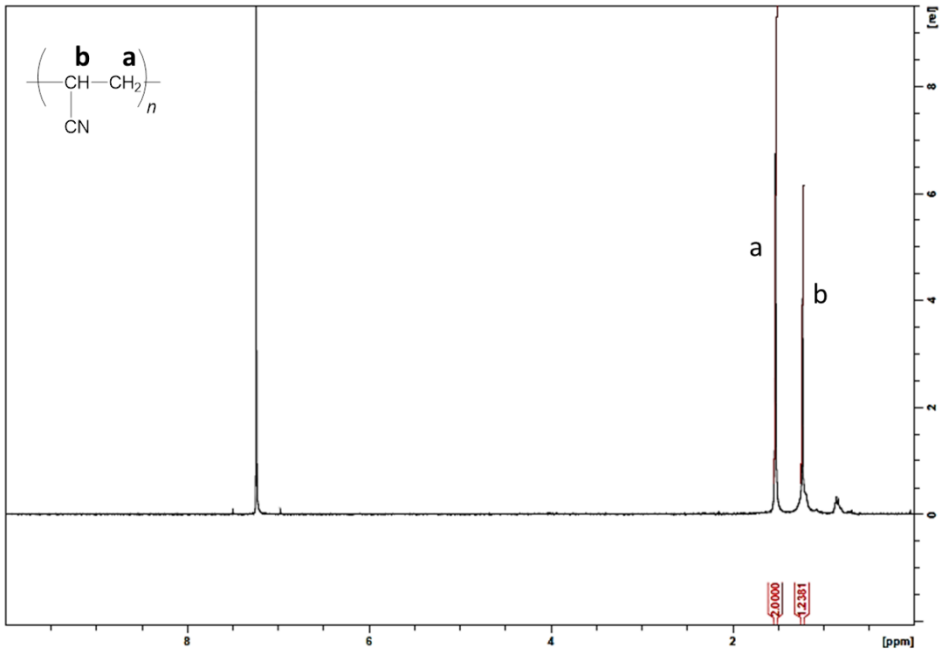

Figure 17 [1]H-NMR spectrum of pure polyacrylonitrile in $CDCl_3$

The [1]H-NMR spectrum of NBR is shown in Figure 18. The result corresponds to the proton signals reported by Liu *et al.* The peak at 2.50 ppm is assigned to one characteristic hydrogen of pendant cynanide groups from copolymerization process.

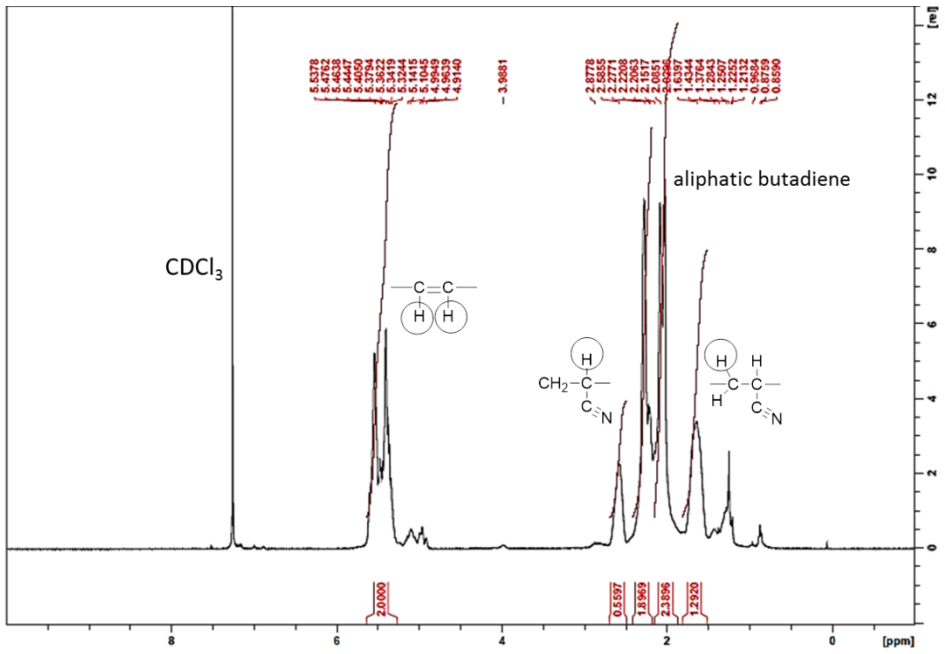

Figure 18 [1]H-NMR spectrum of NBR in $CDCl_3$

Table 5 shows the assigned proton peaks obtained from Figure 18.

Table 5 ^{1}H NMR chemical shifts of some characteristic functional groups

^{1}H chemical shift, ppm	**Description**
1.63	doublet, aliphatic hydrocarbon of acrylonitrile
2.15-2.27	multiplet, seconday aliphatic of butadiene, -CH_2
2.58	doublet, tertiary proton adjacent to the cyanide group
5.36	doublet, olefinic, -C*H*=C*H*-

3.2.1 Quantitative evaluation of monomer

The peak integration from the Figure 18 was directly employed to calculate the structure composition especially the acrylonitrile content.

The olefinic proton integration at 5.36 ppm is 2.000, which composed of two proton from the double bond butadiene. Another one proton attached to the cyanide group is 0.5597.

Olefinic; 2(H) = 2.0000 so, 1(H) = 1.0000

tertiary; 1(H) = 0.5597

Butadiene	**:**	**Acrylonitrile**
1.0000	:	0.5597
1	:	~ 0.56
~ 2	:	~ 1.00
~ 66.7 %	:	~ 33.3 %

From the ^{1}H-NMR calculation, the NBR in this study composed of 67 wt.% unsaturated butadiene and 33 wt.% of acrylonitrile monomer, respectively.

3.3 Isobutylene-isoprene rubber, IIR

A commercial grades of IIR, known for butyl rubber, prepared by copolymerization of polyisobutylene with small amounts ofpolyisoprene. The isoprene content influences for the sulfur vulcanization and the resistance of the copolymer to attack by oxygen, ozone, and UV light. Butyl rubber typically contains 0.5-3.0 wt.% of polyisoprene unsaturation.

Chlorobutyl (CIIR) and bromobutyl (BIIR) are derivertive midified rubber types, which contains 1.2 wt.% of chlorine or bromine molecule, the isoprene unit being the site of halogenation. The halogen gives greater cure flexibility and enhanced cure compatibility with other diene rubbers. Butyl rubber is non-oil resistance due to the hydrocarbon backbone. The [1]H-NMR spectrum of commercial butyl rubber used in this study is shown in Figure 19.

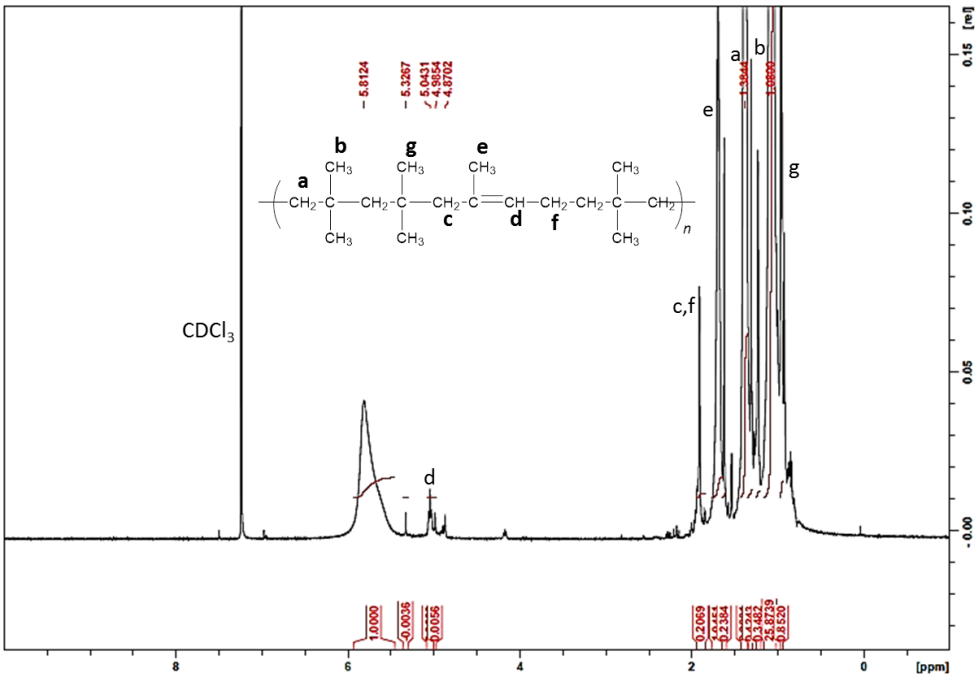

Figure 19 [1]H-NMR spectrum of IIR in $CDCl_3$

From the figure, the peaks were assigned based on the results reported by White and co-workers using 500 MHz [1]H-NMR frequency. The triplet olefinic hydrogen of the 1,4-isoprene unit was detected at 5.05 ppm, which possibly polymerized via 1,4-enchainment.

The chemistry polymerization has shown that the isoprene is predominantly incorporated in 1,4-enchained head-to-tail arrangement, thereby producing a strictly linear polymer backbone. However, it is expected that the isoprene may also incorporate via 1,2- or 4,3-addition as represented below.

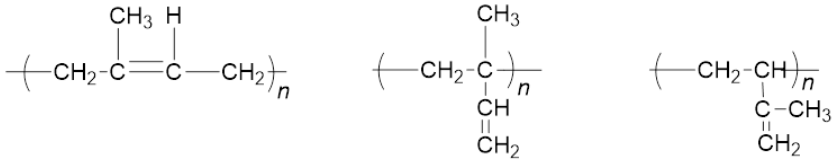

1,4 addition 1,2 addition 3,4 addition

The appearance of the minor peak at 4.8-4.9 ppm from the figure indicated the olefinic proton of the "branched" of isoprene unit, i.e., 1,2 and 4,3-addition, in which 1,2 addition favored sterically. The investigation of butyl rubber microstructure correlated to the results obtained by Makhiyanov using very high ^{1}H-NMR at 600 MHz frequency in chloroform-*d*. Obviously, two types olefinic proton of the isoprene unit and aliphatic hydocarbon were observed;

5.05-5.13 ppm	olefinic protons of the isoprene units in the 1,4 addition
4.93-4.98 ppm	olefinic protons of branched isoprene unit
2.60-0.20 ppm	Methine (tertiary), methylene (secondary), and methyl protons of branched isoprene units, methylene and methyl protons of isoprene units in the 1,4 addition, methylene and methyl protons of unsaturated terminal entities, and methylene and *gem*-dimethyl protons of isobutylene units.

3.4 Ethylene-propylene diene monomer, EPDM

A synthetic rubber polymerized from ethylene and propylene, in which the crystallization being prevented when the ethylene content is in a range of 45-60 %. Due to the lack of unsaturation in the main chain, sulfur cannot be allowed for crosslinking. Therefore, a diene third monomer was commercially added to overcome this drawbacks, i.e.,

dicyclopentadiene, ethylidene norbornene, and 1,4-hexadiene. The EPDM has excellent electrical properties and stability to radiation.

One of the most commercial grade diene using is *5*-ethyllidene-*2*-norbornene or ENB, which being obtained narrow and unimodal chemical composition distribution with metallocene catalysts.

[1]H-NMR spectrum of EPDM for the structural characterization in this study is shown in Figure 20.

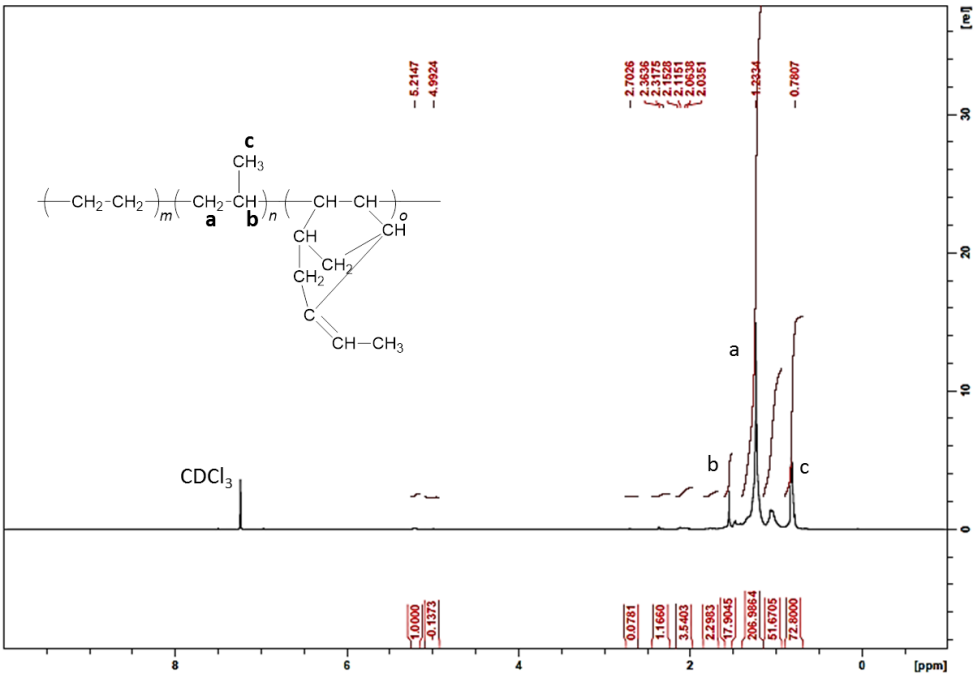

Figure 20 [1]H-NMR spectrum of EPDM in $CDCl_3$

The proton peak characteristics was assigned related to the result obtained by Nuinu et al., in which EPDM was graft with poly(styrene-*co*-methyl methacrylate) to enhance the mechanical and aging resistance. From the figure, the chemical shift at 0.78 ppm was attributed to methyl saturated proton of the propylene unit. For the secondary proton hydrocarbon (methylene), the peak was assigned at 1.23 ppm. This peak is the proton summation for both ethylene and propylene units. Moreover, the trace chemical shift at 5.21

ppm was also observed. This peak was referred to the olefinic proton of the diene (=C*H*); ENB, which is mostly added in EPDM grades.

Additional proton peak determination of tertiary hydrocarbon of the propylene unit is also detected. Mai and Chang assigned this characteristic peak of EPDM raw material at 1.49 ppm. Consequently from the experimental spectrum, the chemical shift of the tertiary hydrocarbon of the propylene unit (b), was observed at 1.52 ppm.

References

1. Becconsall .K. Basic One- and Two- Dimensional NMR Spectroscopy. Weinheim: VCH Verlagsgesellschaft; 1993.
2. Macomber R.S. A Complete Introduction to Modern NMR Spectroscopy. New York: John Wiley&Sons; 1998.
3. Lambert J.B. and Mazzola E.P. Nuclear Magnetic Resonance Spectroopy; An introduction to principles, Aplications, and Experimental methods. New Jersey: Pearson Education; 2004.
4. Balci M. Basic ^{1}H- and ^{13}C-NMR Spectroscopy. Pennsylvania: Elsevier; 2005.
5. Litvinov V.M. and De P.P. Spectroscopy of Rubbers and Rubbery Materials. United Kingdom: Rapra Technology Limited; 2002.
6. Simpson R.B. Rubber Basics. United Kingdom: Rapra Technology Limited; 2002.
7. Khoee S. and Sorkhi M. *Polym. Eng. Sci.* 2007, 47:87-94.
8. Liu Y., Kim H., Pan Q., and Rempell G.L. *Catal. Sci. Technol.* 2013, 3:2689-2698.
9. Song M., Zhao X., Li Y., Hu S., Zhang L., and Wu. *RSC Advances* 2014, 4:6719-6729.
10. Chu .Y. and Vukov R. *Macromolcules* 1985, 18:1423-1430.
11. White J.L., Shaffer T.D., Ruff C.J., and Cross J.P. *Macromolcules* 1995, 28:3290-3300.
12. Makhiyanov N. *Polym. Sci. Ser. A* 2014, 56:241-255.
13. Mitra S., Jørgensen M., Pedersen W.B., Almdal K., and Banerjee D. *J. Appl. Polym. Sci.* 2009, 113:2962-2972.
14. Nuinu P., Pivsa-Art S., and Hinchiranan N. *J. Polym. Res.* 2012, 19:9784-9785.
15. Mai J. and Wang L. *Polym. Chem.* 2014, 5:2118-2129.

Acknowledgements

Before completing this thesis, I recognize this aboard time here must be one of the most memorable times of my life. My journey passed by much faster than I could have imagined.

First and always, I would like to express my sincere thankfulness, appreciation and respect to my great supervisor, Professor Masayuki Yamaguchi for giving me the opportunity to fulfill my dream. He was brave enough to accept me across the globe without knowing any background. His great supervision, helpful suggestion, and professional encouragement are valuable supports to accomplish my degree throughout the tough times. He has always been a door contributing of time, enlightening knowledge, funding, and experience not only for the research, but also the daily life to become a mature person. Only the words written here are still not enough to express my respect to him. It is a great honor for me to be a member in Yamaguchi's laboratory and graduate under his supervision.

Secondly, I would express my appreciate to the members of my committee: Associate Professor Ken-ichi Shinohara, Associate Professor Kazuaki Matsumura, Associate Professor Tsutomu Hamada of JAIST, and Professor Shuichi Maeda of Yamaguchi University for their effort to read my thesis and provide me with helpful comments. I am also profoundly grateful to Professor Tatsuo Kaneko, Dr. Seiji Tateyama, and Shiho Maetani for their generous hospitality and support during the minor research time.

Sincere thanks are also extended to Assistant Professor Shogo Nobukawa, who always provided me a lot of valuable support and thoughtful advice. He is always kindness and friendly to talk in academic and lifestyle. I would like to say thank you to all present and former members of “Yamaguchi family” including all internship members, with all warm support and friendship which make my life here so colorful and memorable. Thanks to Kento Yoshida and Mitsunari Sugiyama for their help and cooperation in our research group.

Finally, I owe deepest gratitude to my family with their endless love and support. They never stopped believing in me and encourage me up in many difficult times. Without them, it was not easy to survive in abroad only by myself and finish this research. Moreover, appreciate thank you to all Thai members in JAIST and everyone else for their love, emotional support, and making me feel less lonely.

Nawaphorn Kuhakongkiat

June 2016

JAIST